PHENOTYPIC, MOLECULAR AND GENETIC CHARACTERIZATION OF DEVELOPMENTAL DEFECTS IN DDX11 AND MGRN1 MUTANT MICE

A Dissertation

Presented to the Faculty of the Graduate School

of Cornell University

In Partial Fulfillment of the Requirements for the Degree of

Doctor of Philosophy

by

Christina D. Cota

May 2012

PHENOTYPIC, MOLECULAR AND GENETIC CHARACTERIZATION OF DEVELOPMENTAL DEFECTS IN DDX11 AND MGRN1 MUTANT MICE

Christina D. Cota, Ph. D.

Cornell University 2012

Early stages in the development of the mouse embryo are characterized by rapid growth and dynamic changes in patterning and morphology. However, technical challenges in accessing and manipulating embryos after implantation in the uterus have hampered the identification of genes involved in these processes. Here I present the characterization of two mouse mutants, *cetus* and *Mgrn1*$^{md\text{-}nc}$. Together these studies have uncovered novel roles for genes in regulating early development and patterning of the mouse embryo.

cetus mutants were isolated from a forward genetic screen for recessive mutations which disrupt the overall morphology of the developing embryo. *cetus* embryos are small with defects in closure of the neural epithelium and a severe reduction in somitic mesoderm. Interestingly, positional cloning of *cetus* revealed a novel point mutation in helicase motif V of the DEAD/H-box helicase, *Ddx11*. I found that the *cetus* mutation in *Ddx11* results in widespread apoptosis at early embryonic stages without disrupting proliferation. These studies identified novel, tissue-specific requirements for DDX11 during mouse development and show that helicase motif V is essential for these processes.

Mgrn1$^{md\text{-}nc}$ is a spontaneous, semi-lethal mutation that results in loss of MGRN1 (Mahogunin RING-finger 1). While the effects of loss of MGRN1 on pigmentation are well studied in *Mgrn1*$^{md\text{-}nc}$ mutant mice, the developmental defects in these mice have not been well characterized. I found that loss of MGRN1 results in the mis-expression of nodal target genes

controlling left-right patterning including *Lefty1*, *Lefty2* and *Pitx2*, resulting in congenital heart defects and death in ~50% of embryos. My characterization of *Mgrn1* mutants uncovered a role for this ubiquitin ligase in the regulation of Nodal signaling and left-right patterning. To this date, MGRN1 remains the only ubiquitin ligase to have been identified with a direct role in left-right patterning.

BIOGRAPHICAL SKETCH

Christina Donata Cota was born in Orlando, FL. The eldest of five children born to Charles Walter and Jill Ann Cota, Christina spent the majority of her childhood in upstate New York. There upon graduation from high school in 1998, Christina first attended the State University of New York (SUNY) at Cobleskill where she received her A.S. in Liberal Arts and Science in 2000. Upon completion of this degree, she transferred to Skidmore College where in 2002 she received a B.A. in Biology. Degree in hand, Christina relocated to Ithaca where she obtained a job as a technician in the lab of Dr. Teresa M. Gunn at Cornell University. Here she was introduced to working with mouse as a model genetic system and began work on the project that would send her to graduate school and result in half of the dissertation that follows this biographical sketch. After two and a half years working as a technician Christina applied to and began graduate school in the Department of Biomedical Sciences at Cornell, first via the employee degree program in 2005 and later as a fulltime student in 2007. In the summer of 2008 Christina moved to the lab of Maria J. Garcia-Garcia in the Department of Molecular Biology and Genetics where she completed her Doctorate of Philosophy in Molecular and Integrative Physiology in 2012.

For my parents Charles and Jill Cota.

ACKNOWLEDGMENTS

There are many people who I would like to thank and without whose support this thesis would not have been possible. I was extremely fortunate to have had the opportunity to work under two great scientists and inspirational women, Maria García-García and Teresa Gunn. I thank them both for their mentorship and support along with the members of my committee; Mark Roberson, Marianna Wolfner and John Schimenti.

I thank all of my labmates for their helpful discussions and critiques, especially my benchmates: Seung-woo Jung, Will Walker, Maho Shibata, Pooneh Bagher and Kristin Blauvelt whose comments, suggestions and friendship I believe have helped to make me a better scientist and lab member. I thank Joe Peters and his lab, especially Qiaojian Shi, for welcoming into their lab and for all of their help with biochemical experiments.

I would like to thank the many wonderful faculty and staff at Cornell University who have made themselves available as resources especially the members of and participants in the Gunn/O'Brien/Garcia-Garcia/Schimenti Joint Lab Meetings (GOGGS), Vertebrate Genomics Club (VERGE), Developmental Biology Journal Club (DBJC) and Replication, Recombination and Repair (R3) group as well as Sylvia Allen, the staff and veterinarians of the Cornell Center for Animal Resources and Education who care for our animals.

Finally I would like to thank my friends and family for their unwavering support and understanding throughout this and all my endeavors. I am truly grateful to you all.

TABLE OF CONTENTS

LIST OF FIGURES

LIST OF TABLES

LIST OF ABBREVIATIONS

AP: anterior-posterior

APC: anaphase promoting complex

AVE: anterior visceral endoderm

BrdU: Bromodeoxyuridine

BSA: Bovine serum albumin

CHD: Congenital Heart Defect

C-terminus: Carboxy-terminus

DNA: Deoxyribonucleic acid

DORV: double-outlet right ventricle

DSB: double-strand break repair

DTT: Dithiothreitol

DV: dorsal-ventral

ECM: extracellular matrix

EMSA: Electrophoretic Mobility Shift Assay

EMT: epithelial-to-mesenchymal-transition

ENU: *N-ethyl-N-nitrosourea*

ESC: Embryonic Stem Cell

ESCRT: Endosomal Sorting *Complex* Required for Transport

H&E: Hematoxylin & Eosin

IAP: Intracisternal A Particle

ICM: inner cell mass

IPTG: isopropyl-β-d-1-thiogalactopyranoside

LPM: lateral plate mesoderm

LR: left-right

MMR: mis-match repair

NTA: Ni^{2+}-nitrilotriacetic acid

N-terminus: Amino-terminus

NVP: Nodal vesicular particle

OCT: Optimal Cutting Temperature medium

PBS: Phosphate buffered saline

PCR: Polymerase Chain Reaction

PD: proximal-distal

RING: Really Interesting New Gene

RNA: Ribonucleic acid

SAC: spindle assembly checkpoint

SF2: Superfamily 2

SSLP: Simple Sequence Length Polymorphism

TB: Terrific broth

TGA: transposition of the great arteries

TUNEL: Terminal deoxynucleotidyl transferase dUTP nick end labeling

X-gal: X-galactosidase

Chapter 1

Introduction

A. Early post-implantation development in the mouse.

Proper development of the mammalian embryo relies on the coordination of three processes; cellular proliferation, specification and morphogenesis. In the mouse, the initial establishment of the proximal-distal axis (PD), initiation of gastrulation and early cellular rearrangements resulting from patterning of the anterior-posterior (AP) axis are all reliant upon cell proliferation (Rossant and P. P. L. Tam, 2004; P. P. Tam and R R Behringer, 1997). Specification of embryonic and extra-embryonic cell lineages, and later those of the endoderm, mesoderm and ectoderm turn on genes that help to regulate this proliferation as well as the cellular and environmental changes that allow for cell movements which ultimately shape the embryo.

In the mouse, attachment of the developing blastocyst to the uterine wall occurs between e4.5 and e5.0. At this time, proliferation and differentiation of the inner cell mass (ICM) generates a radially symmetric epiblast of primitive ectoderm (R. S. P. Beddington, 2001). As the epiblast proliferates and grows along a PD axis, a group of cells located at the distal tip of the developing embryo adjacent to the epiblast in the extra-embryonic visceral endoderm, begin secreting signaling molecules that will pattern the epiblast. These cells comprise a signaling center called the anterior visceral endoderm (AVE). Among the molecules secreted by the AVE are the antagonists LEFTY1 and CERL which are potent inhibitors of NODAL signaling (P. P. L. Tam et al., 2006). Inhibition of *Nodal* in the visceral endoderm at the AVE reduces proliferation in the region which, along with the active migration of these cells, results in the anterior displacement of the AVE (M. Yamamoto et al., 2004). The relocation of the AVE to the anterior additionally results in the restriction of Nodal expression within the epiblast to the

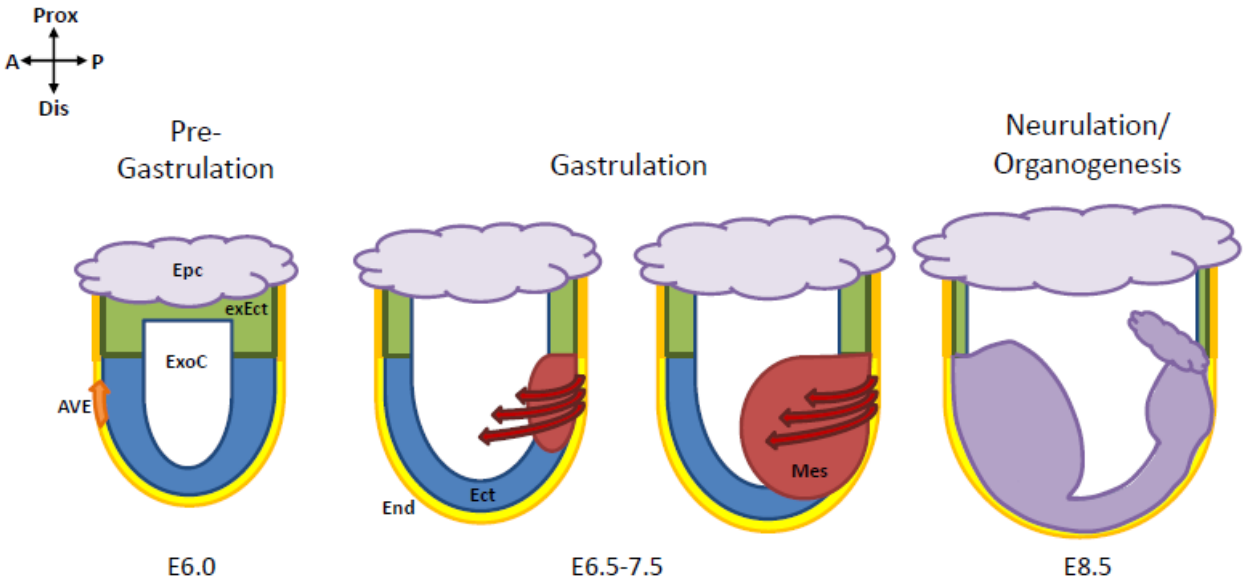

Figure 1.1. Early post-implantation development in the mouse. Illustration of three stages of mouse development; pre-gastrulation, gastrulation and neurulation/organogenesis. Embryonic cell types are indicated in different colors: ectoderm (ect, blue) endoderm (end, yellow) and mesoderm (mes, red). Extra-embryonic tissues are indicated as: ectoplacental cone (epc, grey), extra-embryonic ectoderm (exect, green) and extra-embryonic/visceral endoderm(exend, orange). Exoceloemic (exoc) cavity is indicated. Orange and red arrows indicate the location and direction of movement of the anterior visceral endoderm (AVE) and mesoderm respectively.

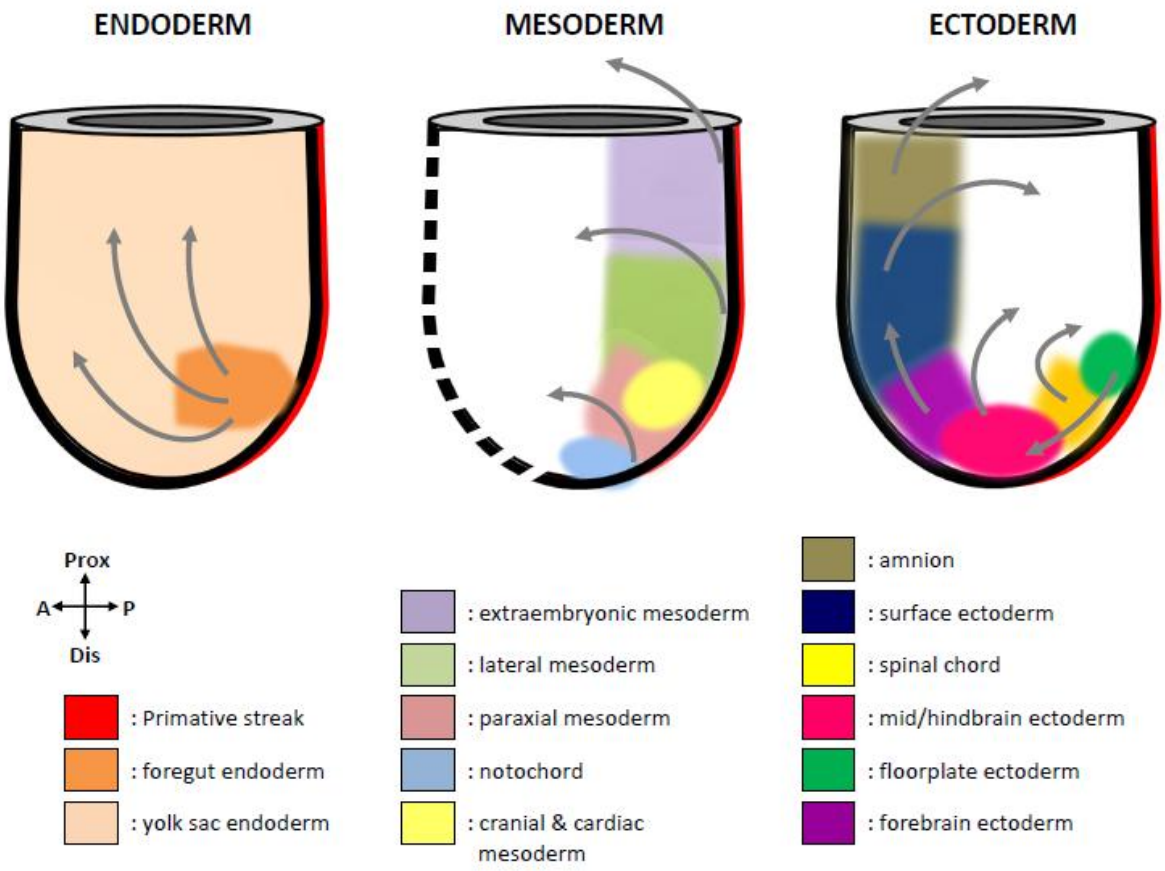

Figure 1.2. Cell fate and morphogenetic movements in the early-to-mid-streak mouse embryo. Illustration of the regional cell fate and directional cell movements (grey arrows) in the developing germ layers. Figure adapted from (P. P. Tam and R R Behringer, 1997).

posterior contributing to the establishment of AP polarity within the embryo (Rossant and P. P. L. Tam, 2004, Figure 1.1).

By e6.5 a group of cells in the posterior region of the epiblast adjacent to the extra-embryonic ectoderm begin to invaginate at the primitive streak indicating the onset of gastrulation. As the primitive streak elongates along the proximal-distal axis of the embryo cells continuously ingress, undergoing an epithelial-to-mesenchymal transition (EMT) which generates the definitive germ layers of the embryo (Figure 1.1; Nowotschin and Hadjantonakis, 2010). The relative order of migration and position of cells within the epiblast at the time of ingression have been correlated with ultimate fate of those cells within the embryo. Cells which ingress first at the most proximal sites within the epiblast contribute to extra-embryonic mesoderm while cells that ingress at the most proximal (anterior) regions of the primitive streak contribute to the cranial and cardiac mesoderm and the definitive endoderm of the gut (Figure 1.2; P. P. Tam and R. S. Beddington, 1987; Lawson et al., 1991).

B. Cell proliferation in early post-implantation development:

Cell proliferation and growth of the murine epiblast.

Upon implantation, the embryonic ectoderm that makes up the epiblast undergoes a burst of proliferation. This proliferative burst peaks during gastrulation and results in an approximate 120 fold increase in cell number over 2 days of development from e5.5 to e7.5 (Snow, 1977). The majority of this increase is seen in the primitive ectoderm, the source of progenitor cells for the embryonic germ layers (Poelmann, 1980). It has been shown that, while not alone sufficient to drive the process, this proliferative burst is necessary to achieve a threshold number of cells required for the initiation of gastrulation (Power and P. Tam, 1993; P. P. Tam, 1988). This likely provides one explanation for the recent observation that blastocyst cell number at implantation is a good predictor of the overall developmental potential of a mouse embryo in embryo transfer

experiments (Ajduk et al., 2011).

Estimates made from careful study of the mitotic cell populations calculate that the average cell cycle duration during gastrulation in the mouse embryo is only 7.5 hours (Lawson et al., 1991; Poelmann, 1981; Snow, 1977). By comparison, cell cycle duration in proliferative tissues of the adult mouse varies greatly, from 18 hours in the rapidly proliferating intestinal crypt to greater than 60 hours in slowly proliferating cells of the corneal epithelium and esophagus (Lehrer et al., 1998; Burholt, 1986; Atlas and Bond, 1965).

In the adult mouse, the length of the cell cycle is typically accomplished by variation in the duration of G1 (Pardee, 1989). However, studies in mouse and rat embryos have determined that the short cell cycle duration at peri-implantation stages is achieved through a shortening of G1, G2 and S phases (Mac Auley et al., 1993; Power and P. Tam, 1993). A major consequence of such a shortening of the cell cycle is that cells in gastrulating mammalian embryos would be predicted to have little, if any, capacity for DNA repair. The most compelling evidence supporting a lack of functional repair pathways during this period stems from experiments in which gastrulating embryos were exposed to low doses of ionizing radiation. Treatment of cells with ionizing radiation induces double-strand breaks in the DNA which must then be recognized and repaired by the cell. In most cells, DNA damage induced by ionizing radiation is recognized by components of the G1/S and G2-M cell cycle checkpoints. Activation of either of these checkpoints results in cell cycle arrest allowing time for the DNA lesions to be repaired (Sancar et al., 2004). In contrast, gastrulating embryos exposed to ionizing radiation displayed wild type levels of proliferation as indicated by Bromodeoxyuridine (BrdU)-incorporation with no evidence for cell cycle arrest. Instead, irradiated embryos showed a massive increase in ATM and p53-dependent apoptosis in embryonic tissues (B. S. Heyer et al., 2000).

In spite of the significant contribution of cell proliferation to the development of the

embryo, and the intriguing mechanistic questions posed by the massive up regulation of the rate of cell proliferation during gastrulation, the mechanisms that regulate the proliferative rate of embryonic tissues at early stages of embryogenesis remain poorly understood. What has become apparent is that the requirement for genes involved in cell cycle progression, cell cycle checkpoints and DNA repair pathway activation in the embryo differs from what has been observed in adult tissues (Artus and Cohen-Tannoudji, 2008; Ciemerych and Sicinski, 2005).

DNA damage checkpoints

DNA damage checkpoints within the cell cycle protect the genome from the accumulation and propagation of deleterious mutations and chromosomal alterations including translocations, deletions, rearrangements and aneuploidies. In mammalian cells, DNA damage checkpoints coincide with points of cell cycle transition at G1/S, intra-S and G2/M (Figure 1.3). These checkpoints, while distinct in timing; are controlled by a common molecular pathway composed of a core set of DNA damage sensors, signal transducers, mediators and effectors that recognize and respond to genetic lesions (Sancar et al., 2004). Loss of individual components of the DNA damage checkpoint machinery, such as *Ataxia telangiectasia and Rad3 related* (*Atr*) or *Hus1 homolog* (*Hus1*), often results in embryonic lethality at or shortly after gastrulation that has been attributed to the increased stress imposed by the rapid proliferation within the embryo (Weiss et al., 2000; E. J. Brown and Baltimore, 2000). (Table 1.1)

Mitotic checkpoint complex

The mitotic spindle assembly checkpoint (SAC) prevents improper chromosome segregation by detecting failed attachment of spindle microtubules to chromosomes at the kinetochore. In the absence of an appropriate kinetochore attachment, the anaphase promoting complex (APC), a large multi-subunit ubiquitin ligase is inactive and unable to degrade securin.

Table 1.1. DNA DAMAGE CHECKPOINTS

Protein Function	Gene Symbol	Gene Name	Null Mutant Phenotype
Sensors			
	Hus1	Hus1 homolog	Abnormal embryonic development appearing at gastrulation accompanied by widespread apoptosis. Embryonic lethal by e10.5 (Weiss et al., 2000).
	Rad9	Rad9 homolog	Abnormal embryonic development appearing at gastrulation accompanied by widespread apoptosis and reduced proliferation. Embryonic lethality occurs between e9.5-12.5 (Hopkins et al., 2004).
	Rad1	Rad1 homolog	Unknown
	Rad17	Rad 17 homolog	Abnormal embryonic development appearing at e8.5. Null embryos display growth retardation, hemorrhage, somite and neural tube closure defects. Embryonic lethal by 11.5 (Budzowska et al., 2004).
	ATM	ataxia telangiectasia mutated homolog	Homozygous null mice are viable. Adults display growth retardation, sensitivity to ionizing radiation and male and female infertility (Barlow et al., 1996).
	ATR	ataxia telangiectasia and Rad3 related	Peri-implantation lethal by e7.5 due to defects in proliferation and caspase-dependent apoptosis downstream of chromosome instability (E. J. Brown and Baltimore, 2000).
	ATRIP	ATR interacting protein	Unknown

Table 1.1 continued. DNA DAMAGE CHECKPOINTS

Protein Function	Gene Symbol	Gene Name	Null Mutant Phenotype
Mediators			
	Mdc1	mediator of DNA damage checkpoint 1	Homozygous null mice are viable and hypersensitive to ionizing radiation. Adults display growth retardation due to defects in proliferation. Homozygous males are infertile and females are sub-fertile (Lou et al., 2006).
	Trp53BP1	transformation related protein 53 binding protein 1; 53BP1	Homozygous null mice are viable and fertile. Adults display growth retardation, immune defects and sensitivity to ionizing radiation (I. M. Ward et al., 2003).
	TopBP1	Topoisomerase (DNA) II binding protein 1	Peri-implantation lethal by e7.5 due to decreased proliferation (Y. Jeon et al., 2011).
	Claspin	claspin homolog	Unknown
	BRCA1	Breast cancer 1	Abnormal embryonic development appearing at gastrulation. Embryos are small, lack mesoderm and display varying degrees of germ layer disorganization due to decreased proliferation. Embryonic lethal by e9.5 (C. Y. Liu et al., 1996; Ludwig et al., 1997)
Transducers			
	Chek1	checkpoint kinase 1 homolog	Peri-implantation lethal by e7.5 due to decreased proliferation and increased apoptosis (Q. Liu, Guntuku, et al., 2000; Takai et al., 2000).
	Chek2	CHK2 checkpoint homolog	Homozygous null mice are viable and fertile (Hirao et al., 2002).
Effectors			
	Trp53	transformation related protein 53; p53	Homozygous null mice are viable and fertile (L A Donehower et al., 1992).
	Cdc25c	cell division cycle 25 homolog C	Homozygous null mice are viable and fertile (M. S. Chen et al., 2001).

The presence of securin inhibits the activity of separase (Xingxu Huang et al., 2005; Ciosk et al., 1998) which is required to degrade cohesion proteins connecting sister chromatids (Hornig et al., 2002) . Checkpoint activation results in prometaphase arrest (Musacchio and Salmon, 2007). Several components of the SAC such as *budding uninhibited by benzimidazoles 3* (*Bub3*; Kalitsis et al., 2000), *MAD2 mitotic arrest deficient-like 1* (*Mad2L1*; Dobles et al., 2000) and *cell division cycle 20* (*Cdc20*; Li et al., 2007) have been knocked out in the mouse and are required for embryo survival at either pre-implantation or peri-implantation stages (Table 1.2).

DNA Repair Pathways

DNA repair pathways during development repair damage to the genome resulting from increased cell proliferation and cell metabolism, reactive oxygen species and both endogenous and exogenous genotoxins (Pachkowski et al., 2011). Three major DNA repair pathways are active in the developing embryo: double-strand break repair (DSB), excision repair (including both base and nucleotide excision repair pathways) and mis-match repair (MMR). Loss of components of these pathways has extremely variable effects on the embryo (Pachkowski et al., 2011). Many components of the MMR pathway are dispensable for embryonic development. Conversely, loss components of the DSB pathway have severe effects on development resulting in early embryonic lethality (Table 1.3). This apparent differential requirement for DNA repair proteins may be reflective of the multiple roles of these genes in a wide variety of processes including cell cycle progression (Ludwig et al., 1997) and redox pathways (Xanthoudakis et al., 1996).

C. Morphogenetic cell movements during gastrulation:

Cell migration and morphogenesis.

While it has been estimated that the high rates of proliferation alone are sufficient to account for the absolute growth of the mouse embryo during gastrulation (Poelmann, 1981), it is

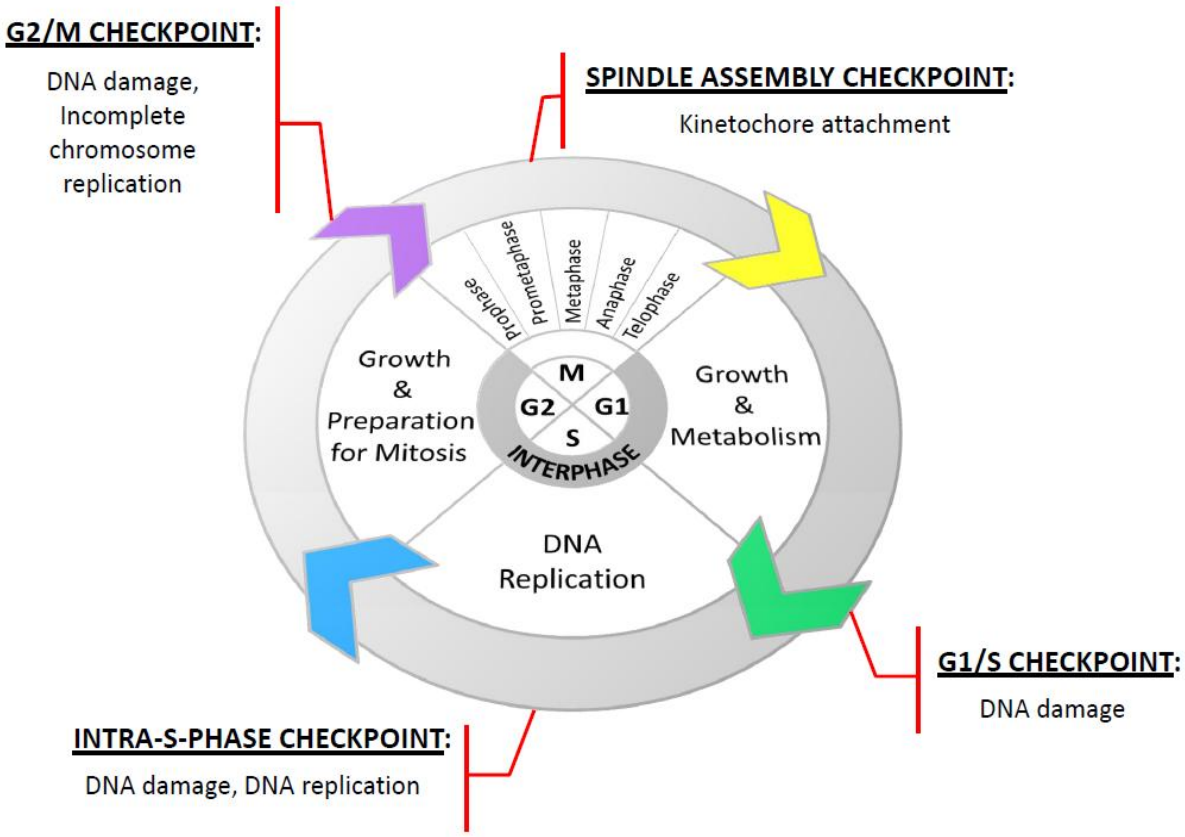

Figure 1.3. Cell cycle and checkpoints. Schematic representation of the eukaryotic cell cycle

Table 1.2. MITOTIC SPINDLE CHECKPOINT			
Protein Function	Gene Symbol	Gene Name	Null Mutant Phenotype
Mitotic Checkpoint Complex			
	Cdc20	cell division cycle 20 homolog	Embryonic lethal at the 2-cell stage due to metaphase arrest (M. Li et al., 2007).
	Bub3	budding uninhibited by benzimidazoles 3 homolog	Peri-implantation lethal by e7.5 with mitotic defects resulting in a progressive cessation of proliferation (Kalitsis et al., 2000).
	Mad211	mitotic arrest deficient 2-like 1	Peri-implantation lethal by e7.5 with defects in proliferation, chromosome segregation and apoptosis (Dobles et al., 2000).
Anaphase Promoting Complex			
	Anapc2	anaphase promoting complex subunit 2	Homozygous lethal by e6.5, no further characterization of the in vivo embryonic defects (Wirth et al., 2004).
	Anapc11	anaphase promoting complex subunit 11	Unknown
Cohesions			
	Smc1a	structural maintenance of chromosomes 1A	Unknown
	Smc3	structural maintenance of chromosomes 3	Unknown
	Stag1	stromal antigen 1; SA1	Unknown
	Rad21	RAD21 homolog; Scc1	Required for zygotic sister chromatid cohesion however in vivo embryonic development remains uncharacterized (Tachibana-Konwalski et al., 2010).

Table 1.2 continued. MITOTIC SPINDLE CHECKPOINT			
Protein Function	Gene Symbol	Gene Name	Null Mutant Phenotype
Regulatory kinases			
	Mad1l1	mitotic arrest deficient 1-like 1	Embryonic lethal, embryonic defects were not characterized (Iwanaga et al., 2007).
	Cdk1	cyclin-dependent kinase 1	Embryonic lethal by e1.5 (Santamaría et al., 2007).
	Bub1	budding uninhibited by benzimidazoles 1 homolog	Peri-implantation lethal by e6.5 (Jeganathan et al., 2007).
	Bub1b	budding uninhibited by benzimidazoles 1 homolog, beta, BubR1	Abnormal peri-implantation development. Embryos are small with elevated apoptosis. Embryonic lethal by e8.5(Q. Wang et al., 2004).
Transient centromere interacting proteins			
	Aurkb	aurora kinase B	Abnormal embryonic development appearing at gastrulation. Embryos are small with elevated proliferation and apoptosis. Embryonic lethal by e9.5 (Fernández-Miranda et al., 2011).
	Birc5	baculoviral IAP repeat-containing 5; Survivin	Null embryos fail to hatch and exhibit abnormal nuclear morphology including micro and macronuclei (Uren et al., 2000).
	Incenp	inner centromere protein	Null embryos fail to hatch and exhibit abnormal nuclear morphology including micro and macronuclei (Cutts, 1999).
Protease			
	Espl1	extra spindle poles-like 1; Separase	Embryos homozygous for a null mutation embryos are peri-implantation lethal with defects chromosome segregation during mitosis (Kumada et al., 2006).

Table 1.3. DNA REPAIR

Protein Function	Gene Symbol	Gene Name	Null Mutant Phenotype
Double-strand Break Repair			
	Mre11a	meiotic recombination 11 homolog A	Embryonic lethal; *in vivo* defects not characterized (Buis et al., 2008).
	Rad50	RAD50 homolog	Abnormal development appearing at gastrulation. Embryos are small and disorganized with embryonic lethality occurring by e7.5 due to decreased proliferation (G. Luo, 1999).
	Nbn	Nibrin	Peri-implantation lethal by e7.5. Embryos are small and cells are disorganized prior to death (J. Zhu et al., 2001).
Mis-match Repair			
	Mlh1	mutL homolog 1	Homozygous null mice are viable and sterile (W Edelmann et al., 1996).
	Msh2	mutS homolog 2	Homozygous null mice are viable with a predisposition to lymphoma (de Wind et al., 1995).
	Msh4	mutS homolog 4	Homozygous null mice are viable and sterile (Kneitz et al., 2000).
	Msh5	mutS homolog 5	Homozygous null mice are viable and sterile (de Vries et al., 1999).
	Msh6	mutS homolog 6	Homozygous null mice are viable with an increased predisposition to GI tumors, B- and T-cell lymphomas resulting in a decreased lifespan (Winfried Edelmann et al., 1997).
	Pms1	postmeiotic segregation increased 1	Homozygous null mice are viable (Prolla et al., 1998).

Table 1.3 continued. DNA REPAIR

Protein Function	Gene Symbol	Gene Name	Null Mutant Phenotype
Excision Repair			
	Apex1	apurinic/apyrimidinic endonuclease 1	Abnormal development appearing post-implantation with embryonic lethality occurring by e7.5 due to apoptosis (Xanthoudakis et al., 1996).
	Fen1	flap structure specific endonuclease 1	Homozygous null embryos are peri-implantation lethal with defects in proliferation and blastocyst outgrowth (Larsen et al., 2003).
	Xrcc1	X-ray repair complementing defective repair in Chinese hamster cells 1	Abnormal development appearing post-implantation with growth retardation and apoptosis resulting in embryonic lethality by e8.5 (Tebbs et al., 1999).
	Ercc1	excision repair cross-complementing rodent repair deficiency, complementation group 1	Peri-natal lethal by weaning. Mice are susceptible to oxidative stress and die due to liver failure (McWhir et al., 1993).
	Ercc8	excision repair cross-complementing rodent repair deficiency, complementation group 8; Csa	Homozygous null mice are viable with increased sensitivity to UV and predisposition to develop skin cancer (Gijsbertus T J van der Horst et al., 2002).
	Ercc6	excision repair cross-complementing rodent repair deficiency, complementation group 6; Csb	Homozygous null mice are viable with increased sensitivity to UV and predisposition to develop skin cancer (Gijsbertus T.J van der Horst et al., 1997)(van der Horst et al., 1997).
	Rad23b	RAD23b homolog; Hr23b	Loss of Rad23b is semi-lethal. Surviving homozygous males are sterile and females are sub-fertile with facial and vascular defects (Ng et al., 2002)(Ng et al., 2002).

Table 1.3 continued. DNA REPAIR

Protein Function	Gene Symbol	Gene Name	Null Mutant Phenotype
Excision Repair			
	Pold1	polymerase (DNA directed), delta 1, catalytic subunit	Homozygous null embryos are peri-implantation lethal with defects in proliferation and blastocyst outgrowth and increased apoptosis (Uchimura et al., 2009)

the migration of these newly formed cells that is essential for the morphogenetic events that shape the basic body plan in gastrula stage embryos (Figure 1.2; Parameswaran and P. P. Tam, 1995; Lawson et al., 1991). A great number of genes and molecules have been identified to play a role in these processes including extracellular matrix (ECM) components, cell surface receptors and signal transduction molecules capable of activating intracellular signaling molecules and cytoskeletal components (P. P. L. Tam et al., 2006). Still the mechanisms that coordinate gene expression, activation and signaling transduction cascades necessary to define the shape of the embryo remains an active area of research. It is clear; however, that morphogenesis of the embryo is dependent upon interactions between cells, their neighbors and their environment.

Integrins

The integrin family of cell surface receptors is the major transducers of signals from the ECM. Upon ligand binding, integrin receptors initiate cascades of intracellular signaling which ultimately result in cell movement. There are 18 α subunits and 8 β integrin subunits in mammals, the subunits heterodimerize to bind ligands (J. T. Yang et al., 1999). Functional redundancies amongst the integrin receptor heterodimers have made separating their functions difficult. However, loss of *αv integrin* in mice results in embryonic lethality with the majority of embryos dying by 10.5 dpc due to vascular defects, defects in cell proliferation, cell survival and posterior mesoderm-derived structures (Goh et al., 1997; Bader et al., 1998; Yang et al., 1993). Intracellularly, integrins have been shown to associate with the cytoskeletal components α-ACTININ, TALIN and FILAMIN as well as the intracellular signaling molecule focal adhesion kinase (FAK) (S Liu, Calderwood, et al., 2000).

More recent work has revealed that four of the αv-integrin heterodimers are capable of activating extracellular transforming growth factor beta (TGFβ) (Asano, Ihn, et al., 2005; Asano, Ihn, et al., 2005; Mu et al., 2002; Munger et al., 1999). TGFβ has been shown to inhibit

cell proliferation and promote cell differentiation (Kitisin et al., 2007). The three mammalian TGFβ isoforms- TGFβ1, 2 and 3- are secreted from the cell in a protected inactive state resulting from interactions between the mature TGFβ isoforms, the cleaved portion of the TGFβ propeptides (latency-associated peptide, LAP) and latent-TGFβ-binding protein (LTBP) (Annes, 2003). Mutating the integrin-binding motif (located in the LAP) of *Tgfβ1* recapitulates the null phenotype including in defects in vasculogenesis (Z. Yang et al., 2007).

Fibronectin

Fibronectin (FN) is a secreted dimeric protein that promotes cytoskeletal rearrangements by forming fibrous associations between integrin heterodimers that result in clustering of these receptors (Wierzbicka-Patynowski and Schwarzbauer, 2003). Twelve *fibronectin* splice isoforms have been identified in mice as well as a fibrillar cellular fibronectin (cFN) which is expressed in most tissues and a non-fibrillar plasma fibronectin (pFN) present in hepatocytes and secreted in blood (Leiss, et al., 2008). In the absence of *fibronectin,* mouse embryos are small with shortened anterior-posterior axes, lack somites, have kinked neural tubes, misshapen headfolds and die by e8.5 (George, 1993).

Like integrins, FN also facilitates TGFβ signaling in cells. However, unlike integrins which directly activate TGFβ by binding the inhibitory LAP; FN is required for the incorporation of the TGFβ inhibitory co-factor, LTBP, into the ECM. Loss of LTBP in the absence of fibronectin results in an inability to retain TGFβ in the ECM (Dallas et al., 2005).

Laminins

The laminins are a family of heterotrimeric extracellular glycoproteins that act as molecular scaffolds and which are essential to for the formation of basement membranes (Sasaki

et al., 2004). Eighteen laminin heterotrimers have been identified in vertebrate species each composed of a single α, β and γ subunit (Durbeej, 2010). *In vivo*, laminins are capable of undergoing calcium-dependent polymerization. It is believed that the polymerization of collagen-associated laminin heterotrimers aides the redistribution of their receptors, integrins, in the plasma membrane, which in turn stimulates the rearrangement of cytoskeletal proteins within cells (Colognato and Yurchenco, 2000). All laminin subunits have been mutated in mouse models, revealing essential roles for *laminin-111* (*Laminin-1*) and *laminin-511* (*Laminin-10*) during embryonic development (Durbeej, 2010). In mice, the absence of the γ1 subunit alone, results in the loss of basement membranes and peri-implantation lethality by 5.5 dpc (Smyth et al., 1999).

Focal Adhesion Kinase (FAK)

FAK is a cytoplasmic tyrosine kinase which becomes autophosphorylated upon binding to integrins and subsequently activated by Src kinases to interact with a number of downstream targets including phosphotidyl inositol 3-kinase (PI3K), GRB2, PAX, and p130CAS activating MAPK, JNK and ERK signal transduction pathways (D D Schlaepfer and Hunter, 1997; Mitra et al., 2005). Mutations which affect Integrin/FAK signaling have also been implicated in the control of cell proliferation and apoptosis presumably via downstream effects on MAPK and PI3 kinase (Sonoda et al., 2000). Knock out models of *Fak* (Furuta et al., 1995; Ilić et al., 1995) and all three mammalian Src kinases; *Src*, *Fyn* and *Yes* (SFY;Klinghoffer, Sachsenmaier, Cooper, & Soriano, 1999); in mice result in gastrulation defects similar those observed in FN null mice and embryo lethality suggesting that FN-stimulated integrin signaling is the major mechanism of activation FAK during this period of development.

Ddx11

Ddx11 is a member of the DEAD/H (Asp-Glu-Ala-Asp/His)-box family of DNA

helicases. Physical interactions have been identified between DDX11 and components of the multimeric cohesin complex that encircles sister chromatids during DNA replication and cell division (Parish et al., 2006; Sherwood et al., 2010; Uhlmann, 2009) as well as cohesion establishment factors (Farina et al., 2008; Leman et al., 2010) and components of the replication fork machinery (Leman et al., 2010). These interactions have implicated a role for DDX11 in the establishment of sister chromatid cohesion.

Consistent with this hypothesis, loss of *Ddx11* in mice results in defects in sister chromatid cohesion and mid-gestation embryonic lethality (A. Inoue et al., 2007). My work presented in this dissertation identifies a novel point mutation in *Ddx11* that results in morphological defects in closure of the neural tube epithelium as well as a severe loss of somitic mesoderm. These defects are reminiscent of those that have been described previously for mice carrying mutations in components of cell adhesion pathways such as *Fn* (George, 1993; Georges-Labouesse et al, 1997) as well as the integrin-activated *FAK* (Ilić et al., 1995; Furuta et al, 1995). Interestingly, a similar loss of somitic mesoderm has also been described in mice lacking components of the DNA check point and repair machinery including the checkpoint component, *Hus1* (Weiss et al., 2000).

D. Post-gastrulation patterning of the embryo.

Establishment of the left-right body axis.

In the mouse, three embryonic axes divide the initially symmetric epiblast. The establishment of the anterior-posterior (AP) and dorsal-ventral (DV) axes occur just prior to and concomitant with gastrulation, respectively (P. P. L. Tam et al., 2006). However, the third and final embryonic axis, which defines the left and right sides of the embryo (LR), is not established

until well after gastrulation. Both the molecular signals and mechanism of axis establishment involved in AP and DV axis establishment are well conserved across vertebrates. Whether this degree of mechanistic conservation exists for the establishment of LR asymmetries remains unclear (Aw and Michael Levin, 2008).

The initial break in bilateral symmetry occurs at the node, a mammalian organizer located at the posterior end of the primitive streak. The node is equivalent to the Hensen's node in the chick or Spemann's organizer in *Xenopus* (R. S. Beddington and E J Robertson, 1999) and results in the asymmetric expression of the TGF-β related gene, *Nodal* (Jane Brennan et al., 2002). This symmetry breaking event, which occurs around e8.0 is dependent on monocilia that cover the ventral surface of the node (S. Takeda et al., 1999; Yasushi Okada et al., 1999; S Nonaka et al., 1998). However, the mechanism by which these cilia contribute to the break in symmetry remains unclear.

Two models have emerged, largely from the analysis of mutations that affect LR patterning. The chemical-gradient model proposes that the break in symmetry begins with the creation of a leftward current of extracellular fluid generated by rotation of beating monocilia. This flow is believed to contribute to the buildup of a nodal vesicular particles (NVPs) released within the node, which carry morphogens important for initiating left-specific signaling in the embryo. As a consequence of the differential distribution of NVPs *Nodal* becomes asymmetrically expressed in the left side of the node (Figure 1.4B, Shigenori Nonaka et al., 2002; Yosuke Tanaka et al., 2005). A second "two-cilia model" recognizes the existence of two populations of cilia within the node; motile cilia that line the ventral surface of the pit and immotile cilia that line the lateral edges. This model proposes leftward nodal flow generated by the motile pit cilia activates, either directly or indirectly, the mechano-sensory immotile cilia at the edges of the node (Figure 1.4C, Tabin and Vogan, 2003). Accompanying these signals it has

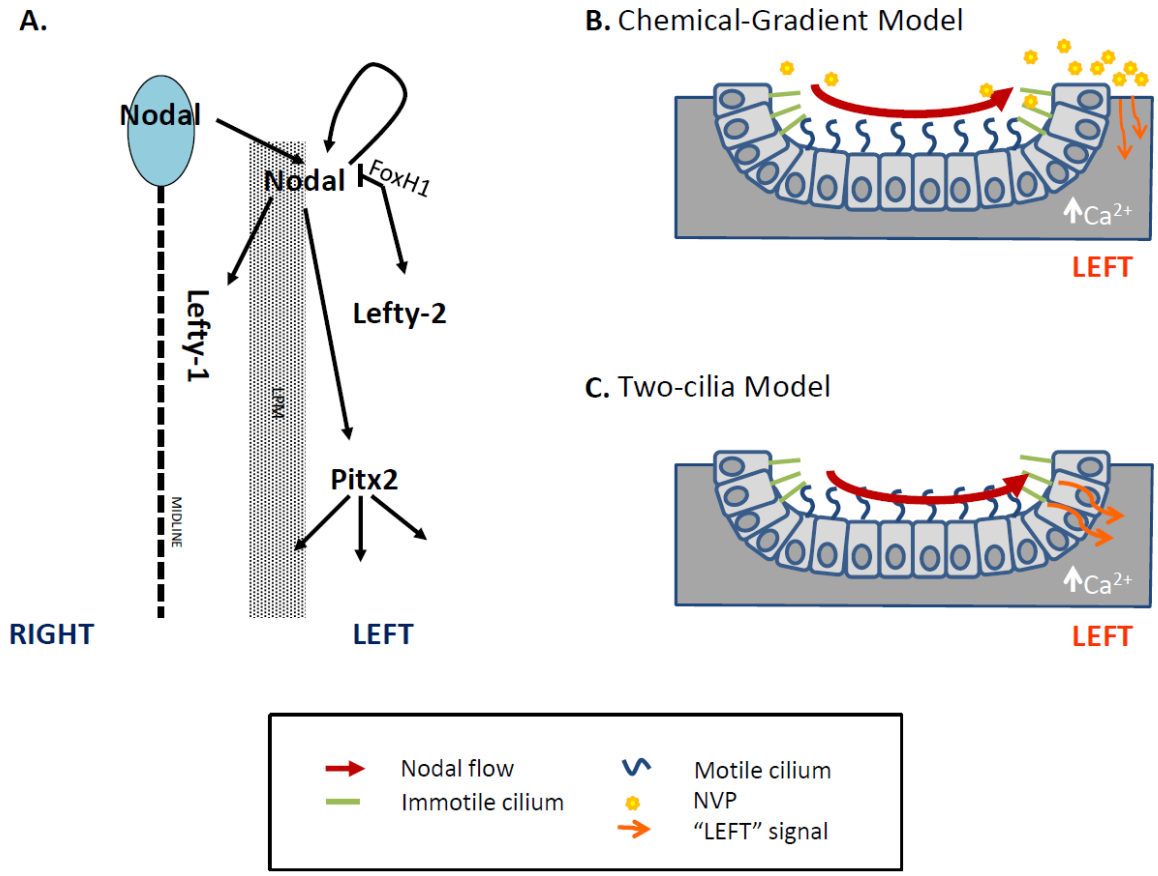

Figure 1.4. Genetic specification of the Left-Right axis and models for breaking symmetry. (A) Left-right patterning pathway: Cilia-dependent asymmetric *Nodal* expression in the node initiates a left-specific *Nodal* signaling cascade in the LPM. *Nodal* in the LPM initiates left-specific *Lefty-1* expression in the floorplate. LEFTY-1 and LEFTY-2 with FOXH1 shut off the *Nodal* signals. (B, C) Two models of nodal flow-dependent symmetry breaking. (B) The chemical-gradient model postulates that cilia-dependent leftward nodal flow carries morphogens in nodal vesicular particles (NVPs) which accumulate on the left side and initiate left-specific signaling. (C) The Two-cilia model of symmetry breaking recognizes that two populations of cilia reside in the node: motile cilia at the surface of the ventral pit and immotile cilia at the lateral edges. This model postulates that the immotile cilia act as mechno-sensors, responding to leftward nodal flow directly or chemical stimuli and initiating left-specific signaling. Both models recognize left-specific genetic signals are accompanied by an increase in intracellular calcium although the mechanism of calcium accumulation remains unclear. Figure adapted from (Shiratori and Hiroshi Hamada, 2006).

been observed that there is an increase in left-specific intracellular calcium at the node although data regarding the contribution of nodal flow to this localization is conflicting (McGrath and Martina Brueckner, 2003; Yosuke Tanaka et al., 2005).

Genetic patterning of the left-right body axis.

Regardless of the symmetry-breaking mechanisms, the end result is the initiation of a cascade of signaling that starts in the node and is propagated to the lateral plate mesoderm (LPM). This cascade initiated with a buildup of *Nodal* on the left side of the node (Collignon J. and E J Robertson, 1996). NODAL then induces asymmetric expression of other signaling molecules in both the left LPM and then the floor plate of the neural tube. Targets of NODAL include two other TGF-β family members, *Lefty1* and *Lefty2* and a bicoid-like homeobox transcription factor, *Pitx2* (Figure 1.4A, Shiratori and Hamada, 2006).

TGF-β molecules signal through heterodimeric receptor complexes to initiate a cascade of SMAD-mediated phosphorylation events which ultimately result in the activation of transcriptional targets. NODAL binds to the ACTR1B/ACVR2B receptor complex with the aid of the EGF-CFC co-receptor, CRIPTO (Reissmann et al., 2001; Yan et al., 2002). The activation of the receptor complex upon ligand binding results in the phosphorylation of SMAD proteins, which in turn associate with the winged-helix transcription factor, FOXH1, to bind activin response elements (AREs) located in the regulatory regions of target genes to activate transcription. Mutations that affect the localization, expression or binding capacity of these molecules have been shown to result in a variety of defects in the expression of LR patterning genes and heart development (Michael M Shen, 2007).

Mgrn1

MGRN1 is a RING-type E3 ubiquitin ligase first identified for its role in pigment-type

switching (Lane, 1960; Phillips, 1963; Miller et al., 1997; L He et al., 2001)). While the exact mechanism by which MGRN1 regulates pigment production remains unclear, genetic studies have indicated a role for MGRN1 as an accessory protein which acts upstream of the Melanocortin 1 receptor (Mc1R) and downstream of *agouti* transcription (Lin He et al., 2003; W. P. Walker and Teresa M Gunn, 2010). Mice lacking *Mgrn1* have completely black fur from the resultant loss of pheomelanin production (Figure 1.5; L He et al., 2001; Lin He et al., 2003) .

In addition to defects in pigment production, *Mgrn1* mutant mice have a variety of pleiotrophic defects including a progressive adult-onset spongiform neurodegeneration, craniofacial defects and embryonic lethality (Lin He et al., 2003; Cota et al., 2006; Phillips, 1963, 1971; Jiao, H. Y. Kim, et al., 2009). My work presented in this dissertation uncovered a previously unidentified role of *Mgrn1* in patterning of the LR axis. Characterization of *Mgrn1* mutants revealed loss of *Mgrn1* results mis-expression of nodal target genes including *Lefty1*, *Lefty2* and *Pitx2* (Cota et al., 2006).

E. Organization of dissertation

The goal of the work presented in this dissertation is to identify genes with novel roles in the regulation of embryonic development.

In Chapter 2, I present work on the identification of a novel mutation in *Ddx11*, characterization of the embryonic defects in these mutants and the biochemical activity of the both wild type and mutant murine DDX11 protein. These results indicate that *Ddx11* is required for genomic stability and embryonic survival in the mouse.

In Chapter 3, I present work on the phenotypic characterization of embryonic patterning defects in *Mgrn1* mutant mice. These results indicate a novel role for *Mgrn1* in the regulation of Nodal signaling and left-right patterning of the mouse embryo.

Appendix A and B contain unpublished data that was not included in previous chapters.

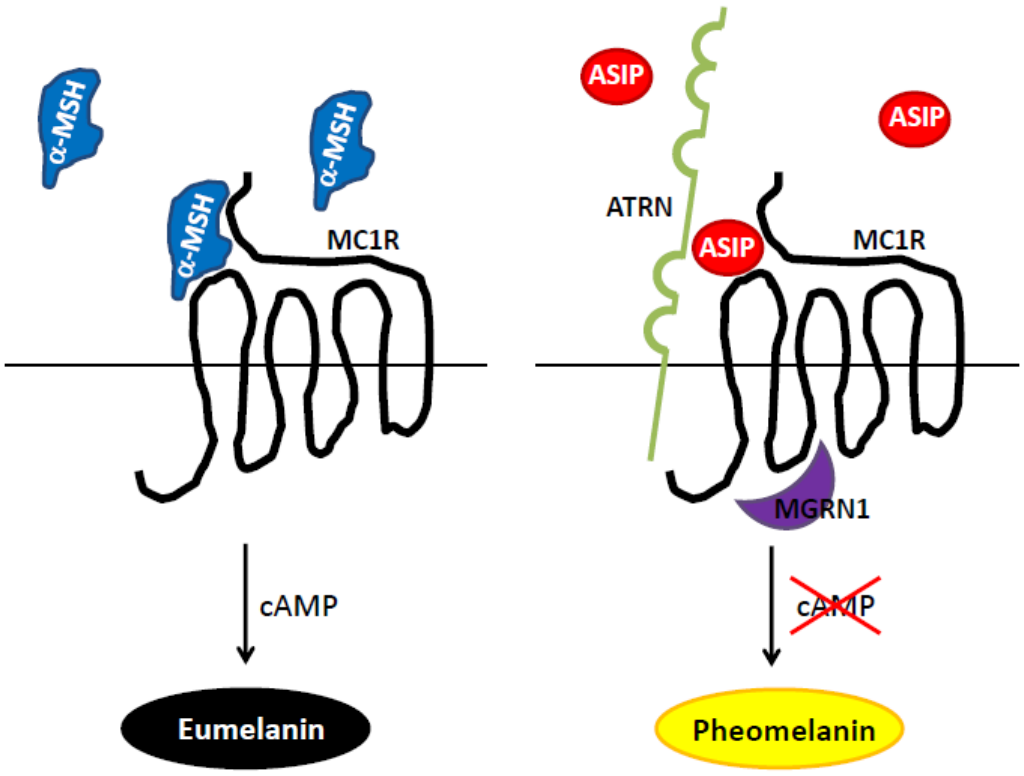

Figure 1.5. Pigment-type switching. Binding of alpha melanocyte stimulating hormone (α-MSH) to the g-protien coupled receptor, MC1R, results in the production cyclic adenocine monophosphate (cAMP) necessary for the conversion of dopaquinone to eumelanin (left). Transient expression of *agouti* during the hair cycle results in the competitive binding of the agouti signaling peptide (ASIP) to MC1R along with the accessory proteins attractin (ATRN) and MGRN1. The interactions of these proteins with the MC1R, in the case of MGRN1 and ATRN via unknown mechanisms, is sufficient to inhibit the production of cAMP and resulting in the conversion of dopaquinone to pheomelanin (right, adapted from Walker and Teresa M Gunn, 2010).

These data are considered supportive and preliminary. Appendix A contains data from co-immunoprecipitation experiments conducted to examine the effect of the *cetus* mutation on interactions between DDX11 and cohesin ring complex proteins. Appendix B contains data from yeast-2-hybrid screens conducted to identify MGRN1 interacting proteins.

REFERENCES

Ajduk, A., Ilozue, T., Windsor, S., Yu, Y., Seres, K. B., Bomphrey, R. J., Tom, B. D., Swann, K., Thomas, A., Graham, C., et al. (2011). Rhythmic actomyosin-driven contractions induced by sperm entry predict mammalian embryo viability. *Nature communications*, **2**, 417.

Annes, J. P. (2003). Making sense of latent TGFbeta activation. *Journal of Cell Science*, **116**, 217-224.

Artus, J. and Cohen-Tannoudji, M. (2008). Cell cycle regulation during early mouse embryogenesis. *Molecular and cellular endocrinology*, **282**, 78-86.

Asano, Yoshihde, Ihn, H., Yamane, K., Jinnin, M., Mimura, Y., and Tamaki, K. (2005). Involvement of alphavbeta5 integrin-mediated activation of latent transforming growth factor beta1 in autocrine transforming growth factor beta signaling in systemic sclerosis fibroblasts. *Arthritis and rheumatism*, **52**, 2897-905.

Asano, Yoshihide, Ihn, H., Yamane, K., Jinnin, M., Mimura, Y., and Tamaki, K. (2005). Increased expression of integrin alpha(v)beta3 contributes to the establishment of autocrine TGF-beta signaling in scleroderma fibroblasts. *Journal of immunology (Baltimore, Md. : 1950)*, **175**, 7708-18.

Atlas, M. and Bond, V. P. (1965). The cell generation cycle of the eleven-day mouse embryo. *The Journal of cell biology*, **26**, 19-24.

Aw, S. and Levin, M. (2008). What's left in asymmetry? *Developmental dynamics : an official publication of the American Association of Anatomists*, **237**, 3453-63.

Bader, Bernhard L, Rayburn, Helen, Crowley, D., and Hynes, Richard O (1998). Extensive Vasculogenesis, Angiogenesis, and Organogenesis Precede Lethality in Mice Lacking All αv Integrins. *Cell*, **95**, 507-519.

Barlow, C., Hirotsune, S., Paylor, R., Liyanage, M., Eckhaus, M., Collins, F., Shiloh, Y., Crawley, J. N., Ried, T., Tagle, D., et al. (1996). Atm-deficient mice: a paradigm of ataxia telangiectasia. *Cell*, **86**, 159-71.

Beddington, R. S. P. (2001). Mammalian Embryo : Establishment of the Embryonic Axes. *Encyclopedia of Life Sciences*, 1-7.

Beddington, R. S. and Robertson, E J (1999). Axis development and early asymmetry in mammals. *Cell*, **96**, 195-209.

Brennan, J., Norris, D. P., and Robertson, Elizabeth J (2002). Nodal activity in the node governs left-right asymmetry. *Genes & development*, **16**, 2339-44.

Brown, E. J. and Baltimore, D. (2000). ATR disruption leads to chromosomal fragmentation and early embryonic lethality. *Genes & Dev.*, **14**, 397-402.

Budzowska, M., Jaspers, I., Essers, J., de Waard, H., van Drunen, E., Hanada, K., Beverloo, B., Hendriks, R. W., de Klein, A., Kanaar, R., et al. (2004). Mutation of the mouse Rad17 gene leads to embryonic lethality and reveals a role in DNA damage-dependent recombination. *The EMBO journal*, **23**, 3548-58.

Buis, J., Wu, Y., Deng, Y., Leddon, J., Westfield, G., Eckersdorff, M., Sekiguchi, J. M., Chang, S., and Ferguson, D. O. (2008). Mre11 nuclease activity has essential roles in DNA repair and genomic stability distinct from ATM activation. *Cell*, **135**, 85-96.

Burholt, D. R. (1986). Oesophageal epithelial cell proliferation and food consumption patterns following irradiation. *The British journal of cancer. Supplement*, **7**, 7-8.

Chen, M. S., Hurov, J., White, L. S., Woodford-Thomas, T., and Piwnica-Worms, H. (2001). Absence of apparent phenotype in mice lacking Cdc25C protein phosphatase. *Molecular and cellular biology*, **21**, 3853-61.

Ciemerych, M. A. and Sicinski, P. (2005). Cell cycle in mouse development. *Oncogene*, **24**, 2877-98.

Ciosk, R., Zachariae, W., Michaelis, C., Shevchenko, A., Mann, M., and Nasmyth, K (1998). An ESP1/PDS1 complex regulates loss of sister chromatid cohesion at the metaphase to anaphase transition in yeast. *Cell*, **93**, 1067-76.

Collignon J., V. I. and Robertson, E J (1996). Relationship Between Asymmetric nodal Expression and the Direction of Embryonic Turning. *Nature*, **381**, 155-158.

Colognato, H. and Yurchenco, P. D. (2000). Form and function: the laminin family of heterotrimers. *Developmental dynamics : an official publication of the American Association of Anatomists*, **218**, 213-34.

Cota, C. D., Bagher, P., Pelc, P., Smith, C. O., Bodner, C. R., and Gunn, Teresa M (2006). Mice with mutations in Mahogunin ring finger-1 (Mgrn1) exhibit abnormal patterning of the left-right axis. *Developmental dynamics : an official publication of the American Association of Anatomists*, **235**, 3438-47.

Cutts, S. M. (1999). Defective chromosome segregation, microtubule bundling and nuclear bridging in inner centromere protein gene (Incenp)-disrupted mice. *Human Molecular Genetics*, **8**, 1145-1155.

Dallas, S. L., Sivakumar, P., Jones, C. J. P., Chen, Q., Peters, D. M., Mosher, D. F., Humphries, M. J., and Kielty, C. M. (2005). Fibronectin regulates latent transforming growth factor-beta (TGF beta) by controlling matrix assembly of latent TGF beta-binding protein-1. *The Journal of biological chemistry*, **280**, 18871-80.

Dobles, M., Liberal, V., Scott, M. L., Benezra, R, and Sorger, P. K. (2000). Chromosome missegregation and apoptosis in mice lacking the mitotic checkpoint protein Mad2. *Cell*, **101**, 635-45.

Donehower, L A, Harvey, M., Slagle, B. L., McArthur, M. J., Montgomery, C. A., Butel, J. S., and Bradley, A (1992). Mice deficient for p53 are developmentally normal but susceptible to spontaneous tumours. *Nature*, **356**, 215-21.

Durbeej, M. (2010). Laminins. *Cell and tissue research*, **339**, 259-68.

Edelmann, W, Cohen, P E, Kane, M., Lau, K, Morrow, B., Bennett, S., Umar, a, Kunkel, T, Cattoretti, G., Chaganti, R., et al. (1996). Meiotic pachytene arrest in MLH1-deficient mice. *Cell*, **85**, 1125-34.

Edelmann, Winfried, Yang, K., Umar, A., Heyer, J., Lau, Kirkland, Fan, K., Liedtke, W., Cohen, Paula E, Kane, Michael F, Lipford, J. R., et al. (1997). Mutation in the mismatch repair gene Msh6 causes cancer susceptibility. *Cell*, **91**, 467-77.

Farina, A., Shin, J.-H., Kim, D.-H., Bermudez, V. P., Kelman, Z., Seo, Y.-S., and Hurwitz, J. (2008). Studies with the human cohesin establishment factor, ChlR1. Association of ChlR1 with Ctf18-RFC and Fen1. *The Journal of biological chemistry*, **283**, 20925-36.

Fernández-Miranda, G., Trakala, M., Martín, J., Escobar, B., González, A., Ghyselinck, N. B., Ortega, S., Cañamero, M., Pérez de Castro, I., and Malumbres, M. (2011). Genetic disruption of aurora B uncovers an essential role for aurora C during early mammalian development. *Development (Cambridge, England)*, **138**, 2661-72.

Furuta, Y., Ilić, D., Kanazawa, S., Takeda, N., Yamamoto, T., and Aizawa, S. (1995). Mesodermal defect in late phase of gastrulation by a targeted mutation of focal adhesion kinase, FAK. *Oncogene*, **11**, 1989-95.

George, E. L. (1993). Defects in mesoderm, neural tube and vascular development in mouse embryos lacking fibronectin. *Development*, **119**, 1079-1091.

Goh, K. L., Yang, J. T., and Hynes, R O (1997). Mesodermal defects and cranial neural crest apoptosis in alpha5 integrin-null embryos. *Development (Cambridge, England)*, **124**, 4309-19.

He, L, Gunn, T M, Bouley, D. M., Lu, X. Y., Watson, S J, Schlossman, S. F., Duke-Cohan, J. S., and Barsh, G S (2001). A biochemical function for attractin in agouti-induced pigmentation and obesity. *Nature genetics*, **27**, 40-47.

He, Lin, Lu, X.-Y. Y., Jolly, A. F., Eldridge, A. G., Watson, Stanley J, Jackson, P. K., Barsh, Gregory S, Gunn, Teresa M, and He L Lu XY, J. A. F. E. A. G. W. S. J. J. P. K. B. G. S. G. T. M. (2003). Spongiform degeneration in mahoganoid mutant mice. *Science (New York, N.Y.)*, **299**, 710-2.

Heyer, B. S., MacAuley, A., Behrendtsen, O., and Werb, Zena (2000). Hypersensitivity to DNA damage leads to increased apoptosis during early mouse development. *Genes & development*, **14**, 2072-84.

Hirao, A., Cheung, A., Duncan, G., Girard, P.-M., Elia, A. J., Wakeham, A., Okada, H., Sarkissian, T., Wong, J. A., Sakai, T., et al. (2002). Chk2 Is a Tumor Suppressor That Regulates Apoptosis in both an Ataxia Telangiectasia Mutated (ATM)-Dependent and an ATM-Independent Manner. *Molecular and Cellular Biology*, **22**, 6521-6532.

Hopkins, K. M., Auerbach, W., Wang, X. Y., Hande, M. P., Hang, H., Wolgemuth, D. J., Joyner, A. L., and Lieberman, H. B. (2004). Deletion of mouse rad9 causes abnormal cellular responses to DNA damage, genomic instability, and embryonic lethality. *Molecular and cellular biology*, **24**, 7235-48.

Hornig, N. C. D., Knowles, P. P., McDonald, N. Q., and Uhlmann, F. (2002). The dual mechanism of separase regulation by securin. *Current biology : CB*, **12**, 973-82.

van der Horst, Gijsbertus T.J, van Steeg, H., Berg, R. J. ., van Gool, A. J., de Wit, J., Weeda, G., Morreau, H., Beems, Rudolf B, van Kreijl, C. F., de Gruijl, F. R., et al. (1997). Defective Transcription-Coupled Repair in Cockayne Syndrome B Mice Is Associated with Skin Cancer Predisposition. *Cell*, **89**, 425-435.

van der Horst, Gijsbertus T J, Meira, L., Gorgels, Theo G M F, de Wit, J., Velasco-Miguel, S., Richardson, J. A., Kamp, Y., Vreeswijk, M. P. G., Smit, B., Bootsma, D., et al. (2002). UVB radiation-induced cancer predisposition in Cockayne syndrome group A (Csa) mutant mice. *DNA repair*, **1**, 143-57.

Huang, Xingxu, Hatcher, R., York, J. P., and Zhang, P. (2005). Securin and separase phosphorylation act redundantly to maintain sister chromatid cohesion in mammalian cells. *Molecular biology of the cell*, **16**, 4725-32.

Ilić, D., Furuta, Y., Kanazawa, S., Takeda, N., Sobue, K., Nakatsuji, N., Nomura, S., Fujimoto, J., Okada, M., and Yamamoto, T. (1995). Reduced cell motility and enhanced focal adhesion contact formation in cells from FAK-deficient mice. *Nature*, **377**, 539-44.

Inoue, A., Li, T., Roby, S. K., Valentine, M. B., Inoue, M., Boyd, K., Kidd, V. J., and Lahti, J. M. (2007). Loss of ChlR1 helicase in mouse causes lethality due to the accumulation of aneuploid cells generated by cohesion defects and placental malformation. *Cell cycle Georgetown Tex*, **6**, 1646-1654.

Iwanaga, Y., Chi, Y.-H., Miyazato, A., Sheleg, S., Haller, K., Peloponese, J.-M., Li, Y., Ward, J. M., Benezra, Robert, and Jeang, K.-T. (2007). Heterozygous deletion of mitotic arrest-deficient protein 1 (MAD1) increases the incidence of tumors in mice. *Cancer research*, **67**, 160-6.

Jeganathan, K., Malureanu, L., Baker, D. J., Abraham, S. C., and van Deursen, J. M. (2007). Bub1 mediates cell death in response to chromosome missegregation and acts to suppress spontaneous tumorigenesis. *The Journal of cell biology*, **179**, 255-67.

Jeon, Y., Ko, E., Lee, K. Y., Ko, M. J., Park, S. Y., Kang, J., Jeon, C. H., Lee, H., and Hwang, D. S. (2011). TopBP1 deficiency causes an early embryonic lethality and induces cellular senescence in primary cells. *The Journal of biological chemistry*, **286**, 5414-22.

Jiao, J., Kim, H. Y., Liu, R. R., Hogan, C. A., Sun, K., Tam, L. M., and Gunn, Teresa M (2009). Transgenic analysis of the physiological functions of Mahogunin Ring Finger-1 isoforms. *Genesis (New York, N.Y. : 2000)*, **47**, 524-34.

Kalitsis, P., Earle, E., Fowler, K J, and Choo, K. H. (2000). Bub3 gene disruption in mice reveals essential mitotic spindle checkpoint function during early embryogenesis. *Genes & development*, **14**, 2277-82.

Kitisin, K., Saha, T., Blake, T., Golestaneh, N., Deng, M., Kim, C., Tang, Y., Shetty, K., Mishra, B., and Mishra, L. (2007). Tgf-Beta signaling in development. *Science's STKE : signal transduction knowledge environment*, **2007**, cm1.

Klinghoffer, R. A., Sachsenmaier, C., Cooper, J. A., and Soriano, P. (1999). Src family kinases are required for integrin but not PDGFR signal transduction. *The EMBO journal*, **18**, 2459-71.

Kneitz, B., Cohen, P E, Avdievich, E., Zhu, L., Kane, M F, Hou, H., Kolodner, R. D., Kucherlapati, R, Pollard, J W, and Edelmann, W (2000). MutS homolog 4 localization to meiotic chromosomes is required for chromosome pairing during meiosis in male and female mice. *Genes & development*, **14**, 1085-97.

Kumada, K., Yao, R., Kawaguchi, T., Karasawa, M., Hoshikawa, Y., Ichikawa, K., Sugitani, Y., Imoto, I., Inazawa, J., Sugawara, M., et al. (2006). The selective continued linkage of centromeres from mitosis to interphase in the absence of mammalian separase. *The Journal of cell biology*, **172**, 835-46.

Lane, P. W. (1960). New Mutants. *Mouse News Letter*, **22**, 35.

Larsen, E., Gran, C., Saether, B. E., Seeberg, E., and Klungland, A. (2003). Proliferation Failure and Gamma Radiation Sensitivity of Fen1 Null Mutant Mice at the Blastocyst Stage. *Molecular and Cellular Biology*, **23**, 5346-5353.

Lawson, K. a, Meneses, J. J., and Pedersen, R. a (1991). Clonal analysis of epiblast fate during germ layer formation in the mouse embryo. *Development (Cambridge, England)*, **113**, 891-911.

Lehrer, M. S., Sun, T. T., and Lavker, R. M. (1998). Strategies of epithelial repair: modulation of stem cell and transit amplifying cell proliferation. *Journal of cell science*, **111 (Pt 1**, 2867-75.

Leiss, M., Beckmann, K., Giros, A., Costell, M., and Fassler, R. (2008). The role of integrin binding sites in fibronectin matrix assembly in vivo. *Current opinion in cell biology*, **20**, 502-507.

Leman, A. R., Noguchi, C., Lee, C. Y., and Noguchi, E. (2010). Human Timeless and Tipin stabilize replication forks and facilitate sister-chromatid cohesion. *Journal of cell science*, **123**, 660-70.

Li, M., York, J. P., and Zhang, P. (2007). Loss of Cdc20 causes a securin-dependent metaphase arrest in two-cell mouse embryos. *Molecular and cellular biology*, **27**, 3481-8.

Liu, C. Y., Flesken-Nikitin, A., Li, S., Zeng, Y., and Lee, W. H. (1996). Inactivation of the mouse Brca1 gene leads to failure in the morphogenesis of the egg cylinder in early postimplantation development. *Genes & development*, **10**, 1835-43.

Liu, Q., Guntuku, S., Cui, X.-S., Matsuoka, S., Cortez, D., Tamai, K., Luo, Guangbin, Carattini-Rivera, S., DeMayo, F., Bradley, Allan, et al. (2000). Chk1 is an essential kinase that is regulated by Atr and required for the G2/M DNA damage checkpoint. *Genes & Dev.*, **14**, 1448-1459.

Liu, S., Calderwood, D. a, and Ginsberg, M. H. (2000). Integrin cytoplasmic domain-binding proteins. *Journal of cell science*, **113 (Pt 2**, 3563-71.

Lou, Z., Minter-Dykhouse, K., Franco, S., Gostissa, M., Rivera, M. A., Celeste, A., Manis, J. P., van Deursen, J., Nussenzweig, A., Paull, T. T., et al. (2006). MDC1 maintains genomic stability by participating in the amplification of ATM-dependent DNA damage signals. *Molecular cell*, **21**, 187-200.

Ludwig, T., Chapman, D. L., Papaioannou, V. E., and Efstratiadis, a (1997). Targeted mutations of breast cancer susceptibility gene homologs in mice: lethal phenotypes of Brca1, Brca2, Brca1/Brca2, Brca1/p53, and Brca2/p53 nullizygous embryos. *Genes & Development*, **11**, 1226-1241.

Luo, G. (1999). Disruption of mRad50 causes embryonic stem cell lethality, abnormal embryonic development, and sensitivity to ionizing radiation. *Proceedings of the National Academy of Sciences*, **96**, 7376-7381.

Mac Auley, a, Werb, Z, and Mirkes, P. E. (1993). Characterization of the unusually rapid cell cycles during rat gastrulation. *Development (Cambridge, England)*, **117**, 873-83.

McGrath, J. and Brueckner, M. (2003). Cilia are at the heart of vertebrate left-right asymmetry. *Current opinion in genetics & development*, **13**, 385-92.

McWhir, J., Selfridge, J., Harrison, D. J., Squires, S., and Melton, D. W. (1993). Mice with DNA repair gene (ERCC-1) deficiency have elevated levels of p53, liver nuclear abnormalities and die before weaning. *Nature genetics*, **5**, 217-24.

Miller, K. A., Gunn, T M, Carrasquillo, M. M., Lamoreux, M. L., Galbraith, D. B., and Barsh, G S (1997). Genetic studies of the mouse mutations mahogany and mahoganoid. *Genetics*, **146**, 1407-15.

Mitra, S. K., Hanson, D. A., and Schlaepfer, David D (2005). Focal adhesion kinase: in command and control of cell motility. *Nature reviews. Molecular cell biology*, **6**, 56-68.

Mu, D., Cambier, S., Fjellbirkeland, L., Baron, J. L., Munger, J. S., Kawakatsu, H., Sheppard, D., Broaddus, V. C., and Nishimura, S. L. (2002). The integrin alpha(v)beta8

mediates epithelial homeostasis through MT1-MMP-dependent activation of TGF-beta1. *The Journal of cell biology*, **157**, 493-507.

Munger, J. S., Huang, Xiaozhu, Kawakatsu, H., Griffiths, M. J., Dalton, S. L., Wu, J., Pittet, J. F., Kaminski, N., Garat, C., Matthay, M. A., et al. (1999). The integrin alpha v beta 6 binds and activates latent TGF beta 1: a mechanism for regulating pulmonary inflammation and fibrosis. *Cell*, **96**, 319-28.

Musacchio, A. and Salmon, E. D. (2007). The spindle-assembly checkpoint in space and time. *Nature reviews. Molecular cell biology*, **8**, 379-93.

Ng, J. M. Y., Vrieling, H., Sugasawa, K., Ooms, M. P., Grootegoed, J. A., Vreeburg, J. T. M., Visser, P., Beems, R. B., Gorgels, T. G. M. F., Hanaoka, F., et al. (2002). Developmental Defects and Male Sterility in Mice Lacking the Ubiquitin-Like DNA Repair Gene mHR23B. *Molecular and Cellular Biology*, **22**, 1233-1245.

Nonaka, S, Tanaka, Y, Okada, Y, Takeda, S., Harada, A., Kanai, Y., Kido, M., and Hirokawa, N (1998). Randomization of left-right asymmetry due to loss of nodal cilia generating leftward flow of extraembryonic fluid in mice lacking KIF3B motor protein. *Cell*, **95**, 829-37.

Nonaka, Shigenori, Shiratori, H., Saijoh, Y., and Hamada, H. (2002). Determination of left-right patterning of the mouse embryo by artificial nodal flow. *Nature*, **418**, 96-9.

Nowotschin, S. and Hadjantonakis, A.-K. (2010). Cellular dynamics in the early mouse embryo: from axis formation to gastrulation. *Current opinion in genetics & development*, **20**, 420-7.

Okada, Yasushi, Nonaka, Shigenori, Tanaka, Yosuke, Saijoh, Y., Hamada, H., and Hirokawa, Nobutaka (1999). Abnormal nodal flow precedes situs inversus in iv and inv mice. *Molecular cell*, **4**, 459-68.

Pachkowski, B. F., Guyton, K. Z., and Sonawane, B. (2011). DNA repair during in utero development: a review of the current state of knowledge, research needs, and potential application in risk assessment. *Mutation research*, **728**, 35-46.

Parameswaran, M. and Tam, P. P. (1995). Regionalisation of cell fate and morphogenetic movement of the mesoderm during mouse gastrulation. *Developmental genetics*, **17**, 16-28.

Pardee, a B. (1989). G1 events and regulation of cell proliferation. *Science (New York, N.Y.)*, **246**, 603-8.

Parish, J. L., Rosa, J., Wang, X., Lahti, J. M., Doxsey, S. J., and Androphy, E. J. (2006). The DNA helicase ChlR1 is required for sister chromatid cohesion in mammalian cells. *Journal of cell science*, **119**, 4857-65.

Phillips, R. J. (1963). New Mutant: non-agouti curly. *Mouse News Letter*, **29**, 38.

Phillips, R. J. (1971). Non-agouti curly (nc). *Mouse News Letter*, **45**, 25.

Poelmann, R. E. (1980). Differential mitosis and degeneration patterns in relation to the alterations in the shape of the embryonic ectoderm of early post-implantation mouse embryos. *Journal of embryology and experimental morphology*, **55**, 33-51.

Poelmann, R. E. (1981). The formation of the embryonic mesoderm in the early post-implantation mouse embryo. *Anatomy and Embryology*, **162**, 29-40.

Power, M. A. and Tam, P. (1993). Onset of gastrulation, morphogenesis and somitogenesis in mouse embryos displaying compensatory growth. *Anatomy and embryology*, **187**, 493–504.

Prolla, T. A., Baker, S. M., Harris, A. C., Tsao, J. L., Yao, X., Bronner, C. E., Zheng, B., Gordon, M., Reneker, J., Arnheim, N., et al. (1998). Tumour susceptibility and spontaneous mutation in mice deficient in Mlh1, Pms1 and Pms2 DNA mismatch repair. *Nature genetics*, **18**, 276-9.

Reissmann, E., Jörnvall, H., Blokzijl, A., Andersson, O., Chang, C., Minchiotti, G., Persico, M. G., Ibáñez, C. F., and Brivanlou, A. H. (2001). The orphan receptor ALK7 and the Activin receptor ALK4 mediate signaling by Nodal proteins during vertebrate development. *Genes & development*, **15**, 2010-22.

Rossant, J. and Tam, P. P. L. (2004). Emerging asymmetry and embryonic patterning in early mouse development. *Developmental cell*, **7**, 155-64.

Sancar, A., Lindsey-Boltz, L. a, Unsal-Kaçmaz, K., and Linn, S. (2004). Molecular mechanisms of mammalian DNA repair and the DNA damage checkpoints. *Annual review of biochemistry*, **73**, 39-85.

Santamaría, D., Barrière, C., Cerqueira, A., Hunt, S., Tardy, C., Newton, K., Cáceres, J. F., Dubus, P., Malumbres, M., and Barbacid, M. (2007). Cdk1 is sufficient to drive the mammalian cell cycle. *Nature*, **448**, 811-5.

Schlaepfer, D D and Hunter, T. (1997). Focal adhesion kinase overexpression enhances ras-dependent integrin signaling to ERK2/mitogen-activated protein kinase through interactions with and activation of c-Src. *The Journal of biological chemistry*, **272**, 13189-95.

Shen, Michael M (2007). Nodal signaling: developmental roles and regulation. *Development (Cambridge, England)*, **134**, 1023-34.

Sherwood, R., Takahashi, T. S., and Jallepalli, P. V. (2010). Sister acts: coordinating DNA replication and cohesion establishment. *Genes & development*, **24**, 2723-31.

Shiratori, H. and Hamada, H. (2006). The left-right axis in the mouse: from origin to morphology. *Development (Cambridge, England)*, **133**, 2095-104.

Smyth, N., Vatansever, H. S., Murray, P., Meyer, M., Frie, C., Paulsson, M., and Edgar, D. (1999). Absence of basement membranes after targeting the LAMC1 gene results in

embryonic lethality due to failure of endoderm differentiation. *The Journal of cell biology*, **144**, 151-60.

Snow, M. (1977). Gastrulation in the mouse: growth and regionalization of the epiblast. *Journal of Embryology and Experimental*, **42**, 293-303.

Sonoda, Y., Matsumoto, Y., Funakoshi, M., Yamamoto, D., Hanks, S. K., and Kasahara, T. (2000). Anti-apoptotic role of focal adhesion kinase (FAK). Induction of inhibitor-of-apoptosis proteins and apoptosis suppression by the overexpression of FAK in a human leukemic cell line, HL-60. *The Journal of biological chemistry*, **275**, 16309-15.

Tabin, C. J. and Vogan, K. J. (2003). A two-cilia model for vertebrate left-right axis specification. *Genes & development*, **17**, 1-6.

Tachibana-Konwalski, K., Godwin, J., van der Weyden, L., Champion, L., Kudo, N. R., Adams, D. J., and Nasmyth, Kim (2010). Rec8-containing cohesin maintains bivalents without turnover during the growing phase of mouse oocytes. *Genes & development*, **24**, 2505-16.

Takai, H., Tominaga, K., Motoyama, N., Minamishima, Y. A., Nagahama, H., Tsukiyama, T., Ikeda, K., Nakayama, K., Nakanishi, M., and Nakayama, K.-ichi (2000). Aberrant cell cycle checkpoint function and early embryonic death in Chk1-/- mice. *Genes & Dev.*, **14**, 1439-1447.

Takeda, S., Yonekawa, Y., Tanaka, Y, Okada, Y, Nonaka, S, and Hirokawa, N (1999). Left-right asymmetry and kinesin superfamily protein KIF3A: new insights in determination of laterality and mesoderm induction by kif3A-/- mice analysis. *The Journal of cell biology*, **145**, 825-36.

Tam, P. P. (1988). Postimplantation development of mitomycin C-treated mouse blastocysts. *Teratology*, **37**, 205-12.

Tam, P. P. L., Loebel, D. a F., and Tanaka, S. S. (2006). Building the mouse gastrula: signals, asymmetry and lineages. *Current opinion in genetics & development*, **16**, 419-25.

Tam, P. P. and Beddington, R. S. (1987). The formation of mesodermal tissues in the mouse embryo during gastrulation and early organogenesis. *Development (Cambridge, England)*, **99**, 109-26.

Tam, P. P. and Behringer, R R (1997). Mouse gastrulation: the formation of a mammalian body plan. *Mechanisms of development*, **68**, 3-25.

Tanaka, Yosuke, Okada, Yasushi, and Hirokawa, Nobutaka (2005). FGF-induced vesicular release of Sonic hedgehog and retinoic acid in leftward nodal flow is critical for left-right determination. *Nature*, **435**, 172-7.

Tebbs, R. S., Flannery, M. L., Meneses, J. J., Hartmann, A., Tucker, J. D., Thompson, L. H., Cleaver, J. E., and Pedersen, R. A. (1999). Requirement for the Xrcc1 DNA base excision repair gene during early mouse development. *Developmental biology*, **208**, 513-29.

Uchimura, A., Hidaka, Y., Hirabayashi, T., Hirabayashi, M., and Yagi, T. (2009). DNA polymerase delta is required for early mammalian embryogenesis. *PloS one*, **4**, e4184.

Uhlmann, F. (2009). A matter of choice: the establishment of sister chromatid cohesion. *EMBO reports*, **10**, 1095-102.

Uren, A. G., Wong, L., Pakusch, M., Fowler, Kerry J., Burrows, F. J., Vaux, D. L., and Choo, K. H. A. (2000). Survivin and the inner centromere protein INCENP show similar cell-cycle localization and gene knockout phenotype. *Current Biology*, **10**, 1319-1328.

de Vries, S. S., Baart, E. B., Dekker, M., Siezen, A., de Rooij, D. G., de Boer, P., and te Riele, H. (1999). Mouse MutS-like protein Msh5 is required for proper chromosome synapsis in male and female meiosis. *Genes & Development*, **13**, 523-531.

Walker, W. P. and Gunn, Teresa M (2010). Piecing together the pigment-type switching puzzle. *Pigment cell & melanoma research*, **23**, 4-6.

Wang, Q., Liu, T., Fang, Y., Xie, S., Huang, Xuan, Mahmood, R., Ramaswamy, G., Sakamoto, K. M., Darzynkiewicz, Z., Xu, M., et al. (2004). BUBR1 deficiency results in abnormal megakaryopoiesis. *Blood*, **103**, 1278-85.

Ward, I. M., Minn, K., van Deursen, J., and Chen, J. (2003). p53 Binding protein 53BP1 is required for DNA damage responses and tumor suppression in mice. *Molecular and cellular biology*, **23**, 2556-63.

Weiss, R. S., Enoch, T., and Leder, P. (2000). Inactivation of mouse Hus1 results in genomic instability and impaired responses to genotoxic stress. *Genes & Dev.*, **14**, 1886-1898.

Wierzbicka-Patynowski, I. and Schwarzbauer, J. E. (2003). The ins and outs of fibronectin matrix assembly. *Journal of cell science*, **116**, 3269-76.

de Wind, N., Dekker, M., Berns, A., Radman, M., and te Riele, H. (1995). Inactivation of the mouse Msh2 gene results in mismatch repair deficiency, methylation tolerance, hyperrecombination, and predisposition to cancer. *Cell*, **82**, 321-30.

Wirth, K. G., Ricci, R., Giménez-Abián, J. F., Taghybeeglu, S., Kudo, N. R., Jochum, W., Vasseur-Cognet, M., and Nasmyth, Kim (2004). Loss of the anaphase-promoting complex in quiescent cells causes unscheduled hepatocyte proliferation. *Genes & development*, **18**, 88-98.

Xanthoudakis, S., Smeyne, R. J., Wallace, J. D., and Curran, T. (1996). The redox/DNA repair protein, Ref-1, is essential for early embryonic development in mice. *Proceedings of the National Academy of Sciences of the United States of America*, **93**, 8919-23.

Yamamoto, M., Saijoh, Y., Perea-Gomez, A., Shawlot, W., Behringer, Richard R, Ang, S.-L., Hamada, H., and Meno, C. (2004). Nodal antagonists regulate formation of the anteroposterior axis of the mouse embryo. *Nature*, **428**, 387-92.

Yan, Y.-T., Liu, J.-J., Luo, Y., E, C., Haltiwanger, R. S., Abate-Shen, C., and Shen, M. M. (2002). Dual Roles of Cripto as a Ligand and Coreceptor in the Nodal Signaling Pathway. *Molecular and Cellular Biology*, **22**, 4439-4449.

Yang, J. T., Bader, B L, Kreidberg, J. A., Ullman-Culleré, M., Trevithick, J. E., and Hynes, R O (1999). Overlapping and Independent Functions of Fibronectin Receptor Integrins in Early Mesodermal Development. *Developmental biology*, **215**, 264-277.

Yang, J. T., Rayburn, H, and Hynes, R O (1993). Embryonic mesodermal defects in alpha 5 integrin-deficient mice. *Development (Cambridge, England)*, **119**, 1093-105.

Yang, Z., Mu, Z., Dabovic, B., Jurukovski, V., Yu, D., Sung, J., Xiong, X., and Munger, J. S. (2007). Absence of integrin-mediated TGFbeta1 activation in vivo recapitulates the phenotype of TGFbeta1-null mice. *The Journal of cell biology*, **176**, 787-93.

Zhu, J., Petersen, S., Tessarollo, L., and Nussenzweig, A. (2001). Targeted disruption of the Nijmegen breakage syndrome gene NBS1 leads to early embryonic lethality in mice. *Current Biology*, **11**, 105-109.

Chapter 2

The *cetus* ENU-induced mutation in the mouse DNA helicase Ddx11 reveals an essential role of its motif V for embryonic development

ABSTRACT

DDX11 (DEAD/H (Asp-Glu-Ala-Asp/His)-box polypeptide 11) is a member of the highly conserved FANCJ family of Superfamily 2 (SF2) DNA helicases. Studies in yeast and human cells have demonstrated an involvement of DDX11 in sister chromatid cohesion, cell cycle progression and genome stability. In mouse, loss of DDX11 has been previously shown to result in embryonic lethality. However, the developmental defects that lead to embryonic death in mice lacking *Ddx11* are still poorly understood. Here we describe the phenotypic characterization and positional cloning of *cetus*, a mouse ENU-induced mutation that disrupts *Ddx11*. Homozygous *cetus* mutant embryos are small, display shortening of the anterior-posterior axis and fail to thrive beyond E8.5. Analysis of cell-type specific gene expression by *in situ* hybridization showed a specific reduction in paraxial mesoderm structures in *cetus* mutant embryos including somites. Positional cloning of *cetus* revealed a non-synonymous point mutation in the sequence encoding motif V of DDX11. The *cetus* mutation failed to complement a null allele of *Ddx11*, indicating that the point mutation in motif V completely disrupts DDX11 function. Together these results indicate a role for *Ddx11* in early development of the mouse embryo and a essential role for motif V in mediating DDX11 function.

.

INTRODUCTION

Initially identified in genetic screens for mating type switching and chromosome transmission fidelity in *saccharomyces cerevisiae*, *Ddx11* (*Chl1* ,yeast) has been found to aid in the proper segregation of sister chromatids (Liras et al., 1978; F Spencer et al., 1990). Sister chromatid cohesion ensures the proper segregation of chromosomes during mitosis and is facilitated by a number of proteins collectively known as the cohesin complex. In mammals, the cohesin complex contains two structural maintenance of chromosomes proteins (SMC1 and SMC3) as well as a sister chromatid cohesion subunit (SCC3) and a single α-kleisin protein, SCC1 (RAD21) (Ciemerych and Sicinski, 2005; Razqallah Hakem, 2008). In human cells, physical interactions have been identified between DDX11 and components of the cohesin complex, SCC1, SMC1 and SMC3 (Parish et al., 2006) as well as the cohesion establishment factor Ctf18-RFC and the endonuclease, FEN1 (Farina et al., 2008). These interactions indicate a role for DDX11 in the establishment of cohesion (for a recent review see Sherwood et al., 2010).

Loss of *Ddx11* both in yeast (S. L. L. Gerring et al., 1990) and mouse (A. Inoue et al., 2007) has been shown to result in a G2/M cell cycle delay. In human cells, RNAi knockdown of *Ddx11* results in prometaphase arrest, mitotic failure and aneuploidy (Parish et al., 2006). Furthermore, mutations in members of this family of proteins that also includes the ERCC2 (Excision Repair Cross-Complementation Group 2), FANCJ (Fanconi Anemia Group J) and RTEL1 (Regulator of Telomere Length 1) have been identified in a number of human diseases. These include Fanconi anemia (MIM 609054), xeroderma pigmentosum (MIM 278730) and cerebro-oculo-facio-skeletal syndrome (MIM 610756). Recently, mutations in *hDdx11* were found to be the genetic defect in a patient with Warsaw Breakage Syndrome (WBS, MIM 613398), a human cohesinopathy characterized by hypersensitivity to DNA damaging agents and defects in sister chromatid segregation resulting in severe developmental defects (van der Lelij et

al., 2010).

The importance of *Ddx11* during development has been further highlighted by the recent generation of a targeted *Ddx11* knockout in the mouse ($Ddx11^{KO}$, also referred to as $ChlR1^{KO}$). These mice develop post-implantation with defects in cell cycle progression and apoptosis. Death of $Ddx11^{KO}$ embryos has been attributed to a failure to form placental structures (A. Inoue et al., 2007). However, the embryonic defects in these mutants remain poorly understood. Additionally, while the biochemical activity of DDX11 is well established (Hirota and J M Lahti, 2000; Farina et al., 2008; Yuliang Wu et al., 2012), comparatively little is known regarding how individual motifs contribute to DDX11 activity (reviewed by Fairman-Williams et al., 2010).

Here we describe the identification and characterization of *cetus*, a novel *N-ethyl-N-nitrosourea* (ENU)-induced allele of *Ddx11*. Positional cloning and genetic complementation analysis of *cetus* revealed a mutation in DDX11 helicase motif V that generates a null allele. $Ddx11^{cetus}$ mutant embryos display shortening of the anterior-posterior axis and a loss of mesodermal structures including somites. We have found that both $Ddx11^{cetus}$ and $Ddx11^{KO}$ embryos display widespread cell death during gastrulation. These cellular defects precede the gross morphological abnormalities in the mutant embryos and result in embryonic death by mid gestation. In contrast to mutations in the motif V of other SF2 helicases, which have been shown to disrupt ATP hydrolysis or DNA binding, no defect was detected in the ATP hydrolysis or DNA binding activities of the $DDX11^{cetus}$ mutant protein. Together, these results demonstrate a specific role for *Ddx11* during early development of the mouse embryo and that motif V is essential for DDX11 function.

MATERIALS AND METHODS

Positional cloning and sequencing of *cetus*

The *cetus* mutation was generated by ENU-mutagenesis as described previously (Garcia-Garcia et al., 2005; Kasarskis et al., 1998). Mapping with polymorphic MIT (www.informatics.jax.org) and SKI (http://mouse.ski.mskcc.org) SSLP markers indicated linkage to distal mouse chromosome 17. Additional markers were generated from genome sequence data with the etandem EMBOSS software (http://bioweb2.pasteur.fr/docs/EMBOSS/etandem.html) for high-resolution refinement of the candidate interval. Primer sequences for these novel Simple Sequence Length Polymorphic (SSLP markers are specified below (Table 2.1). cDNAs of all annotated genes (www.ensembl.org) in the *cetus* candidate interval (*E13009J12Rik, VapA, Txndc2, Rab31,Ppp4r1, Ralbp1, Twsg1, Ankrd12, Ndufv2, Orf19* and *Ddx11*) were amplified by RT-PCR (Superscript One-Step RT-PCR, Invitrogen) using RNA from E8.5 *cetus* and C57BL/6J (control) embryos extracted using RNA-STAT (Tel-Test). Amplification products were sequenced at the Cornell University Life Sciences Core Laboratory Center (CLC). A single T to C mutation was identified at amino acid 2228 of the *Ddx11* ORF. This point mutation generated a *BseR*I restriction fragment length polymorphism that was assayed for by digestion of PCR products generated from amplification of genomic DNA.

Mouse (mus musculus) strains

Ddx11^{cetus} was analyzed in CAST/Ei and C3H/FeJ genetic backgrounds and genotyped with D17CU33 and D17CU40 or D17CU35 and D17CU39 SSLP markers respectively (Table 2.1). *Ddx11*^{KO} were obtained from Dr Jill Lahti (A. Inoue et al., 2007) and backcrossed to C3H/FeJ.

Table 2.1. SSLP Primers

Name	Sequence
D17CU33L	5'-ACACAGGAGAACGGAATGGA-3'
D17CU33R	5'-TTTTTAGGTGAGTTAGCCCAACA-3'
D17CU35L	5'-TGCGTTCAGCTTACAGAGGA-3'
D17CU35R	5'-CAATCATTTCTATCAGTTGACATGG-3'
D17CU39L	5'-GCCACTCCATTACCACACG-3'
D17CU39R	5'-GGATTCAGGGGAGTCCATTT-3'
D17CU40L	5'-CTCCCTCTGCTTCCAAAGTG-3'
D17CU40R	5'-AATGCAGCTCCAGGACATCT-3'
D17CU38L	5'-TCAGTGACACAGGCACTTCC-3'
D17CU38R	5'-TGGCCTTTTGTCTCCTCATT-3'
D17CU41L	5'-TCCTCTCACACATAAATTGAGCA-3'
D17CU41R	5'-AGAGCTCTTACCGCATTGGT-3'
D17CU44L	5'-TGTACAGCATTTGGCAGAGC-3'
D17CU44R	5'-AAGCACAGAGGATGCCACTC-3'
D17CU45L	5'-GGTGTGAGTCAGCGGAAAAG-3'
D17CU45R	5'-GTCCCCAAAGACGGAGATTA-3'
D17CU39L	5'-GCCACTCCATTACCACACG-3'
D17CU39R	5'-GGATTCAGGGGAGTCCATTT-3'
D17CU29L	5'-TGACCTAACTGGCTCGCTCT-3'
D17CU29R	5'-GGTGGGAGAGAAAATGGACA-3'
D17CU47L	5'-AAGCCCCAAATGGTTTGTTT-3'
D17CU47R	5'-CATGGCAACTACAGGGAAGAA-3'
D17CU48L	5'-TCCTCCCTCATGAGTCTTGC-3'
D17CU48R	5'-AGGCTCAGTCATCTGCCAAA-3'
D17CU49L	5'-CAAATTCCTTAGGGTGTCAAGC-3'
D17CU49R	5'-GAAAGCCTAGCACTCCAGCA-3'
D17CU51L	5'-CCCAGTGTCCAGGACCAATA-3'
D17CU51R	5'-ACTGGTTATGCCCCATCAAA-3'

Analysis of Mutant embryos

Embryos were dissected in PBS containing 0.4% BSA at different stages as indicated. Whole-mount RNA in situ hybridization was performed as described (Belo et al., 1997). For phospho-histone-H3 immunohistochemistry and TUNEL, e7.5 embryos were cryosectioned at 10μm as previously described (García-García and Kathryn V Anderson, 2003). All comparisons of wild type and mutant embryos are at the same magnification unless otherwise noted. Anti-phospho-histone H3 (Ser10) (Upstate) was used at 1/250. TUNEL was performed using the ApopTag Detection Kit (Chemicon). As positive controls for TUNEL, sections were treated with DNAse I. Extra-embryonic tissue was removed prior to embedding and used for genotyping with primers 5'- GAGTCCACTGCCTCTGGAAG-3' and 5'-CTAGGTCGACGGTTATACCAGACTTGGGTGTG-3'.

Protein expression & purification

The coding region of the full length murine *Ddx11* was amplified from cDNA isolated from e10.5 C57BL/6J mouse embryos using the primers 5'-CTAGAGATCTATGGCTGACGAAAACCAGGA-3' and 5'-CTAGGTCGACGGTTATACCAGACTTGGGTGTG-3'. The resulting sequence was cloned into the Not1 and SalI sites of the ppSUMO (Navarro et al., 2009). This generated an in frame N-terminal His/SUMO-tagged construct. HIS/SUMO-DDX11^{cetus} and HIS/SUMO-DDX11^{K50R} mutant sequences were generated by site-directed mutagenesis of the wild type vector using the primers 5'-CTGACAGGGGCCTTGCCCCTCTCTGTGGTTGGAG-3'/ 5'-CTCCAACCACAGAGAGGGGCAAGGCCCCTGTCAG-3' and 5'-TCCAACTGGCACGGGAAGGTCCTTAAGTCTGATTTG-3'/ 5'-CAAATCAGACTTAAGGACCTTCCCGTGCCAGTTGGA-3' respectively. All sequences were verified by Sanger sequencing at the Cornell University Life Sciences Laboratories Center.

BL21(DE3) cells were transformed and grown at 37^{o}C overnight in Terrific Broth (TB) with 50 mg/L kanamycin. Expression was induced by the addition of 0.3 mM isopropyl-β-d-1-thiogalactopyranoside (IPTG) when cultures reached an OD_{600} of 0.8. After 3 hours, cells were lysed in Lysis buffer, pH 8.0 (50 mM NaH_2PO_4, 300 mM NaCl, 10 mM Imidazole). Lysates were purified under native conditions by affinity chromatography using Ni^{2+}-nitrilotriacetic acid (NTA) agarose (Protocol 9, The QIAexpressionist, 2003). Eluted fractions were combined and subjected to dialysis overnight at 4^{o}C in storage buffer (50 mM NaH_2PO_4, 300 mM NaCl, 5% glycerol). Dialyzed samples were further concentrated and loaded on a Superdex-200 size exclusion column (GE Healthcare) which had been equilibrated with storage buffer. Fractions were collected, glycerol concentration was adjusted to a final concentration of 10% and purification was verified by SDS-PAGE and western blot.

Western Blot

Proteins were denatured by boiling in an equal volume of 2X Laemmli sample buffer (126 mM Tris-Cl (pH 6.8), 20% glycerol, 4% sodium dodecyl sulfate (SDS), 0.005% Bromophenol Blue, 5% β-mercaptoethanol (BME) or 200 mM Dithiothreitol (DTT)) and separated by SDS-PAGE (4-6% w/v acrylamide). Proteins were transferred to F-polyvinylidene difluoride (PVDF) membranes, blocked in either 5% BSA or non-fat dry milk in Tris-buffered saline (pH 7.6) with 0.1% Tween-20. Primary antibody binding was accomplished by overnight incubation of blots at 4^{o}C in Tris-buffered Saline (pH 7.6) with 0.1% Tween-20 and either 5% BSA or non-fat dry milk. Washes and secondary antibody binding were performed at room temperature in Tris-buffered saline (pH 7.6) with 0.1% Tween-20. Antibodies used included anti-DDX11 (1: 1500, SantaCruz) and anti-Goat HRP (1:5000, SantaCruz). Proteins were detected using an enhanced chemiluminescence (ECL) detection kit (Pierce).

ATP hydrolysis assays

Gel filtration fractions collected for recombinant HIS/SUMO-DDX11^{WT} or mutant proteins were incubated at 37°C in 100 mL reactions containing 5 or 10 μL of the recombinant protein fraction, 25 mM Tris-Cl (pH 7.5), 200 μg/ml bovine serum albumin, 50 mM cold ATP, 3 mM $Mg(CH_3OO)_2$, 2 mM DTT, 45 fmol ssM13mp18 DNA (NEB) and 30 nM [γ^{32}P]ATP (Perkin Elmer) for ≤120 min. Reactions were stopped by the addition of 10 μL of 0.5 mM EDTA. Separation of ADP from ATP was achieved by thin layer chromatography on PEI–cellulose sheets (Merck, Darmstadt, Germany) in 0.6 M K_2HPO_4 (pH 3.4). Plates were dried and exposed to phosphor imaging screens overnight. ATPase activity was determined by quantification of [γ^{32}P]ADP on a STORM 860 PhosphorImager (Amersham Life Sciences, Inc.) using the ImageQuant 5.2 software package.

Gel mobility Shift Assays

Experiments were performed as native polyacrylamide gel electrophoresis assays using [γ^{32}P]ATP (Perkin Elmer) as described (López de Saro and O'Donnell, 2001). Each 50μL reaction contained 25 mM Tris-Cl (pH 7.5), 5% glycerol, 200 μg/ml bovine serum albumin, 25 mM KCl, 2 mM DTT, 100 μg/mL poly-dIdC (Sigma), 25mM $Mg(CH_3OO)_2$, 100 mM ATP and 85 fmol of ^{32}P-labeled substrate (Table 2.2). Recombinant HIS/SUMO-DDX11 wild type or mutant proteins were included as indicated in the figure legends. In some cases, RecQ (Abcam) was used as positive control. Samples were incubated at 37°C for 20 min, and then 20 μl of the reaction was run on a 6% native polyacrylamide gel (6% acrylamide/bisacrylamide 29:1, 0.5 × TBE buffer). Electrophoresis was performed in 0.5 × TBE buffer (45 mM Tris borate, 45 mM boric acid, and 2.5 mM EDTA) at 150 V for 3 hr. Binding affinities (dissociation constants) were calculated as the reciprocal of the protein concentration at which half the available labeled substrate was bound (Hishida et al., 2004).

Table 2.2. DNA substrate oligonucleotides

Name	Sequence	Reference
JEP167 (100nt)	5'-CCATTAGCAAGGCCGGAAACGTCACCAATGCAACGATCAGCCAACTAAACTAGGACATCTTTGCCTTTTTGGCAAAGATGTCCTAGTTTAGTTGGCTGAT-3’	N/A
JEP325 (65nt)	5’-ATCAGCCAACTAAACTAGGACATCTTTGCCTTTTTGGCAAAGATGTCCTAGTTTAGTTGGCTGAT-3’	N/A
NLC710 (30nt)	5’-GGCAAAGATGTCCTAGTTTAGTTGGCTGAT-3’	Peters & Craig, 2001
NLC707 (65nt)	5’-CCATTAGCAAGGCCGGAAACGTCACCAATGCAACGATCAGCCAACTAAACTAGGACATCTTTGCC-3’	Peters & Craig, 2001

RESULTS

Morphogenetic defects in *cetus* mutant embryos

The *cetus* mutation was isolated from an *N-ethyl-N-nitrosourea* (ENU) mutagenesis screen designed to identify recessive lethal mutations that disrupt the overall morphology of the developing embryo (Garcia-Garcia et al., 2005). Homozygous *cetus* mutant embryos implant normally and are morphologically indistinguishable from their wildtype littermates at E6.5. A subset of *cetus* mutant embryos arrest during gastrulation (53.1% on a C3H/HeJ congenic genetic background and 88.9% on a CAST/Ei mixed background) yet many survive the process albeit with widespread morphological defects. *cetus* mutant embryos with late developmental arrest are approximately one third the size of their wild type littermates. These embryos display a shortened anterior-posterior axis and lack distinguishable somites (Figure 2.1). The neural tube epithelium in *cetus* mutants appears distorted and/or wavy and fails to fuse in even the most developmentally advanced embryos, a defect highlighted by analysis of the expression of the gene *Sox2* (Figure 2.1, Figure 2.2I-J). Additionally, many *cetus* mutant embryos have rudimentary headfolds and prominent epithelial blisters on the dorsal surface (Figure 2.1B).

To characterize the developmental defects of *cetus* embryos, I analyzed by *in situ* hybridization the expression of genes expressed in the allantois (*Tbx4*, Chapman et al., 1996), lateral plate mesoderm (*FoxF1*, Mahlapuu et al., 2001), paraxial/somitic mesoderm (*Mox1*, Candia et al., 1992) and axial mesoderm (*brachyury, T*, Wilkinson et al., 1990). *Tbx4* was found to be expressed in *cetus* mutants, but the allantois was found to be disproportionate, rudimentary and/or round in shape (Figure 2.2 A-B &D). The lateral plate mesoderm marker *FoxF1* was expressed normally in *cetus* embryos (Figure 2.2E-F) as shown by whole mount *in situ* hybridization as was the expression of *T* was also normal in these embryos (Figure 2.2G-H). However, analysis of the expression of *Mox1* revealed an extreme reduction in somitic

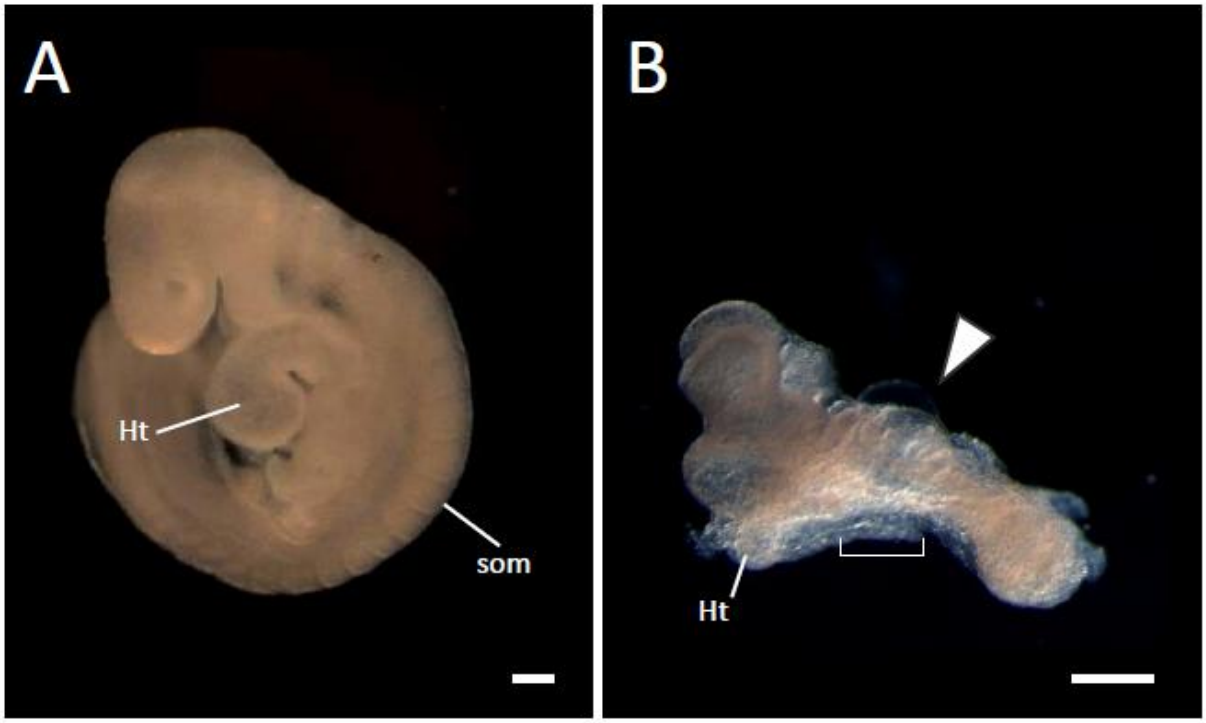

Figure 2.1. Morphologic defects in *cetus* mutants. Lateral views of wild type (A) and *cetus* mutant (B) embryos at E9.5. In the *cetus* mutant the neural epithelium tube remains open and the heart (Ht) fails to loop and remains as a straight tube. Arrowhead in B points to dorsal blisters which are devoid of cells. Bracket in B highlights the absence of discernible somites (som). Scale bars in A and B represents 200μm and 100μm, respectively.

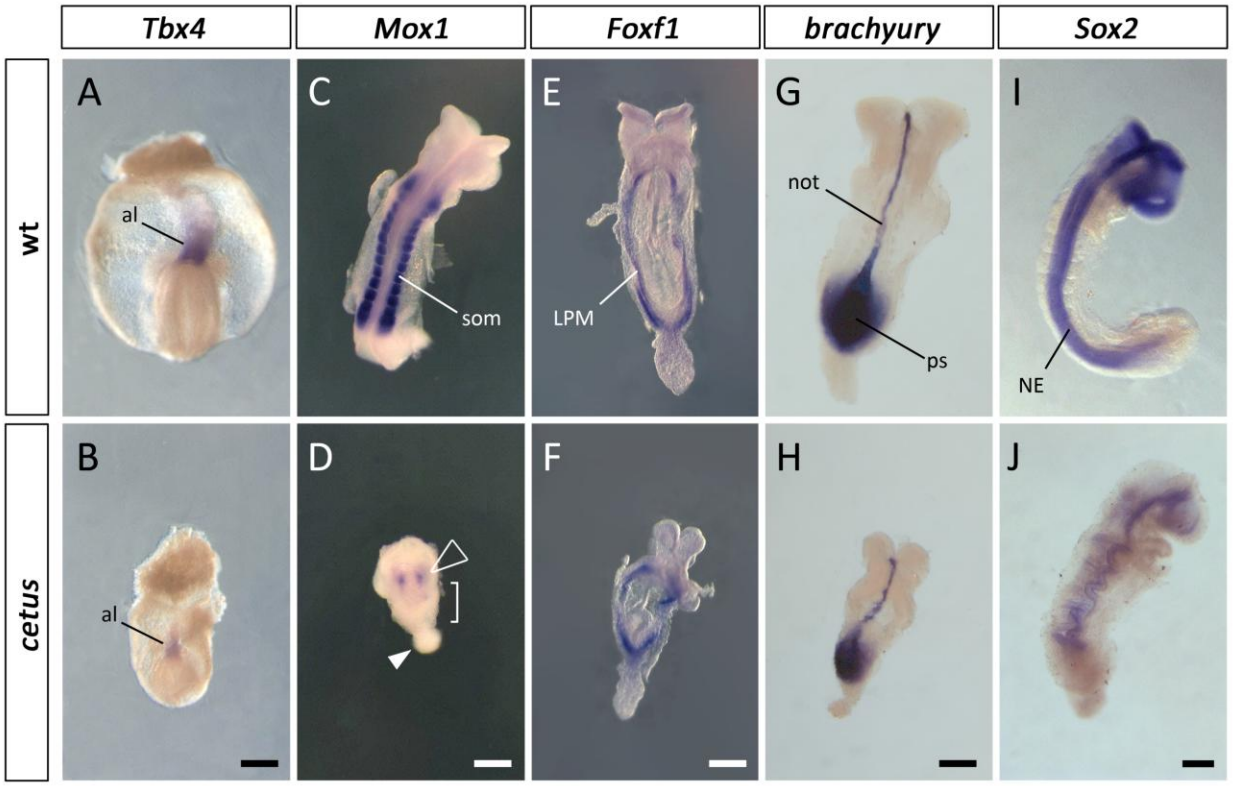

Figure 2.2. *cetus* mutant embryos have severe embryonic defects. Whole mount *in situ* hybridizations with *Tbx4* (A-B), *Mox1* (C-D), *Foxf1* (E-F), *T* (G-H) and *Sox2* (I-J) probes on E8.5 wild type (A, C, E, G, I) and *cetus* mutant (B, D, F, H, J) embryos. Solid arrowhead in D points to the ball-like allantois of a *cetus* mutant. Empty arrowhead in D points to vestigial expression of *Mox1* in the anterior part of a *cetus* embryo. This phenotype was only observed in a few cases, most cetus mutants completely lacked *Mox1* expression as shown in Figure 2. Bracket in D highlights the lack of somites (som). al, allantois. LPM, lateral plate mesoderm. not, notochord (axial mesoderm). ps, primitive streak. NE, neuroepithelia. Scale bars represent 200µm.

mesoderm in *cetus* mutants relative to wild type littermates, and a failure of these cells to condense in the mutant embryos. Most embryos lacked *Mox1* expression entirely, while a small proportion retained a low level of bilateral expression in the anterior region of the embryo (Figure 2.2C-D). Together, these results indicate the *cetus* mutation results in a severe and specific reduction in somitic mesoderm, but not other mesenchymal cell types.

The *cetus* mutation disrupts the DEAD/H-box helicase DDX11

Microsatellite based linkage analysis mapped the *cetus* mutation to a 1.1Mb interval on chromosome 17. All 11 genes within the candidate interval were sequenced and subsequent analysis identified a single T-C base transition in the DEAD/H-box helicase, *Ddx11* (Figure2.3A-B). No mutations were found in any of the other genes in the interval. Further analysis of *Ddx11* by *in situ* hybridization found the expression of this gene to be ubiquitous in both embryonic and extra-embryonic tissues at e8.5 and e9.5 (Figure 2.4).

DDX11 (DEAD/H (Asp-Glu-Ala-Asp/His)-box polypeptide 11) is as a member of the FANCJ sub-family of the super family 2 (SF2) DNA helicases that also includes the ERCC2, FANCJ and RTEL1 (reviewed by Wu et al., 2009). The *cetus* mutation results in a Leu-Pro amino acid substitution in a highly conserved residue of motif V, one of the seven conserved motifs characteristic of these proteins (Figure 2.3C). To confirm that the mutation in *Ddx11* is responsible for the *cetus* phenotype, and determine the severity of the allele, I performed a genetic complementation test with a previously described null allele of *Ddx11* (*Ddx11*^{KO}). *Ddx11*^{KO} mice were generated by the targeted deletion of exons 3-5 which encode the Walker A domain required for the ATP hydrolysis activity of the DDX11 protein (A. Inoue et al., 2007). We generated both *Ddx11*$^{cetus/KO}$ and *Ddx11*^{KO} homozygous embryos. Like *Ddx11*^{cetus}, compound heterozygous and *Ddx11*^{KO} embryos were small and lacked epithelial

Figure 2.3. Positional cloning of *cetus*. (A) *cetus* was mapped to a 1.1 Mb interval on chromosome 17 containing 11 genes (red line). Numbers to the right of the chromosome indicate the number of independent recombinants separating the mutation from the corresponding SSLP markers indicated to the left. For linkage analysis, a total of 2,018 chromosomes were analyzed. (B) Sequence chromatograms showing the *Ddx11* nucleic acid sequence in wild type and *cetus* mutant embryos. Indicated in red is the T-C base transition in the *cetus* mutant sequence which is predicted to result in a L743P amino acid substitution. (C) Schematic representation of the DDX11 protein structure. Conserved helicase motifs are indicated (not to scale). The location of the *cetus* mutation in helicase motif V is indicated in red. The positions of known human disease-associated mutations in the vicinity are indicated (adapted from Fan et al., 2008). Black arrowhead, Warsaw Breakage syndrome (WBS); Green stars, xeroderma pigmentosum (XP) ; Blue stars, trichothiodistrophy (TTD); Orange star, cockayne syndrome (CS). Red arrow indicates the position of the leucine residue mutated in *cetus*.

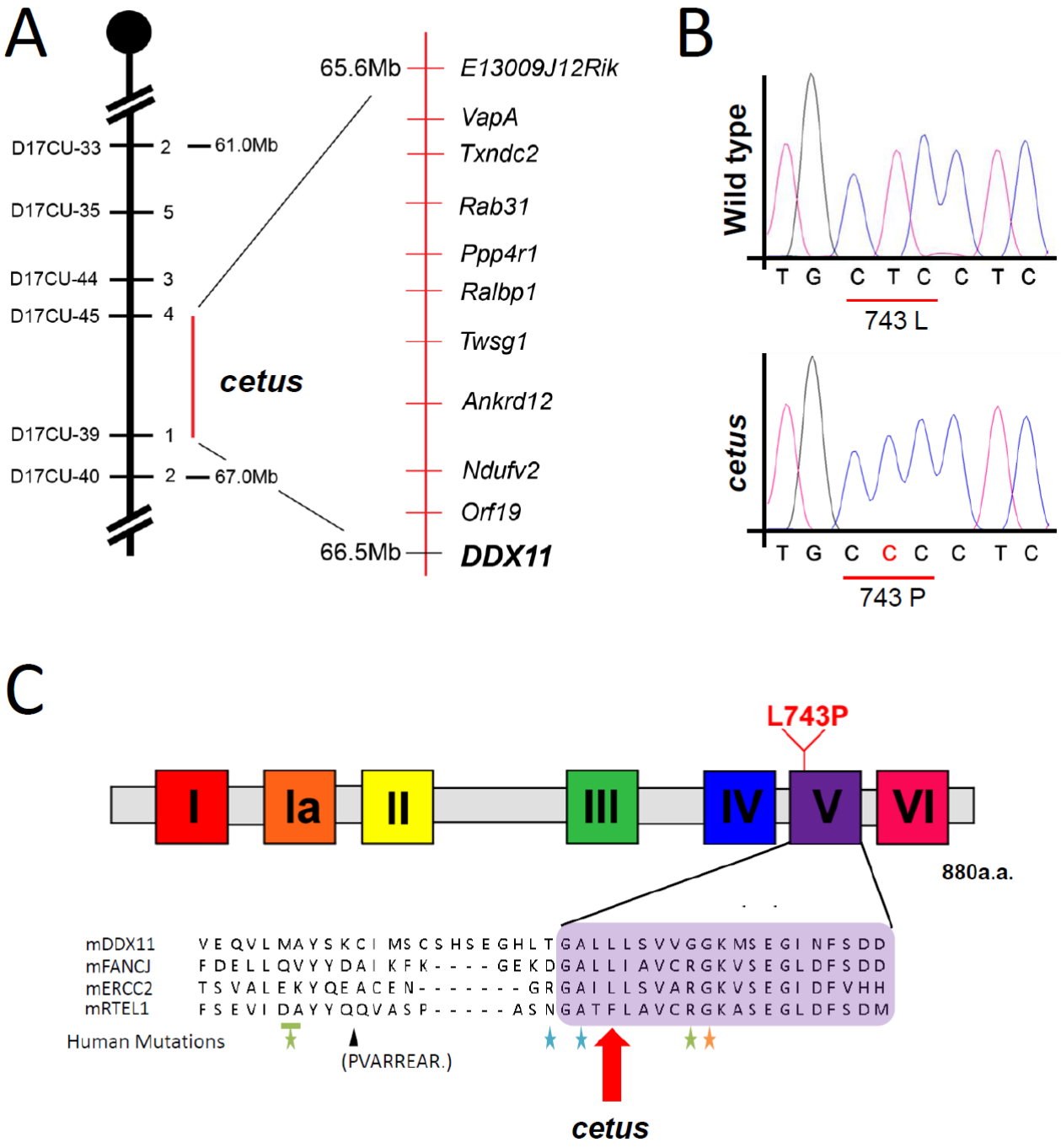
A
65.6Mb
E13009J12Rik
VapA
Txndc2
Rab31
Ppp4r1
Ralbp1
Twsg1
Ankrd12
Ndufv2
Orf19
66.5Mb
DDX11
D17CU-33
2
61.0Mb
D17CU-35
5
D17CU-44
3
D17CU-45
4
cetus
D17CU-39
1
D17CU-40
2
67.0Mb
B
Wild type
T G C T C C T C
743 L
cetus
T G C C C C T C
743 P
C
L743P
I
Ia
II
III
IV
V
VI
880a.a.
mDDX11 VEQVLMAYSKCIMSCSHSEGHLTGALLLSVVGGKMSEGINFSDD
mFANCJ FDELLQVYYDAIKFK----GEKDGALLIAVCRGKVSEGLDFSDD
mERCC2 TSVALEKYQEACEN-------GRGAILLSVARGKVSEGIDFVHH
mRTEL1 FSEVIDAYYQQVASP-----ASNGATFLAVCRGKASEGLDFSDM
Human Mutations
(PVARREAR.)
cetus

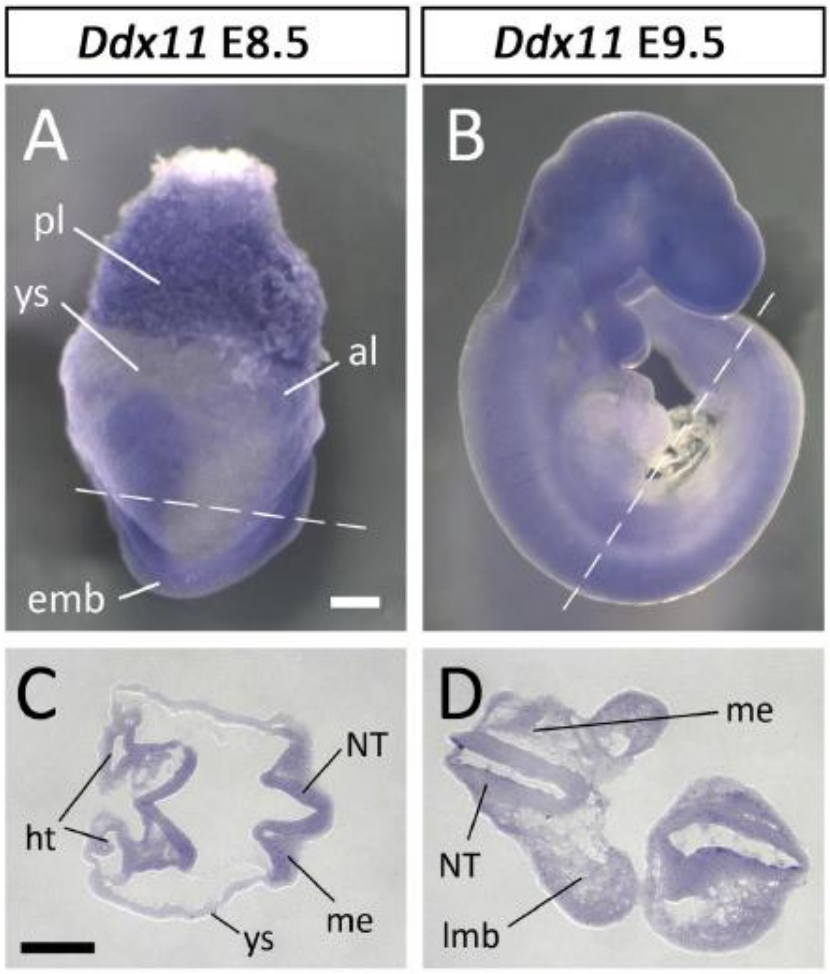

Figure 2.4. Expression of *Ddx11* at E8.5 and E9.5. (A-B) Whole mount *in situ* hybridizations with a *Ddx11* probe in wild type E8.5 (A) and E9.5 (B) embryos. The discontinuous lines in A-B indicate the section planes shown in C-D, respectively. emb, embryo. pl, placenta. al, allantois. ys, yolk sac. ht, heart. me, mesoderm. NT, neural tube. lmb, limb. Scale bar in A (for A-B pictures) represents 200µm and in C (for pictures in C-D) 50µm.

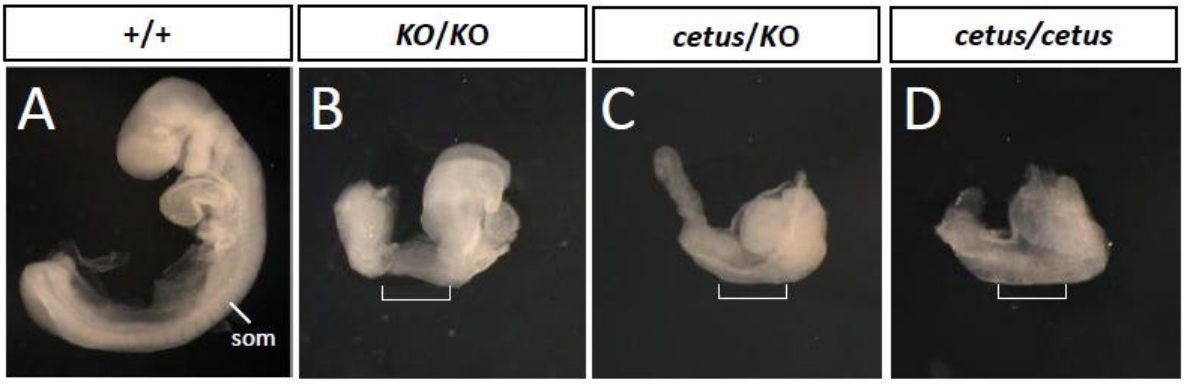

Figure 2.5. The *cetus* mutation disrupts *Ddx11*. Genetic analysis revealed that the *cetus* mutation did not complement a null (*KO*) allele of *Ddx11*, as judged from the similarities between the phenotypes of *KO* (C), *cetus/KO* (D) and *cetus* (E) embryos dissected at E9.5. Brackets highlight the absence of somites (som). All images depicted represent at 20X magnification.

somites (Figure 2.5B-D). These results indicate the ENU-induced *cetus* mutation represents a null allele of *Ddx11*.

In these experiments, we also noted the accumulation of a substantial number of cells in the amniotic cavity of *Ddx11* mutants. Many of these cells contained nuclei with pyknotic morphology indicating that they might be undergoing apoptosis. To confirm this, I performed TUNEL staining on cryosections from gastrulation stage embryos (Figure 2.6A, C, E). Quantification of the TUNEL positive cells in these assays revealed $Ddx11^{cetus}$ mutant and $Ddx11^{KO}$ embryos displayed a greater than 15-fold increase in the levels of apoptosis compared to wild type (Figure 2.6G). This apopotosis was widespread, occurring throughout the embryo in both epithelial and mesenchymal cell layers, an observation consistent with the ubiquitous expression pattern of the *Ddx11* transcript (Figure 2.4). At e7.5 both $Ddx11^{cetus}$ and $Ddx11^{KO}$ null mutant embryos were also noticeably smaller than their wild type littermates. However proliferation rates as detected by phospho-histone-3 (pH3) staining in the nucleus were comparable (Figure 2.6B, D, F & H), indicating that apoptosis, and not a lack of proliferation, is responsible for the small size of *Ddx11* mutants.

DDX11^{cetus} maintains DNA-binding and ATP hydrolysis activity

Previous studies have shown experimentally that hDDX11 is capable of acting as a ATP-dependent DNA helicase *in vitro* (Hirota and J M Lahti, 2000; Farina et al., 2008; Yuliang Wu et al., 2012). Several mutations that have been implicated in human disease that occur within or in close proximity to motif V in related FANCJ helicases have implicated this motif in ATP hydrolysis, DNA binding and helicase activity (Figure 2.3C; Fan et al., 2008). To address the possibility that the *cetus* mutation disrupts DDX11 ATP hydrolysis activity, recombinant HIS/SUMO-DDX11^{WT} and HIS/SUMO-DDX11^{cetus} mutant proteins were expressed in bacteria and affinity purified. As a control for these assays, a second mutant protein, HIS/SUMO-

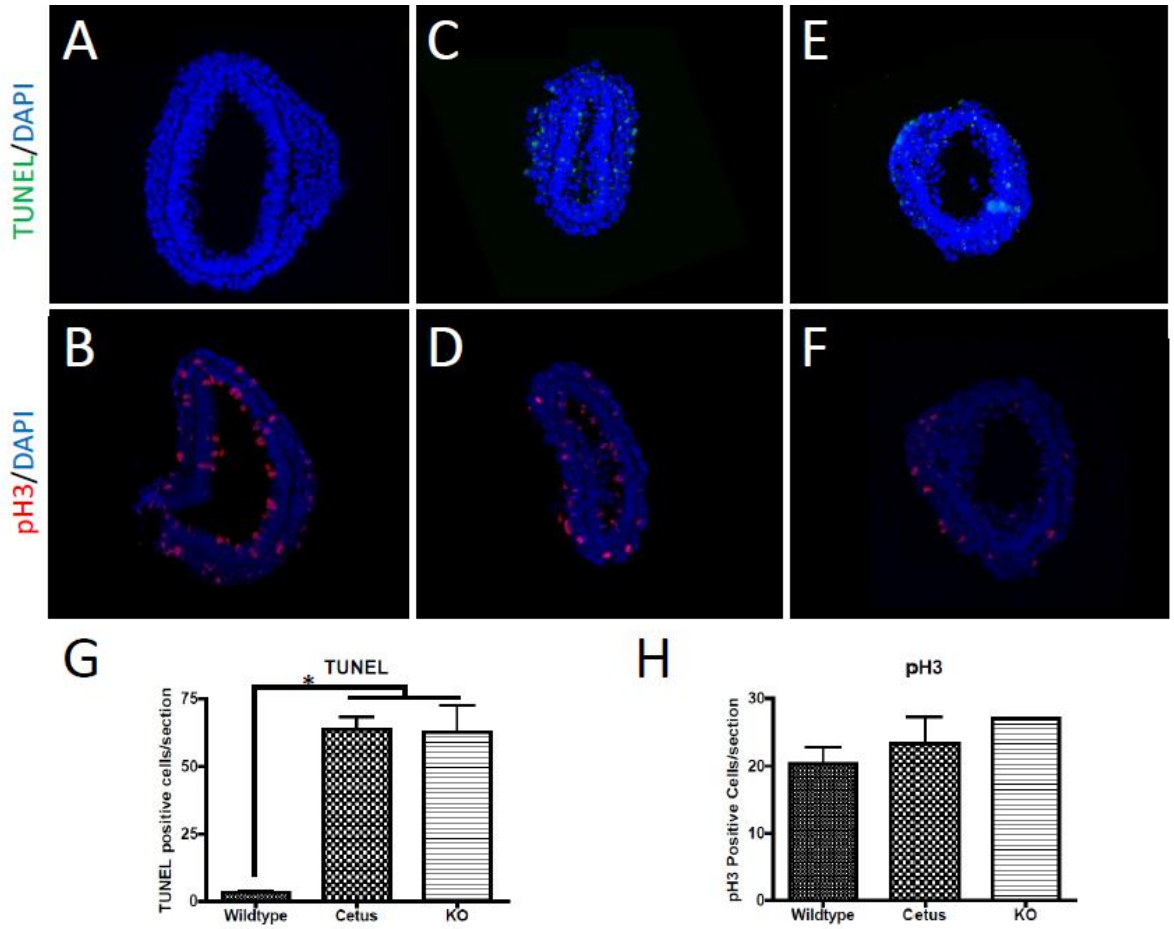

Figure 2.6. Apoptosis and proliferation in *Ddx11* mutant embryos. (A,C,E) TUNEL (green) and DAPI (blue) staining in E7.5 wild type (A), *Ddx11*^{cetus} (B) and *Ddx11*^{KO} (C) embryos. (G) Quantification of TUNEL positive cells revealed a dramatic increase in apoptosis in *Ddx11* mutants as compared to wild type littermates. (B, D, F) Phospho-histone 3 (pH3; red) and DAPI (blue) staining in E7.5 wild type (B), *Ddx11*^{cetus} (D) and *Ddx11*^{KO} (F) embryos. (H) Quantification of Phospho-histone 3 positive cells failed to reveal statistically significant differences between wild type and *Ddx11* mutants. Error bars represent the standard deviation across 4 or more sections from 3 independent embryos. Asterisk indicated $p<0.05$.

DDX11^{K50R}, was also generated. This *K50R* mutation affects the ATP-binding site and has been previously shown to significantly reduce the ATP hydrolysis activity of the hDDX11 protein (Hirota and J M Lahti, 2000; Yuliang Wu et al., 2012). Protein fractions were analyzed by western blot for the presence of full-length HIS/SUMO-DDX11 protein and ATP hydrolysis activity (Figure 2.7). The presence of ATP hydrolysis activity corresponded well with fractions containing HIS/SUMO-DDX11^{WT} and HIS/SUMO-DDX11^{cetus} mutant proteins. As expected, little ATP hydrolysis activity was observed in fractions containing HIS/SUMO-DDX11^{K50R} mutant protein. Taken together these results serve as validation of the purification of the recombinant HIS/SUMO-DDX11 proteins.

ATP hydrolysis activity was further assayed quantitatively in fractions containing HIS/SUMO-DDX11 protein. Quantification of the rate of ATP hydrolysis by the HIS/SUMO-DDX11 proteins showed there was no significant difference between the HIS/SUMO-DDX11^{WT} and HIS/SUMO-DDX11^{cetus} mutant proteins (Figure 2.8). These results indicate that the *cetus* mutation does not disrupt ATP hydrolysis.

DDX11 ATP hydrolysis activity has previously been shown to be dependent upon DNA binding (Hirota and J M Lahti, 2000), suggesting that the HIS/SUMO-DDX11^{cetus} mutant protein would also retain this function. Using electrophoretic mobility shift assays (EMSA), I found the murine HIS/SUMO-DDX11^{WT} protein was indeed able to bind single-stranded DNA and 3' recessed end structured DNA *in vitro* but not blunt-end double strand structures (Figure 2.9; data not shown). HIS/SUMO-DDX11^{cetus} mutant protein and the HIS/SUMO-DDX11^{K50R} protein bound DNA with similar affinities to the wild type (Figure 2.9D). These results are consistent with the known role of DDX11 as a DNA helicase and indicate that the *cetus* mutation does not disrupt HIS/SUMO-DDX11 DNA binding.

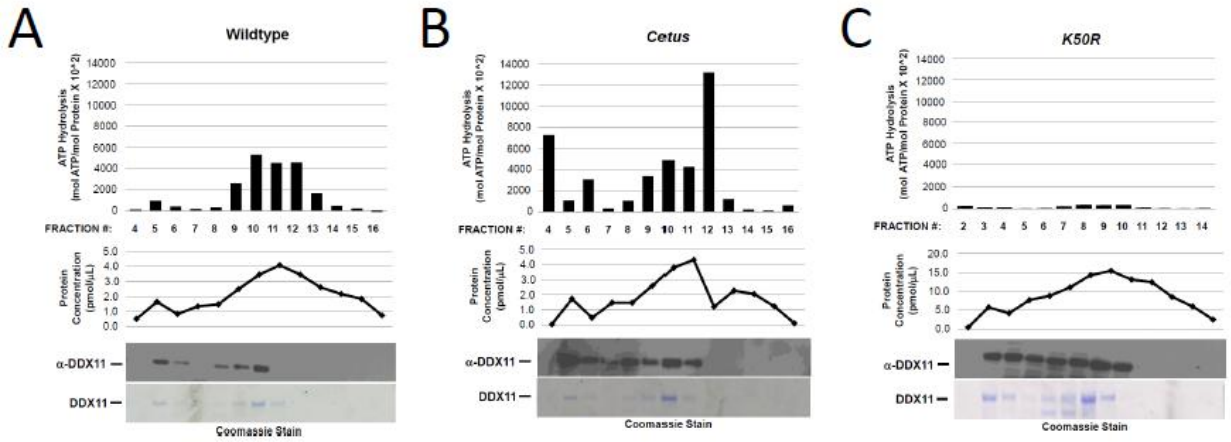

Figure 2.7. Purification of recombinant DDX11proteins. Analysis of recombinant wild type (A), *cetus* mutant (B) and *K50R* (C) His/SUMO-DDX11 protein purification. Bar graphs in each panel depict quantification of ATP hydrolysis activity calculated for individual protein fractions as described in the Materials & Methods. Protein concentrations were determined by Bradford assay (BioRad) and represent the total protein concentration in each fraction. Signal and staining in western blots and coomassie stained SDS-PAGE gels depict the location and relative concentrations of His/SUMO-DDX11 protein present in each fraction.

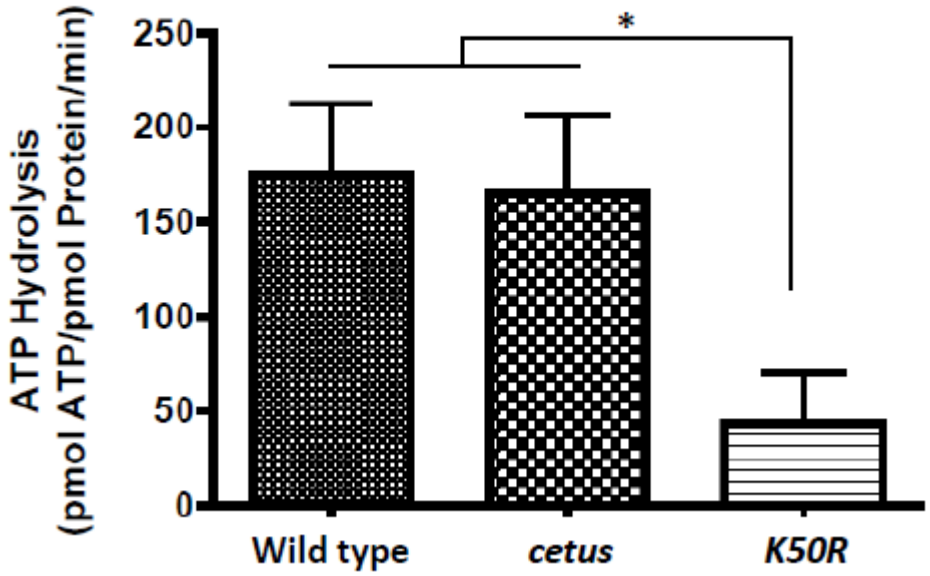

Figure 2.8. ATPase activity of DDX11 proteins. The graph depicts a comparison of the ATP hydrolysis activities of recombinant wild type, *cetus* and *K50R* mutant HIS/SUMO-DDX11 proteins. All proteins were assayed in the presence of single stranded DNA. Error bars represent the standard deviation across experiments conducted on samples prepared from two independent protein purifications. The asterisk indicates $p<0.05$.

Figure 2.9. Gel mobility shift analysis of DDX11 binding to single strand DNA structures. Analysis of DNA binding by wild type, *cetus* and *K50R* mutant HIS/SUMO-DDX11 proteins DDX11 as detected by electrophoretic mobility shift assays (EMSA) to (A) linear single strand, (B) 3' recessed and (C) 3' recessed foldback DNA structures. HIS/SUMO-DDX11 proteins were added at 0.425 μM, 4.25 μM, 21.25 μM and 42.5 μM concentrations. Recombinant RECQ (425 μM, Abcam) was used as a binding control. Binding reaction conditions and calculations were performed as described in the Materials & Methods. A summary of dissociation constants for HIS/SUMO-DDX11 proteins with various substrates is provided (D).

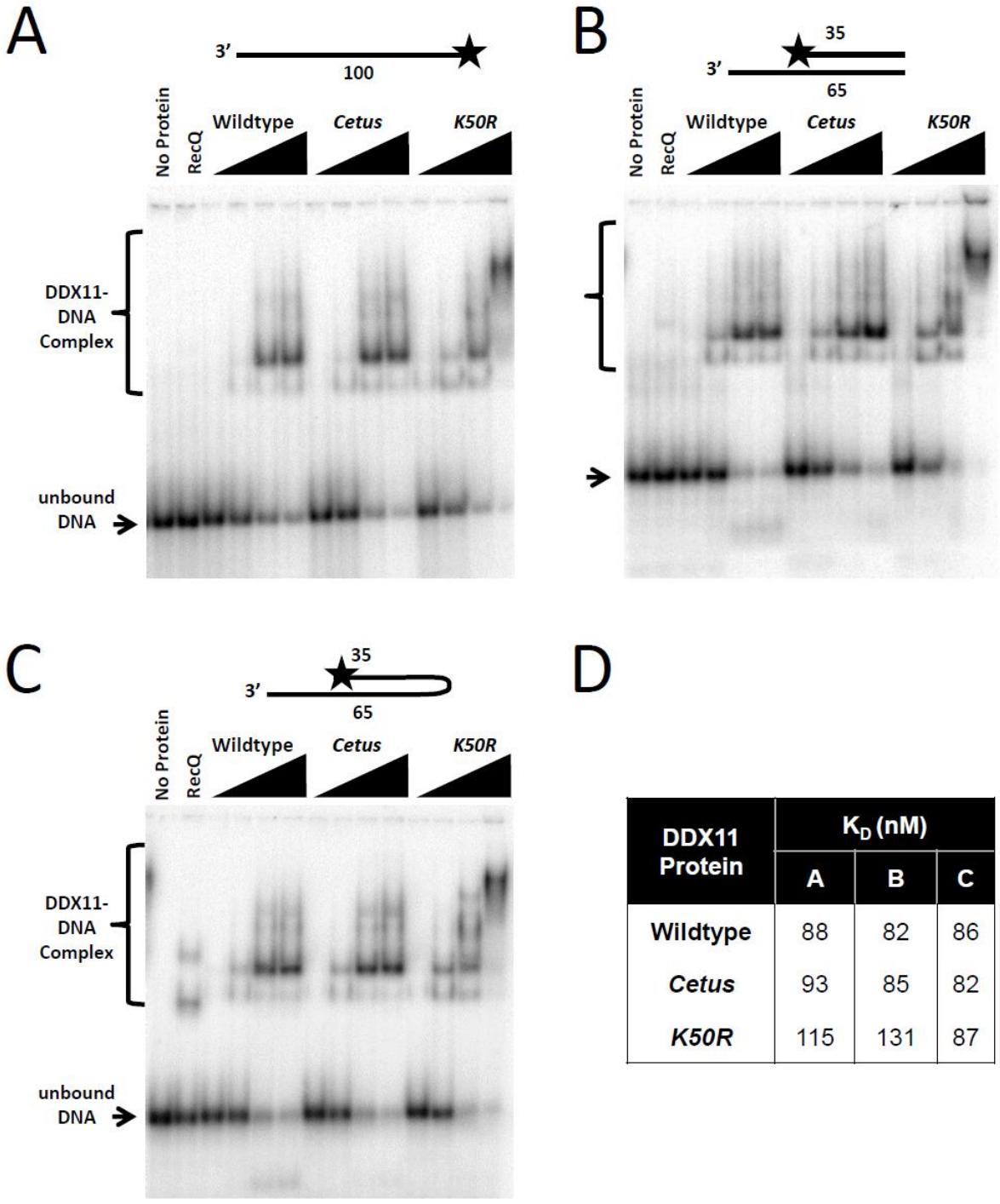

DDX11 Protein	K_D (nM)		
	A	B	C
Wildtype	88	82	86
Cetus	93	85	82
K50R	115	131	87

DISCUSSION

DDX11 is required for development of the early mouse embryo

Previous studies have demonstrated that *Ddx11* is essential for maintaining genome integrity and that loss of *Ddx11* results in embryonic lethality in mice (S. L. L. Gerring et al., 1990; A. Inoue et al., 2007; Parish et al., 2006). However, the embryonic defects of $Ddx11^{KO}$ were poorly characterized. Analysis of $Ddx11^{cetus}$ and $Ddx11^{KO}$ mutants showed that these embryos arrest by E8.5 with widespread morphological defects including a severe reduction in somitic mesoderm. The L743P *cetus* mutation disrupts motif V, one of seven highly conserved motifs characteristic of DEAD/H box helicases. Genetic complementation revealed that disruption of this motif in the $Ddx11^{cetus}$ mutants likely generates a null allele. Together, these results indicate a specific requirement for motif V in mediating essential DDX11 functions during development.

Genome instability and mesoderm defects

The original characterization of the $Ddx11^{KO}$ embryos showed defects in sister chromatid cohesion and cell cycle progression (A. Inoue et al., 2007). Consistent with a role for DDX11 in these processes, I found that loss of DDX11 in $Ddx11^{KO}$ and $Ddx11^{cetus}$ mutant embryos resulted in significant widespread apoptosis at very early embryonic stages. However, despite evidence for apoptosis throughout the embryo and ubiquitous expression of *Ddx11* transcript, our results show that some mesodermal populations are substantially more sensitive to these defects (Figure 2.1). $Ddx11^{cetus}$ mutant embryos display an extreme reduction in paraxial mesoderm as detected by expression of *Mox1* while lateral plate mesoderm and notochord are relatively unaffected.

Precisely why some mesodermal populations appear to be more sensitive to the defects present in $Ddx11^{cetus}$ mutants is unclear. It has been well established that cohesion and cohesion-related proteins are important regulators of development (reviewed in Dorsett, 2011; Wood et al.,

2010). However, understanding the nature of cohesion-related protein involvement in the regulation of developmental processes has been hampered by the complexity of separating mitotic defects from potentially direct regulation of developmental pathways by these proteins.

During early mouse embryogenesis, epithelial cells that comprise the embryo undergo a massive up-regulation in proliferation that generates the 120-fold increase in cell number between e6.5 and e7.5 (Snow, 1977; Lawson et al., 1991). In contrast, mesodermal cell populations have been described to divide at a rate similar to that of adult populations and significantly slower than corresponding ectodermal cell populations at the same stage of development (Snow, 1977; Solter et al., 1971). This degree of variation in the duration of the cell cycle is dependent, at least in part, upon a loss of DNA damage checkpoint and repair pathway activation in the embryo (reviewed by Artus & Cohen-Tannoudji, 2008). In yeast, inactivation of the mitotic spindle checkpoint in conjunction with the loss of *chl1* significantly increased the occurrence of cell death in progeny of dividing cells (R. Li and A. W. Murray, 1991). Furthermore, loss of function mutations in other determinants of proper cell cycle progression such as the tumor suppressors *Brca2* (R Hakem et al., 1998) and *Palb2* (Rantakari et al., 2010) as well as a component of the RAD9/RAD1/HUS1 checkpoint complex, *Hus1* (Levitt et al., 2005) cause defects in somitic mesoderm similar to those we observe in *Ddx11* mutants. Thus the increased cell cycle duration in mesodermal cell populations coupled with properties intrinsic to the somitic mesoderm such as small differences in the length of the cell cycle and the mitotic index might make this tissue particularly sensitive to DNA damage.

DNA binding and DNA-dependent ATP hydrolysis are not sufficient for DDX11 function

Previously characterized mutations in motif V of related FANCJ helicases which are associated with xeroderma pigmentosum in humans have been shown to reduce, but not abolish, both DNA binding and ATP hydrolysis activity (L. Fan et al., 2008). Furthermore, it has

recently been shown that the DDX11$^{\Delta K897}$ associated with Warsaw Breakage Syndrome in humans, reduced DNA binding and DNA-dependent ATP hydrolysis in *in vitro* assays (Yuliang Wu et al., 2012). The structural incompatibility of a leucine to proline amino acid substitution (Gray et al., 1996) like the L743P *cetus* mutation in the DDX11 protein implies that folding of the region surrounding the *cetus* mutation in the DDX11 protein is perturbed. However, I was unable to detect any obvious defect in the ability of the DDX11^{cetus} protein to mediate either ATP hydrolysis or DNA binding. These results indicate that while the DNA binding and ATP hydrolysis activity of DDX11 may be required for proper DDX11 function *in vivo*, they are not alone sufficient to mediate these processes. Additional studies aimed at identifying the biochemical, protein and/or DNA interactions that are required for DDX11 functions during development are necessary to identify which of these may be compromised in the *cetus* mutants (see Appendix A).

CONCLUSIONS

Results of our phenotypic and biochemical analysis of *Ddx11^{cetus}* mutants, suggest that the *cetus* mutation disrupts a crucial function of DDX11 that is critical for embryonic development. The identification of mutations in *Ddx11* in human patients underscores the importance of understanding the functions of this gene. Further investigation in to the molecular and biochemical nature of the defects in *Ddx11^{cetus}* mutants should provide novel insight into the role of this protein in sister chromatid cohesion as well as the function of helicase motif V in FANCJ helicases.

ACKNOWLEDGMENTS

Mark Roberson, Mariana Wolfner, John Schimenti, Joseph Peters, Qiaojuan Shi, Maria Spies and members of the Garcia lab for helpful discussions and comments on the data presented in this study; Jill Lahti, Eishi Noguchi, John Schimenti and Holger Sondermann for mice and reagents; Joseph Peters and Qiajuan Shi for help with protein purification, ATPase and gel mobility shift assays. Cornell's CARE staff for mice husbandry and care.

REFERENCES

Artus, J., & Cohen-Tannoudji, M. (2008). Cell cycle regulation during early mouse embryogenesis. *Molecular and cellular endocrinology*, *282*(1-2), 78-86. doi:10.1016/j.mce.2007.11.008

Belo, J. a, Bouwmeester, T., Leyns, L., Kertesz, N., Gallo, M., Follettie, M., & De Robertis, E. M. (1997). Cerberus-like is a secreted factor with neutralizing activity expressed in the anterior primitive endoderm of the mouse gastrula. *Mechanisms of development*, *68*(1-2), 45-57. Retrieved from http://www.ncbi.nlm.nih.gov/pubmed/9431803

Candia, A. F. F., Hu, J., Crosby, J., Lalley, P. A. A., Noden, D., Nadeau, J. H. H., & Wright, C. V. V. (1992). Mox-1 and Mox-2 define a novel homeobox gene subfamily and are differentially expressed during early mesodermal patterning in mouse embryos. *Development (Cambridge, England)*, *116*(4), 1123-1136. Retrieved from http://dev.biologists.org/cgi/content/abstract/116/4/1123

Chapman, D. L., Garvey, N., Hancock, S., Alexiou, M., Agulnik, S. I., Gibson-Brown, J. J., Cebra-Thomas, J., et al. (1996). Expression of the T-box family genes, Tbx1-Tbx5, during early mouse development. *Developmental dynamics : an official publication of the American Association of Anatomists*, *206*(4), 379-90. doi:10.1002/(SICI)1097-0177(199608)206:4<379::AID-AJA4>3.0.CO;2-F

Ciemerych, M. A., & Sicinski, P. (2005). Cell cycle in mouse development. *Oncogene*, *24*(17), 2877-98. doi:10.1038/sj.onc.1208608

Dorsett, D. (2011). Cohesin: genomic insights into controlling gene transcription and development. *Current opinion in genetics & development*, *21*(2), 199-206. doi:10.1016/j.gde.2011.01.018

Fairman-Williams, M. E., Guenther, U.-P., & Jankowsky, E. (2010). SF1 and SF2 helicases: family matters. *Current opinion in structural biology*, *20*(3), 313-24. doi:10.1016/j.sbi.2010.03.011

Fan, L., Fuss, J. O., Cheng, Q. J., Arvai, A. S., Hammel, M., Roberts, V. a, Cooper, P. K., et al. (2008). XPD helicase structures and activities: insights into the cancer and aging phenotypes from XPD mutations. *Cell*, *133*(5), 789-800. doi:10.1016/j.cell.2008.04.030

Farina, A., Shin, J.-H., Kim, D.-H., Bermudez, V. P., Kelman, Z., Seo, Y.-S., & Hurwitz, J. (2008). Studies with the human cohesin establishment factor, ChlR1. Association of ChlR1 with Ctf18-RFC and Fen1. *The Journal of biological chemistry*, *283*(30), 20925-36. doi:10.1074/jbc.M802696200

Garcia-Garcia, M. J., Eggenschwiler, J. T., Caspary, T., Alcorn, H. L., Wyler, M. R., Huangfu, D., Rakeman, A. S., et al. (2005). Analysis of mouse embryonic patterning and morphogenesis by forward genetics. *Proceedings of the National Academy of Sciences*, *102*(17), 5913-5919.

García-García, M. J., & Anderson, K. V. (2003). Essential role of glycosaminoglycans in Fgf signaling during mouse gastrulation. *Cell*, *114*(6), 727-37. Retrieved from http://www.ncbi.nlm.nih.gov/pubmed/14505572

Gerring, S. L. L., Spencer, F., & Hieter, P. (1990). The CHL 1 (CTF 1) gene product of Saccharomyces cerevisiae is important for chromosome transmission and normal cell cycle progression in G2/M. *The EMBO journal*, *9*(13), 4347. Nature Publishing Group. Retrieved from http://www.pubmedcentral.nih.gov/articlerender.fcgi?artid=552222&tool=pmcentrez&rendertype=abstract

Gray, T. M., Arnoys, E. J., Blankespoor, S., Born, T., Jagar, R., Everman, R., Plowman, D., et al. (1996). Destabilizing effect of proline substitutions in two helical regions of T4 lysozyme: leucine 66 to proline and leucine 91 to proline. *Protein science : a publication of the Protein Society*, *5*(4), 742-51. doi:10.1002/pro.5560050419

Hakem, R, de la Pompa, J. L., & Mak, T. W. (1998). Developmental studies of Brca1 and Brca2 knock-out mice. *Journal of mammary gland biology and neoplasia*, *3*(4), 431-45. Retrieved from http://www.ncbi.nlm.nih.gov/pubmed/10819537

Hakem, Razqallah. (2008). DNA-damage repair; the good, the bad, and the ugly. *The EMBO journal*, *27*(4), 589-605. doi:10.1038/emboj.2008.15

Hirota, Y., & Lahti, J. M. (2000). Characterization of the enzymatic activity of hChlR1, a novel human DNA helicase. *Nucleic acids research*, *28*(4), 917-24. Retrieved from http://www.pubmedcentral.nih.gov/articlerender.fcgi?artid=102573&tool=pmcentrez&rendertype=abstract

Hishida, T., Han, Y.-W., Shibata, T., Kubota, Y., Ishino, Y., Iwasaki, H., & Shinagawa, H. (2004). Role of the Escherichia coli RecQ DNA helicase in SOS signaling and genome stabilization at stalled replication forks. *Genes & development*, *18*(15), 1886-97. doi:10.1101/gad.1223804

Inoue, A., Li, T., Roby, S. K., Valentine, M. B., Inoue, M., Boyd, K., Kidd, V. J., et al. (2007). Loss of ChlR1 helicase in mouse causes lethality due to the accumulation of aneuploid cells generated by cohesion defects and placental malformation. *Cell cycle Georgetown Tex*, *6*(13), 1646-1654. Retrieved from http://www.ncbi.nlm.nih.gov/pubmed/17611414

Kasarskis, a, Manova, K., & Anderson, K. V. (1998). A phenotype-based screen for embryonic lethal mutations in the mouse. *Proceedings of the National Academy of Sciences of the United States of America*, *95*(13), 7485-90. Retrieved from http://www.pubmedcentral.nih.gov/articlerender.fcgi?artid=1460985&tool=pmcentrez&rendertype=abstract

Lawson, K. a, Meneses, J. J., & Pedersen, R. a. (1991). Clonal analysis of epiblast fate during germ layer formation in the mouse embryo. *Development (Cambridge, England)*, *113*(3), 891-911. Retrieved from http://www.ncbi.nlm.nih.gov/pubmed/1821858

Levitt, P. S., Liu, H., Manning, C., & Weiss, R. S. (2005). Conditional inactivation of the mouse Hus1 cell cycle checkpoint gene. *Genomics*, *86*(2), 212-24. doi:10.1016/j.ygeno.2005.04.007

Li, R., & Murray, A. W. (1991). Feedback control of mitosis in budding yeast. *Cell*, *66*(3), 519-531. doi:10.1016/0092-8674(81)90015-5

Liras, P., McCusker, J., Mascioli, S., & Haber, J. E. (1978). Characterization of a mutation in yeast causing nonrandom chromosome loss during mitosis. *Genetics*, *88*(4 Pt 1), 651-71. Retrieved from http://www.pubmedcentral.nih.gov/articlerender.fcgi?artid=1213811&tool=pmcentrez&rendertype=abstract

López de Saro, F. J., & O'Donnell, M. (2001). Interaction of the beta sliding clamp with MutS, ligase, and DNA polymerase I. *Proceedings of the National Academy of Sciences of the United States of America*, *98*(15), 8376-80. doi:10.1073/pnas.121009498

Mahlapuu, M., Ormestad, M., Enerback, S., & Carlsson, P. (2001). The forkhead transcription factor Foxf1 is required for differentiation of extra-embryonic and lateral plate mesoderm. *Development*, *128*(2), 155-166.

Navarro, M. V. A. S., De, N., Bae, N., Wang, Q., & Sondermann, H. (2009). Structural analysis of the GGDEF-EAL domain-containing c-di-GMP receptor FimX. *Structure (London, England : 1993)*, *17*(8), 1104-16. doi:10.1016/j.str.2009.06.010

Parish, J. L., Rosa, J., Wang, X., Lahti, J. M., Doxsey, S. J., & Androphy, E. J. (2006). The DNA helicase ChlR1 is required for sister chromatid cohesion in mammalian cells. *Journal of cell science*, *119*(Pt 23), 4857-65. doi:10.1242/jcs.03262

Peters, J. E., & Craig, N. L. (2001). Tn7 recognizes transposition target structures associated with DNA replication using the DNA-binding protein TnsE. *Genes & development*, *15*(6), 737-47. doi:10.1101/gad.870201

Rantakari, P., Nikkilä, J., Jokela, H., Ola, R., Pylkäs, K., Lagerbohm, H., Sainio, K., et al. (2010). Inactivation of Palb2 gene leads to mesoderm differentiation defect and early embryonic lethality in mice. *Human molecular genetics*, *19*(15), 3021-9. doi:10.1093/hmg/ddq207

Sherwood, R., Takahashi, T. S., & Jallepalli, P. V. (2010). Sister acts: coordinating DNA replication and cohesion establishment. *Genes & development*, *24*(24), 2723-31. doi:10.1101/gad.1976710

Snow, M. (1977). Gastrulation in the mouse: growth and regionalization of the epiblast. *Journal of Embryology and Experimental*, *42*(2), 293-303. Retrieved from http://dev.biologists.org/content/42/1/293.short

Solter, D., Skreb, N., & Damjanov, I. (1971). Cell cycle analysis in the mouse EGG-cylinder. *Experimental cell research*, *64*(2), 331-4. doi:10.1016/0014-4827(71)90084-X

Spencer, F, Gerring, S. L., Connelly, C., & Hieter, P. (1990). Mitotic chromosome transmission fidelity mutants in Saccharomyces cerevisiae. *Genetics*, *124*(2), 237-49. Retrieved from http://www.pubmedcentral.nih.gov/articlerender.fcgi?artid=1203917&tool=pmcentrez&rendertype=abstract

Wilkinson, D. G., Bhatt, S., & Herrmann, B. G. (1990). Expression pattern of the mouse T gene and its role in mesoderm formation. *Nature*, *343*(6259), 657-659. Nature Publishing Group. doi:10.1038/343657a0

Wood, A. J., Severson, A. F., & Meyer, B. J. (2010). Condensin and cohesin complexity: the expanding repertoire of functions. *Nature reviews. Genetics*, *11*(6), 391-404. doi:10.1038/nrg2794

Wu, Y, Suhasini, a N., & Brosh, R. M. (2009). Welcome the family of FANCJ-like helicases to the block of genome stability maintenance proteins. *Cellular and molecular life sciences : CMLS*, *66*(7), 1209-22. doi:10.1007/s00018-008-8580-6

Wu, Yuliang, Sommers, J. A., Khan, I., de Winter, J. P., & Brosh, R. M. (2012). Biochemical characterization of warsaw breakage syndrome helicase. *The Journal of biological chemistry*, *287*(2), 1007-21. doi:10.1074/jbc.M111.276022

van der Lelij, P., Chrzanowska, K. H., Godthelp, B. C., Rooimans, M. A., Oostra, A. B., Stumm, M., Zdzienicka, M. Z., et al. (2010). Warsaw breakage syndrome, a cohesinopathy associated with mutations in the XPD helicase family member DDX11/ChlR1. *American journal of human genetics*, *86*(2), 262-6. doi:10.1016/j.ajhg.2010.01.008

CHAPTER 3

Mice with mutations in *Mahogunin Ring Finger-1* (*Mgrn1*) exhibit abnormal patterning of the left-right axis.[1]

[1]This work has been published as Cota CD, Bagher P, Pelc P, Smith CO, Bodner CR & Gunn TM (2006), Mice with mutations in Mahogunin Ring Finger-1 (*Mgrn1*) exhibit abnormal patterning of the left-right axis. *Dev Dyn*. DOI: 10.1002/dvdy.20992.
Authors contributions are as follows: Analysis of left-right gene expression defects in *Mgrn1* mutants and generation of the *Mgrn1*^{XC712} mice was done by Cota CD. Bodner CR performed preliminary *in situ* experiments and provided initial technical support. Analysis of cardiac and pulmonary defects as well as expression of *Mgrn1*was done by Bagher P with technical support from Pelc P and Smith OC. Cota CD, Bagher PB and Gunn TM all contributed to the writing of the manuscript.
Modifications to fit the dissertation format requirements of Cornell University have been made by Cota CD.

ABSTRACT

Mahogunin Ring Finger 1 (*Mgrn1*) encodes a RING-containing protein with ubiquitin ligase activity that has been implicated in agouti pigment-type switching. In addition to having dark fur, mice lacking MGRN1 develop adult-onset spongy degeneration of the central nervous system and have reduced embryonic viability. Observation of complete *situs inversus* in a small proportion of adult *Mgrn1* mutant mice suggested that embryonic lethality resulted from congenital heart defects (CHDs) due to defective establishment and/or maintenance of the left-right (LR) axis. Here we report that *Mgrn1* is expressed in a pattern consistent with a role in LR patterning during early development and that many *Mgrn1* mutant embryos show abnormal expression of asymmetrically expressed genes involved in LR patterning. A range of complex heart defects was observed in 20% of mid-late gestation *Mgrn1* mutant embryos and another 20% were dead. This was consistent with 46-60% of mutants being dead by weaning age. Our results indicate that *Mgrn1* acts early in the LR signaling cascade and is likely to provide new insight into this developmental process as *Nodal* expression was uncoupled from expression of other nodal-responsive genes in *Mgrn1* mutant embryos. Our work identifies a novel role for MGRN1 in embryonic patterning and suggests that the ubiquitination of MGRN1 target genes is essential for the proper establishment and/or maintenance of the LR axis.

INTRODUCTION

The establishment of the left-right (LR) body axis during early development in vertebrate embryos is essential to proper morphology and placement of the visceral organs. The LR axis is the final of the three body axes to be established during development, with the initial symmetry breaking event occurring at the late neural fold stage (Hiroshi Hamada et al., 2002). Over the past decade, a number of genes involved in these steps have been identified including those encoding the transforming growth factor-β (TGF- β)-related signaling molecules *Nodal, Lefty1 and Lefty2* and the bicoid-type homeobox gene, *Pitx2* (Collignon J. and E J Robertson, 1996; L. A. Lowe et al., 1996; C Meno et al., 1998; Yoshioka et al., 1998). The initial symmetry-breaking event has been attributed to a leftward flow that is a result of beating monocilia located on the ventral surface of the mammalian node. This flow is thought to cause a build-up of NODAL on the left side of the node which is then transferred to the lateral plate mesoderm (LPM) where it sets off a cascade of signaling on the left side of the developing embryo maintained by a midline barrier (Shigenori Nonaka et al., 2002; S Nonaka et al., 1998). While this theory of nodal flow has been widely accepted and modified to include means for both chemical (S Nonaka et al., 1998; Yasushi Okada et al., 2005) and physical (McGrath et al., 2003) modes of generating a left-specific signaling event, other theories have been presented including a prolonged and stable upregulation of Ca^{2+} in the left side of the node which has been proposed to be involved regulating the left-sided signaling cascade (McGrath et al., 2003; Yosuke Tanaka et al., 2005). Mice lacking the membrane cation channel Polycystin-2 (PKD2) have impaired left–right axis determination and do not show left-sided elevation of Ca^{2+} in the node (Pennekamp et al., 2002; McGrath et al., 2003). Although the mechanism of $Ca2^{+}$-dependent regulation of left–right asymmetry remains unclear, work in chick embryos has shown that transient accumulation of extracellular calcium leads to asymmetric activation of Notch (A. Raya et al., 2004). In mice,

Notch activity has been shown to regulate *Nodal* expression around the node (Krebs et al., 2003; A. Raya et al., 2003).

Nodal expression in the node is required to induce *Lefty1* expression in the floorplate and *Nodal* expression in the left LPM (M. Yamamoto et al., 2003; J Brennan et al., 2001). *Lefty1* is a feedback inhibitor of nodal that restricts its signaling and duration of expression. *Nodal* in the left LPM acts as a left-side determinant and activates *Lefty2* expression (M. Yamamoto et al., 2003). In the absence of *Lefty1* or *Lefty2*, early *Nodal* expression in the LPM is asymmetric but it subsequently becomes bilateral (C Meno et al., 1998, 2001). Abnormal expression of any of these genes typically results in LR patterning defects.

LR patterning defects result in a variety of *situs* abnormalities including *situs inversus* (complete reversal of the left and right body axes), isomerism (resulting in symmetrical *situs* of an organ or organs) or heterotaxia (reversed symmetry of at least one but not all organs). Morbidity and mortality of laterality defects are generally attributed to associated complex congenital heart defects (CHDs), suggesting that the developing heart is particularly susceptible to disturbances in LR patterning (Kathiriya and Srivastava, 2000). Individuals with *situs inversus* have a higher incidence of CHDs than individuals with normal LR development (~3% vs. <0.1%), while ~90% of individuals with heterotaxia or isomerism are estimated to show complex CHDs (Ferencz et al., 1985; Bowers et al., 1996; Freed, 2001; Walmsley et al., 2004; Ramsdell, 2005). Cardiac malformations most commonly associated with LR patterning defects include atrial and ventricular septal defects, single (common) ventricle, transposition of the great arteries (TGA), double-outlet right ventricle (DORV), and pulmonary stenosis or atresia (Freed, 2001).

Mahogunin RING Finger-1 (*Mgrn1*) encodes a C3HC4 RING domain-containing protein with ubiquitin ligase activity (Lin He et al., 2003). Mutations in mouse *Mgrn1* were first

identified for their effect on pigmentation (Lane, 1960; Phillips, 1963; Miller et al., 1997). Mice homozygous for a null allele, *Mgrn1*$^{md\text{-}nc}$, produce no detectable mRNA transcript, have black fur and exhibit reduced embryonic viability (Phillips, 1963, 1971; Lin He et al., 2003). Mice homozygous for a hypomorphic allele, *Mgrn1*$^{md\text{-}2J}$, produce reduced amounts of aberrant mRNA transcript, have dark fur and also exhibit reduced embryonic viability (Phan et al., 2002; Bagher et al., 2006). We observed complete *situs inversus* in a small number (<1%) of adult *Mgrn1*$^{md\text{-}nc}$ mutant mice, which led to the hypothesis that reduced viability in *Mgrn1* mutants was due to congenital heart defects resulting from abnormal LR patterning. Histological examination revealed a range of complex heart defects in 20% of mid-to-late gestation *Mgrn1* mutant embryos, while another 20% of 12.5-19.5 d.p.c. embryos were dead. These observations were consistent with 46-60% mortality of homozygotes by weaning age. MGRN1 expression during embryogenesis was consistent with a role in LR patterning, and while most *Mgrn1* mutant embryos showed normal expression of *Nodal*, a high proportion had aberrant (absent, bilateral and/or right-sided) expression of *Lefty1*, *Lefty2* and *Pitx2*. Our work suggests that MGRN1 acts early in the LR signaling cascade and that studying *Mgrn1* mutants will provide novel insight into the molecular mechanisms of LR patterning.

MATERIALS & METHODS

Mice

Mgrn1$^{md\text{-}nc}$ mutant mice (Lin He et al., 2003) were maintained on an inbred (>20 generations of brother-sister inbreeding) C3H X 101 (C3.101) background. Attempts to make this allele congenic on the C3H/HeJ or 129S1/SvImJ backgrounds were unsuccessful as embryonic lethality approached 100% by the 5th backcross generations. C3H/HeJ-*Mgrn1*$^{md\text{-}2J}$ mice (Sweet and Davisson, 1995) have an ~8 kb IAP insertion in exon 13 that results in the production of aberrant *Mgrn1* RNA transcripts (Phan et al., 2002; Bagher et al., 2006). Mice

were obtained from a cryopreserved stock at the Jackson Laboratory and subsequently maintained by intercrossing siblings. As these mice did not breed well, a homozygous mutant was mated to a non-mutant 129S1/SvImJ mouse to obtain F1 heterozygotes, which were intercrossed to obtain *Mgrn1*$^{md\text{-}2J}$ homozygotes; experiments were performed using these mice and further intercrossed progeny. C3H/HeJ and 129S1/SvImJ control mice were originally obtained from the Jackson Laboratory and maintained in-house by brother-sister inbreeding.

Mgrn1$^{Gt(pGT1Lxf)XC712Wcs}$ (abbreviated to *Mgrn1*^{XC712}) mutant mice were generated from a mouse embryonic stem cell (ESC) line generated by BayGenomics that carries a gene-trap insertion in intron 17 of the *Mgrn1* locus, trapping 2 of the 4 normal RNA isoforms (Bagher et al., 2006). The gene-trap vector is composed of a strong splice acceptor sequence upstream of a *β-geo* reporter gene (*β-galactosidase* fused to neomycin phosphotransferase) followed by a poly adenylation signal (Stryke et al., 2003). The trapped ESC, generated from 129P2 ESC lines, were injected into C57BL/6J blastocysts. One chimeric male was mated to a 129S1/SvImJ female and genotyped progeny were intercrossed for 6-8 generations to generate animals used for experiments described herein. Mice homozygous for the *Mgrn1*^{XC712} mutation have slightly darker fur on the dorsum but no discernible embryonic patterning defects.

Histology

Mgrn1$^{md\text{-}nc}$ and *Mgrn1*$^{md\text{-}2J}$ homozygous embryos were collected from timed pregnancies between 16.5 and 18.5 d.p.c and fixed in 10% formalin. Embryos were ethanol-dehydrated and paraffin-embedded for sectioning. Transverse serial sections were made at 8 μm and subsequently stained with hematoxylin and eosin (H&E) using a standard protocol.

X-Galactosidase Staining and Cryosectioning Sectioning

Mgrn1^{XC712} homozygous embryos were collected from timed pregnancies at 7.5-9.5 d.p.c., fixed

in 4% paraformaldehyde for 10-15 minutes and assayed for β-GEO expression by X-galactosidase staining following a standard protocol (www.rodentia.com/wmc/docs/lacz_bible.html). Stained embryos were embedded in 1% agarose and cryoprotected in 60% sucrose prior to secondary embedding in OCT. Sagittal or transverse serial cryosections were made at 25-30 μm.

Whole-Mount *in situ* Hybridization

Whole mount *in situ* hybridization was performed as previously described (IC et al., 2000). RNA probes for *Nodal*, *Lefty* (which recognizes *Lefty1* and *Lefty2)* and *Pitx2* have been described previously (L. A. Lowe et al., 1996; C Meno et al., 1996; Yoshioka et al., 1998). The *Mgrn1* probe was a 420-bp portion of the 3'UTR (common to all 4 isoforms) generated by PCR using forward primer CAGTTCCCCCGCACAGGTC and reverse primer AGGAAGGAGCAGGGTTAGAGTCAG and IMAGE cDNA clone 3481878 as template. All embryos were collected from timed pregnancies where females were checked daily for copulatory plugs and the day of detection of a plug was considered 0.5 d.p.c. Developmental age of embryos was verified by somite number.

RESULTS

LR patterning defects in *Mgrn1* mutant mice

The pigmentation phenotype of *Mgrn1* mutant mice is fully penetrant. Based on crosses between heterozygous and homozygous *Mgrn1* mutants where equal proportions of heterozygous (agouti) and homozygous (dark) pups are expected, 46% of C3.101-*Mgrn1*$^{md\text{-}nc}$ and 60% of CeH/HeJ-*Mgrn1*$^{md\text{-}2J}$ homozygotes die before birth or during the first 3 weeks of life (Table 3.1). Surviving animals have other phenotypes, including dark fur and adult-onset spongy degeneration of the central nervous system (*Mgrn1*$^{md\text{-}nc}$ only). In addition, while most adult *Mgrn1* mutants show normal situs of asymmetric internal organs such as the heart, lungs, liver,

Table 3.1. Lethality in *Mgrn1* mutants at weaning

Cross	mice born n	died before weaning* n (%)	animals weaned: heterozygotes n (%)	animals weaned: homozygotes** n (%)	homozygotes missing at weaning
Mgrn1md-nc/+ x Mgrn1md-nc/md-nc	2009	32	1285 (65%)	692 (35%)	46% [1-(692/1285)]
Mgrn1md-2J/+ x Mgrn1md-2J/md-2J	581	12	406 (71%)	163 (29%)	60% [1-(163/406)]

* Genotype of dead embryos unknown

**Number of homozygotes are expected to be equivalent to heterozygotes in this cross

Figure 3.1. Situs defects in *Mgrn1* mutant mice. (**A-C**) Wild-type, C3H/HeJ, mice show *situs solitus* (normal) (**A**) as do most *Mgrn1*$^{md\text{-}nc/md\text{-}nc}$ mutant mice (**B**), although a small proportion of adults were observed with complete *situs inversus* (**C**). Upper panel shows the positions of the heart (H), stomach, spleen (Sp), lungs (Lu) and liver (Lv). Lower panels show reversed positions of the left (lK) and right (rK) kidneys in the affected animal. (**D-K**) Situs defects were also observed in some *Mgrn1* mutants during embryonic development. 16.5 d.p.c. wild-type (C3H/HeJ) pup (**D**) and an unaffected *Mgrn1*$^{md\text{-}nc/md\text{-}nc}$ pup (**E**) showed normal positioning of the heart (black arrows) while an affected *Mgrn1*$^{md\text{-}nc/md\text{-}nc}$ (**F**) that was runted (E and F are at same scale) had mesocardia (**F**, black arrow). The heart of the runted animal (**K**, right, designated with *) was also hypoplastic relative to wild-type (**J**) and to its unaffected littermate (**K,** left).

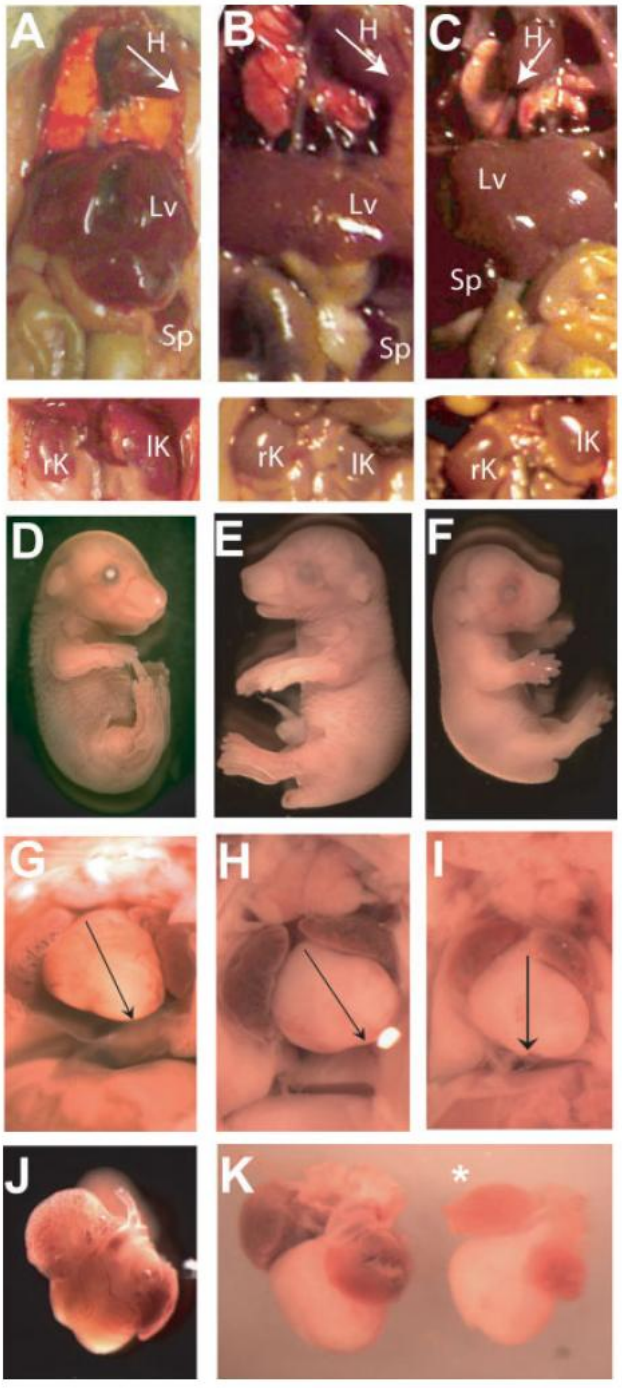
A
H
Lv
Sp
B
H
Lv
Sp
C
H
Lv
Sp
rK
lK
rK
lK
rK
lK
D
E
F
G
H
I
J
K
*

Table 3.2. Embryonic lethality at late stages of gestation in *Mgrn1* mutants

Genotype	Age (dpc)	# embryos	# resorptions (%)	# with hemorrhage (%)
Mgrn1$^{mdnc\text{-}nc/md\text{-}nc}$	12.5	16	2 (11%)	0
Mgrn1$^{mdnc\text{-}2J/md\text{-}2J}$	12.5	16	7 (30%)	0
Mgrn1$^{mdnc\text{-}nc/md\text{-}nc}$	14.5	17	3 (15%)	2 (10%)
Mgrn1$^{mdnc\text{-}2J/md\text{-}2J}$	14.5	15	4 (21%)	1 (5%)
Mgrn1$^{mdnc\text{-}nc/md\text{-}nc}$	15.5	5	2 (30%)	0
Mgrn1$^{mdnc\text{-}2J/md\text{-}2J}$	15.5	17	2 (11%)	2 (11%)
Mgrn1$^{mdnc\text{-}nc/md\text{-}nc}$	16.5	4	2 (33%)	0
Mgrn1$^{mdnc\text{-}2J/md\text{-}2J}$	16.5	9	0	1 (11%)
Mgrn1$^{mdnc\text{-}nc/md\text{-}nc}$	18.5-19.5	5	3 (38%)	0
Mgrn1$^{mdnc\text{-}2J/md\text{-}2J}$	18.5-19.5	6	2 (25%)	0
	Total	110	27 (20%)	6 (4%)

Figure 3.2. Cardiac and pulmonary defects in 16.5 d.p.c. *Mgrn1* mutant mice. (**A-D**) Normal C3H/HeJ embryo (**A**) and two *Mgrn1*$^{md\text{-}nc/md\text{-}nc}$ embryos with hemorrhage (black arrows). Boxed region in C is shown at higher magnification in D. (**E-J**) H&E-stained transverse sections of a control C3H/HeJ, an unaffected *Mgrn1* mutant mouse and a *Mgrn1* mutant mouse exhibiting cardiac and pulmonary defects. The affected embryo corresponds to embryo 5 in Table 2 and is labeled in the bottom right corner. Individual structures are labeled, with abnormal structures in capital letters. (**E-F**) C3H/HeJ embryo with normal anatomy and situs. (**E**) An intact inter-atrial septum (ias) separates the left and right atria, the left ventricle (lv) and right ventricle (rv) are separated by an inter-ventricular septum (ivs). (**F**) Normal positioning of the aorta (ao) and pulmonary artery (pa) with a normal right ventricular outflow tract (rvot) and the esophagus (es) slightly left of the midline. (**G-H**) Unaffected *Mgrn1*$^{md\text{-}nc/md\text{-}nc}$ embryo with anatomy and situs comparable to the C3H/HeJ control. Partial penetrance of the phenotype results in homozygous mutants with normal positioning and development of the heart. (**I-J**) *Mgrn1*$^{md\text{-}nc/md\text{-}nc}$ embryo with cardiac and pulmonary defects**.** (**I**) A ventricular septal defect (VSD) and common atrium (CA) are present with a visible thinning of the ventricular myocardium in the compact zone (arrow). This embryo also exhibits left pulmonary isomerism (LPI), having two left lungs (LL), and mesocardia of the heart in the body cavity. (**J**) The outflow tract developed normally with correct positioning of the great vessels but midline positioning of the esophagus. All images in D-I were taken at 5x magnification.

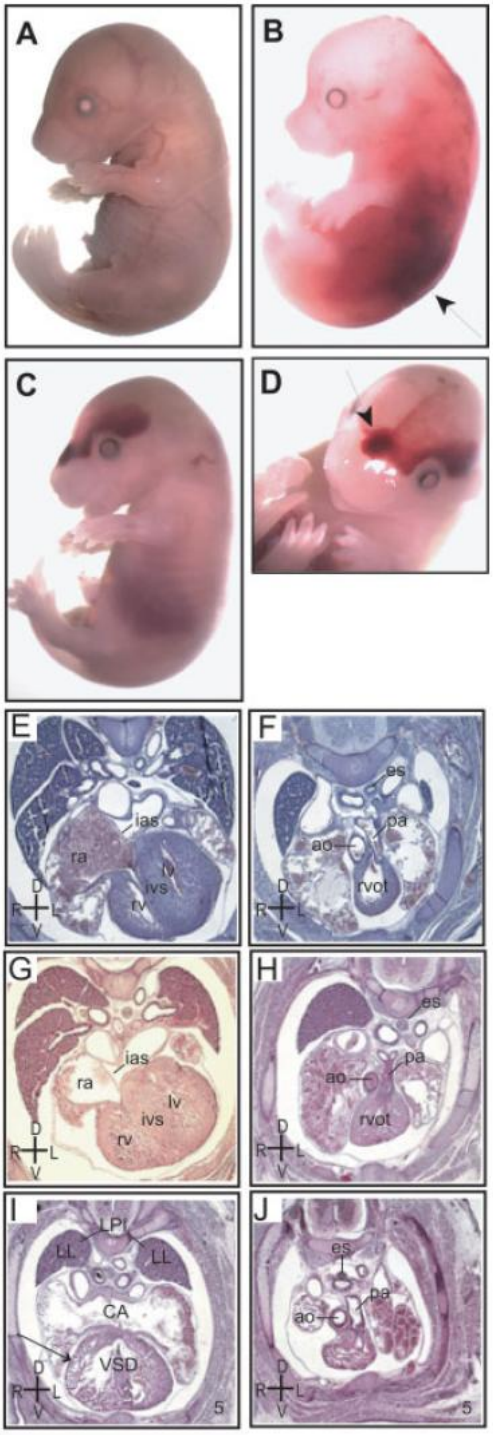
A
B
C
D
E
ias
ra
lv
ivs
rv
D
R
L
V
F
es
pa
ao
rvot
G
H
I
LPl
LL
LL
CA
VSD
5
J

stomach, spleen and kidneys (Figure 3.1A-B), complete reversal (*situs inversus*) was observed in a very small proportion (estimated to be <1%) of adult *Mgrn1*$^{md\text{-}nc/md\text{-}nc}$ mice (Figure 3.1C). This suggested that loss of *Mgrn1* causes a defect in LR patterning.

To further investigate the hypothesis that LR patterning is altered in *Mgrn1* mutants, we examined embryos for laterality defects. Between 12.5 and 19.5 d.p.c, 20% of *Mgrn1* mutant embryos were dead (Table 3.2). Gross examination of resorbed embryos indicated that they did not all die at the same stage of development as they varied greatly in size and condition of the tissue; in some cases, only a small, dark mole was observed while in the same litter, the anatomical structures of a pale, degenerating embryo could still be discerned. When examined at 9.5-10.5 d.p.c 1% (1/106) of *Mgrn1* mutant embryos exhibited leftward heart looping, reversed axial rotation (tail positioned to the left of the midline/head), and/or improperly placed attachment points of extra-embryonic membranes, while another 2% (2/106) exhibited ambiguous heart looping with no other apparent *situs* defects. At later stages of development (12.5-18.5 d.p.c.), 4% (5/109) embryos showed hemorrhage (Figure 3.2A-D) and 25% (5/20) displayed complex CHD including atrial and ventricular septal defects, thinning of the myocardium, right aortic arch, double outlet right ventricle, unroofed coronary sinus, malposition of the great arteries, retroesophageal left subclavian artery, abnormal heart situs (mesocardia or dextrocardia), and/or pericardial and pleural effusion (Figures 3.1-3.3 and Table 3.3). Some embryos also showed left pulmonary isomerism and/or pulmonary hemorrhage (Figure 3.3 and Table 3.3). Additional *situs* defects would not have been detected as only the chest region of these embryos were sectioned and analyzed. Taken together, our observations support the hypothesis that LR patterning is abnormal in *Mgrn1* mutant embryos and leads to

Figure 3.3. Cardiac and outflow tract defects in 18.5 d.p.c. *Mgrn1* mutant mice. H&E-stained transverse sections of wild-type and *Mgrn1* mutant mice. Affected embryos are labeled in the bottom right corner and their numbers correspond to embryos in Table 2. Individual structures are labeled, with abnormal structures in capital letters. (**A-B**) C3H/HeJ embryo with normal anatomy and situs. (**A**) The left ventricle (lv) and right ventricle (rv) are separated by an inter-ventricular septum (ivs). (**B**) Normal positioning of the aorta (ao) and pulmonary artery (pa). (**C-D**) *Mgrn1*$^{md\text{-}nc/md\text{-}nc}$ embryo with normal anatomy and situs. (**E-F**) *Mgrn1*$^{md\text{-}2Jnc/md\text{-}2J}$ embryo (#10) with cardiac defects and symptoms of congestive heart failure. (**E**) Pericardial and pleural effusion signifying congestive heart failure in this embryo. Atrioventricular septal defect (AVSD) resulting in one large heart chamber with thinning of the ventricular myocardium (arrow). (**F**) The outflow tract developed normally relative to wild-type and unaffected *Mgrn1* mutant. (**G-H**) *Mgrn1*$^{md\text{-}nc/md\text{-}nc}$ embryo (#13) with cardiac and outflow tract defects. (**G**) Presence of an AVSD results in one large heart chamber. This embryo also exhibited dextrocardia. (**F**) Associated outflow tract abnormalities including a right aortic arch (RAA) emerging from a double outlet right ventricle (DORV) were also observed. (**I-J**) *Mgrn1*$^{md\text{-}nc/md\text{-}nc}$ embryo (#18) with cardiac, situs and outflow tract defects. (**I**) An unroofed coronary sinus (UCS) drains into a common atrium (CA). This animal exhibits dextrocardia and abnormal ventricular situs with reversal of the lv and rv relative to unaffected animals. (**J**) Malposition of the great arteries (MGA) with a more ventral PA as compared to wild-type. The AO continues to the right of the es as a RAA, with a retroesophageal left subclavian artery (LRESA). (**K-L**) *Mgrn1*$^{md\text{-}nc/md\text{-}nc}$ (#19) embryo with cardiac, situs and outflow tract defects. (**K**) This embryo had similar cardiac defects to Embryo #18 (I-J), such as dextrocardia, UCS, CA, and reversal of ventricular situs. In addition, this embryo had reversed lung situs, pericardial effusion and transposition of the great arteries (TGA) **(K-L)**. Although the global situs of this animal is unknown, both the heart and lungs developed reversed situs. All images were taken at 5x magnification.

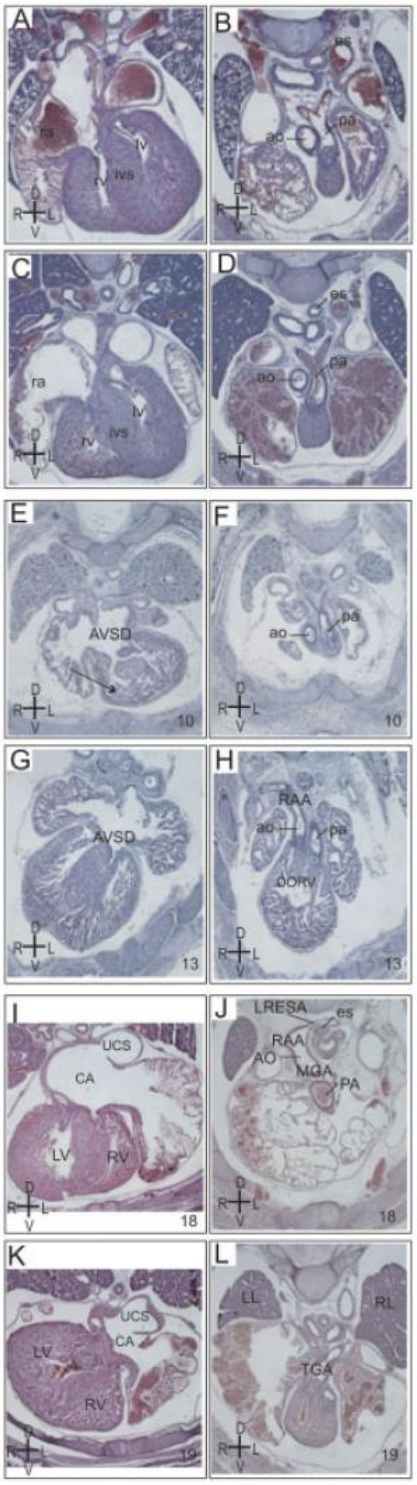
A
ra
lv
rv
ivs
B
as
pa
ao
C
ra
lv
ivs
rv
D
as
pa
ao
E
AVSD
10
F
pa
ao
10
G
AVSD
13
H
RAA
ao
pa
DORV
13
I
UCS
CA
LV
RV
18
J
LRESA
es
RAA
AO
MCA
PA
18
K
UCS
CA
LV
RV
19
L
LL
RL
TGA
19

Table 3.3 Cardiovascular and pulmonary phenotypes in *Mgrn1* mutant mice

Embryo	Age (dpc)	Phenotype
5	16.5	thinning of the myocardium (compact zone), left pulmonary isomerism, common atrium, ventricular septal defect, mesocardia
10	18.5	pericardial effusion, pleural effusion, atrioventricular septal defect, thinning of the myocardium, malposition of the great arteries
13	18.5	atrioventricular septal defect, right aortic arch, double outlet right ventricle, dextrocardia
18	18.5	right aortic arch, retroesophageal left subclavian artery, double outlet right ventricle, common atrium, unroofed coronary sinus, dextrocardia, reversed heart situs
19	18.5	dextrocardia, reversed lung situs, common atrium, pericardial effusion, transposition of the great arteries, reversed heart situs

Figure 3.4. Embryonic expression of *Mgrn1* RNA and protein. The MGRN1-β-GEO fusion protein expressed in *Mgrn1*$^{XC712/XC712}$ embryos was detected by X-gal staining **(A, E-I, K)** and *Mgrn1* mRNA was detected by *in situ* hybridization in wild-type embryos using a 3'UTR probe **(B-D, J)**. Similar expression patterns were observed with both methods. (**A**) MGRN1-β-GEO was expressed in the node (arrow) of pre-somite embryos. (**B-D**) Ventral (**B**, boxed region enlarged in **C**) and right lateral (**D**) views of a 2-3 somite embryo showing strong *Mgrn1* expression in the node (arrow) and heart (h). (**E**) Right lateral view of a 6 somite embryo in which X-gal was developed for 24 hours, showing with expression in the node (arrow), neuroepithelium, floorplate, paraxial mesoderm, somites and heart (h). (**F**) Sagittal section of 6-7 somite embryo showing strong expression in node (arrow, boxed region enlarged in **G**) as well as expression in neuroepithelium, heart (h) and mesoderm. Angle and approximate position of section is represented by line on adjacent sketch of 8.5 d.p.c. embryo. **(H)** Ventral view of a 6 somite embryo developed for 12 hours showing strong MGRN1-β-GEO expression in the midline (arrow) and heart (h). **(I)** Transverse section of a 13 somite embryo developed for 12 hours, showing symmetric floorplate expression (arrow) of MGRN1-β-GEO. Angle and approximate position of section is represented by line on adjacent sketch of 8.5-8.75 d.p.c. embryo. **(J-K)** By 9.5 d.p.c., MGRN1-β-GEO **(J)** and Mgrn1 mRNA **(K)** are broadly expressed.

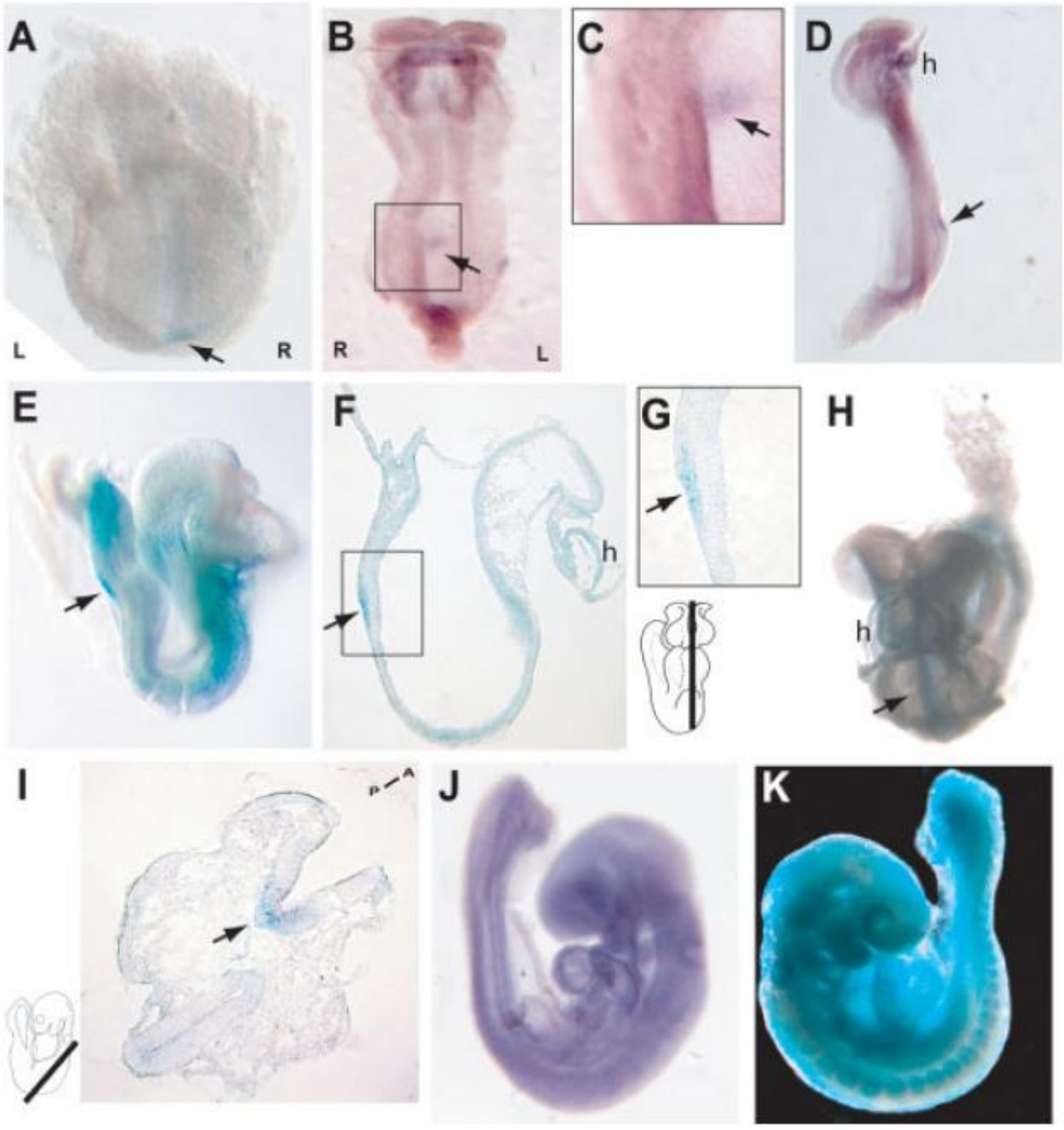
A
L
R
B
R
L
C
D
h
E
F
h
G
H
h
I
J
K

high a proportion of embryonic and early post-natal lethality due to complex congenital heart defects.

Mgrn1 expression in the developing embryo

We determined whether the expression pattern of MGRN1 was consistent with a role in LR patterning. MGRN1 expression was examined in normal mouse embryos from the late neural fold (pre-somite) stage through gastrulation and up to 10.5 d.p.c by *in situ* hybridization of wild-type embryos and X-galactosidase (X-gal) staining of homozygous *Mgrn1*^{XC712} embryos, which carry a gene-trap insertion in intron 17 (Bagher et al., 2006), to visualize the MGRN1-β-GEO fusion protein they produce. X-gal staining and *in situ* hybridization gave comparable results. Embryos were examined in whole mount and/or frozen sections. In pre-somite and early somite-stage embryos, *Mgrn1* was strongly expressed in the node (Figure 3.4A-D) and more weakly in the neuroepithelium. In 6- to 12- somite embryos, *Mgrn1* was strongly expressed in the node, symmetrically in the floorplate of the neural tube, and in the developing heart (Figure 3.4E-I). Weaker staining was observed in paraxial mesoderm, somites, the neuroepithelium and the hind- and fore-gut pockets. By E9.5, expression was virtually ubiquitous (Figure 3.4J-K).

Mgrn1 acts downstream of *Nodal* but upstream of *Lefty-1, Lefty-2* and *Pitx2*

To determine where MGRN1 acts in the known LR patterning pathway, we examined the expression of the (normally) asymmetrically expressed genes *Nodal*, *Lefty1*, *Lefty2* and *Pitx2* in *Mgrn1*$^{md\text{-}nc}$ and *Mgrn1*$^{md\text{-}2J}$ mutant embryos. In control embryos (Figure 3.5A and Table 3.4), *Nodal* was expressed in the node at pre- and early-somite stages and in the left LPM from 3-4 somites until 8-10 somites, consistent with other reports (L. A. Lowe et al., 1996). *Nodal* expression was normal in 98% (47/48) of *Mgrn1* mutant embryos examined (Figure 3.5A-B and Table 3.4). One *Mgrn1*$^{md\text{-}2J}$ homozygote had no *Nodal* expression in the node and bilateral

expression in the cardiac LPM (Figure 3.5C and Table 3.4). For *Lefty1*, *Lefty2* and *Pitx2*, abnormal patterns of expression were observed in a large proportion (17-50%) of *Mgrn1* mutant embryos (Figure 3.5D-L and Table 3.3). In control embryos, *Lefty1* was expressed in the midline and *Lefty2* was expressed in the left LPM (Figure 3.5D). In *Mgrn1* mutant embryos, *Lefty1* was either normal (76%) or absent (24%) while *Lefty2* was normal (50%), reversed (right-sided only; 3%), symmetric (bilateral; 25%) or absent (22%) (Figure 3.5E-I and Table 3.4). Mis-expression of *Lefty2* in *Mgrn1* mutant embryos did not correspond with absence of *Lefty1* expression, supporting the hypothesis that NODAL activates *Lefty2* independent of *Lefty1* (Hiroshi Hamada et al., 2002; Mercola, 2003). In control embryos, *Pitx2* was expressed in the headfold region and left LPM (Figure 3.5J). *Pitx2* expression was normal in the headfold region of all *Mgrn1* mutant embryos examined but either normal (66.7%), reversed (3.9%), symmetric (5.9%) or absent (23.5%) in the LPM (Figure 3.5K-L and Table 3.3). These observations suggest that *Mgrn1* acts early in LR patterning. It is intriguing that such a small proportion of *Mgrn1* mutants show abnormal expression of *Nodal* relative to the proportion with altered expression of other NODAL target genes. It is possible that a higher proportion of mutant embryos show low levels of aberrant *Nodal* expression that cannot be detected by *in situ* hybridization but can impact the expression of downstream target genes. However, the observation that the vast majority of *Mgrn1* mutant embryos express *Nodal* in the node would not explain the high frequency at which no *Lefty1* expression was observed in the floorplate, given that *Nodal* expression in the node induces *Lefty1* expression. In addition, *Nodal* expression was always observed in the left LPM yet more than 25% of *Mgrn1* mutants displayed no detectable *Lefty2* expression in the left LPM. Thus, our results are particularly intriguing as *Nodal* expression appears to be uncoupled from

Figure 3.5. *In situ* hybridization analysis of *Nodal, Lefty* and *Pitx2 e*xpression in *Mgrn1* mutant embryos. (**A-C**) Ventral views of *Nodal* expression in 5 somite C3H/HeJ (control) (**A**) and 3 somite *Mgrn1*$^{md\text{-}2Jmd\text{-}/2J}$ (**B**) embryos showing normal expression in the node and left lateral plate (lpm) mesoderm in both. One 6 somite, *Mgrn1*$^{md\text{-}2Jmd\text{-}/2J}$, embryo (**C**) expressed reduced levels of *Nodal* bilaterally in the cardiac lateral plate mesoderm (arrows). (**D-I**) Normal and various patterns of abnormal *Lefty1/2* expression were observed in 8-8.5 d.p.c. C3H/HeJ and *Mgrn1* mutant embryos. Ventral views of a C3H/HeJ (**D**) and *Mgrn1*$^{md\text{-}nc/md\text{-}nc}$ (**E**) embryo with normal *Lefty1* expression in the floorplate and normal *Lefty2* expression in the left lpm**,** and *Mgrn1*$^{md\text{-}2J/md\text{-}2J}$ embryos with no *Lefty1* expression in the floorplate and normal *Lefty2* expression in the left lpm (**F**)**,** no *Lefty1* in the floorplate and bilateral *Lefty2* in the lpm (**G**), no *Lefty1* expression in the floorplate and strong *Lefty2* expression in the right lpm (low level of *Lefty2* expression in the left lpm) (**H**) and normal *Lefty1* expression in the floorplate and symmetric *Lefty2* expression in the right and left lpm (**I**). (**J-L**) Normal and various patterns of abnormal *Pitx2* expression were also observed in 8-8.5 d.p.c. *Mgrn1* mutant embryos. Ventral views of C3H/HeJ (**J**) and *Mgrn1*$^{md\text{-}2J/md\text{-}2J}$ embryos with normal *Pitx2* expression in the headfold and in the left lpm (**K**) and normal *Pitx2* expression in the headfold and symmetric expression in the right and left lpm (**L**).

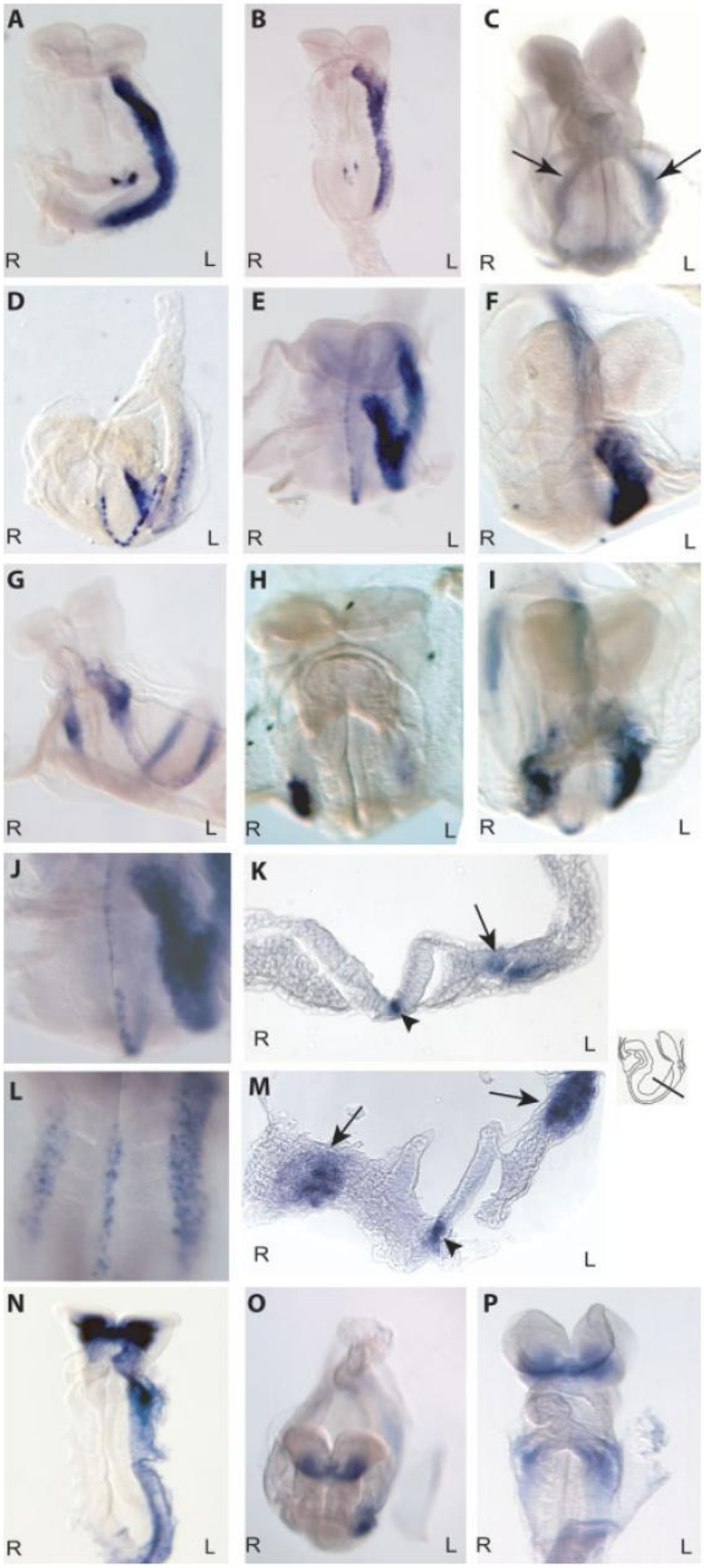
A
R
L
B
R
L
C
R
L
D
R
L
E
R
L
F
R
L
G
R
L
H
R
L
I
R
L
J
K
R
L
L
M
R
L
N
R
L
O
R
L
P
R
L

Table 3.4. Asymmetric gene expression in *Mgrn1* mutant embryos

			LPM				Node		
Gene	Genotype	Somites	% Left	% Right	% Bilateral	% Absent	% Normal	% Absent	Total (n)
Nodal	+/+[1]	0-2	---	---	---	---	100	---	2
		3-7	100	---	---	---	100	---	15
		8-10	100	---	---	---	100	---	5
	Mgrn1$^{md\text{-}nc/md\text{-}nc}$	0-2	---	---	---	---	100	---	5
		3-7	100	---	---	---	100	---	10
		8-10	50	---	---	50	50	50	8
	Mgrn1$^{md\text{-}2J/md\text{-}2J}$	0-2	---	---	---	---	100	---	1
		3-7	91.7	---	8.3 [2]	---	91.7	8.3 [2]	12
		8-10	41.7	---	---	58.3	41.7	58.3	12
Lefty2 [3,4]	+/+[1]	4-8	100 (0)	---	---	---			16
	Mgrn1$^{md\text{-}nc/mc\text{-}nc}$	4-8	50 (3)	---	22.2 (0)	27.8 (1)			18
	Mgrn1$^{md\text{-}2J/md\text{-}2J}$	4-8	27.3 (1)	9 (0)	36.4 (2)	27.3 (1)			11
Pitx2	+/+*	5-12	100	---	---	---			8
		13-21	100	---	---	---			27
	Mgrn1$^{md\text{-}nc/mc\text{-}nc}$	5-12	50	8.3	---	41.7			12
		13-21	66.6	16.7	---	16.7			6
	Mgrn1$^{md\text{-}2J/md\text{-}2J}$	5-12	71.5	---	7.1	21.4			14
		13-21	73.7	---	10.5	15.8			19

			Floorplate			
			% Left	% Right	% Bilateral	% Absent
Lefty1 [3]	+/+[1]	2-7	100	---	---	---
	Mgrn1$^{md\text{-}nc/md\text{-}nc}$	2-7	66.7	---	---	33.3
	Mgrn1$^{md\text{-}2J/md\text{-}2J}$	2-7	75	---	---	25

[1] +/+ (control) embryos were collected from 129S1/SvImJ and/or C3H/HeJ animals

[2] *Nodal* expression in 1 *Mgrn1*$^{md\text{-}2J/md\text{-}2J}$ embryo (Fig. 5C) was bilateral in the cardiac LPM and absent from the node

[3] *Lefty1* and *Lefty2* expression were detected simultaneously using a single probe

[4] Number of embryos scored for *Lefty2* expression with abnormal (absent) *Lefty1* expression indicated in ( ) after %

expression of the *Lefty* genes and *Pitx2* in *Mgrn1* mutant embryos. This suggests a novel mechanism of gene regulation. To our knowledge, our work demonstrates the first instance of a component of the ubiquitination pathway being involved in LR patterning.

DISCUSSION

We have identified a novel role for the MGRN1 ubiquitin ligase in LR patterning. Ubiquitination has been implicated in regulation of transcription (Z.-W. Sun et al., 2002; Gillette et al., 2004), endocytic trafficking and receptor down-regulation (Stang et al., 2000; Haglund et al., 2003) and marking of proteins for degradation by the 26S proteasome (Pickart, 2004). Based on gene expression patterns in *Mgrn1* mutant mice, *Mgrn1* acts early in the LR signaling cascade. MGRN1 is strongly expressed in the node from pre-somite stages onward, preceding asymmetric expression of *Nodal*. At later stages, it is also expressed in the floorplate but no significant or asymmetric expression was detected in the LPM. This expression pattern suggests that MGRN1 could be involved in early LR patterning in the node as well as later events, perhaps contributing to the midline barrier. Intriguingly, *Nodal* expression was normal in the node and LPM in the vast majority of *Mgrn1* mutant embryos yet other nodal-responsive genes (*Lefty1*, *Lefty2*, *Pitx2*) showed high frequencies of aberrant expression. This suggests that understanding the role of MGRN1 in LR patterning will provide new insight into the previously described signaling pathways involved in this critical developmental process.

A high proportion of *Mgrn1* mutant embryos develop CHDs that are consistent with LR patterning defects. MGRN1 is expressed in the developing heart, however, and in neuroepithelial cells (most likely including neural crest cells). Some of the CHDs observed in *Mgrn1* mutant mice, such as double outlet right ventricle and malposition of the great arteries, could also result from neural crest cell defects (Kirby and Waldo, 1995). It will be of future interest to examine whether *Mgrn1* has a role in heart development independent of its role in LR patterning.

CONCLUSIONS

While the pigment defects in *Mgrn1* mutants have been extensively studied and defects in the embryonic viability of these animals had been previously reported, no prior studies had sought to identify the underlying defects in these mice. My analysis of the expression of genes required for proper patterning of the LR axis in *Mgrn1* mutant embryos has revealed a requirement for *Mgrn1* in this process. The precise mechanism by which MGRN1 mediates LR patterning is unknown, however, it is likely that ubiquitin-mediated trafficking and/or degradation of MGRN1 target proteins will be required. Future work should focus on the identification of the direct MGRN1-interacting proteins and the characterization of the role of these interactions in left-right axis specification (see Appendix B). It will be of special interest to determine contribution of MGRN1's ligase activity to these processes.

ACKNOWLEDGEMENTS

Lori Mon Tam and Lisa Lai-Ming Chan for assistance with early *in situ* hybridization experiments, Hiroshi Hamada and Timothy O'Brien and Ian Welsh for *in situ* probes and/or advice on the *in situ* hybridization protocol, Maria García-García for assistance with agarose embedding of embryos, Drew Noden for assistance with photographing embryos, and Fraz Ahmed Ismat for advice on CHD analysis. This work was supported by AHA Scientist Development Grant #0330010N to T.M.G.

REFERENCES

Bagher, P., Jiao, J., Owen Smith, C., Cota, C. D., & Gunn, T. M. (2006). Characterization of Mahogunin Ring Finger-1 expression in mice. *Pigment cell research / sponsored by the European Society for Pigment Cell Research and the International Pigment Cell Society*, *19*(6), 635-43. doi:10.1111/j.1600-0749.2006.00340.x

Bowers, P. N., Brueckner, M., & Yost, H. J. (1996). The genetics of left-right development and heterotaxia. *Seminars in perinatology*, *20*(6), 577-88. Retrieved from http://www.ncbi.nlm.nih.gov/pubmed/9090782

Brennan, J., Lu, C. C., Norris, D. P., Rodriguez, T. A., Beddington, R. S., & Robertson, E. J. (2001). Nodal signalling in the epiblast patterns the early mouse embryo. *Nature*, *411*(6840), 965-9. doi:10.1038/35082103

Collignon J., V. I., & Robertson, E. J. (1996). Relationship Between Asymmetric nodal Expression and the Direction of Embryonic Turning. *Nature*, *381*, 155-158.

Ferencz, C., Rubin, J. D., McCarter, R. J., Brenner, J. I., Neill, C. A., Perry, L. W., Hepner, S. I., et al. (1985). Congenital heart disease: prevalence at livebirth. The Baltimore-Washington Infant Study. *American journal of epidemiology*, *121*(1), 31-6. Retrieved from http://www.ncbi.nlm.nih.gov/pubmed/3964990

Freed, M. (2001). The pathology, pathophysiology, recognition, and treatment of congenital heart disease. In V. Fuster, R. Alexander, & R. O'Rourke (Eds.), *Hurst's The Heart* (10th ed., pp. 1837-1905). McGraw-Hill.

Gillette, T. G., Gonzalez, F., Delahodde, A., Johnston, S. A., & Kodadek, T. (2004). Physical and functional association of RNA polymerase II and the proteasome. *Proceedings of the National Academy of Sciences of the United States of America*, *101*(16), 5904-9. doi:10.1073/pnas.0305411101

Haglund, K., Di Fiore, P. P., & Dikic, I. (2003). Distinct monoubiquitin signals in receptor endocytosis. *Trends in biochemical sciences*, *28*(11), 598-603. Retrieved from http://www.ncbi.nlm.nih.gov/pubmed/14607090

Hamada, Hiroshi, Meno, C., Watanabe, D., & Saijoh, Y. (2002). Establishment of vertebrate left-right asymmetry. *Nature reviews. Genetics*, *3*(2), 103-13. doi:10.1038/nrg732

He, L., Lu, X.-Y. Y., Jolly, A. F., Eldridge, A. G., Watson, S. J., Jackson, P. K., Barsh, G. S., et al. (2003). Spongiform degeneration in mahoganoid mutant mice. *Science (New York, N.Y.)*, *299*(5607), 710-2. doi:10.1126/science.1079694

IC, O. T. P. W., Welsh, I. C., & O'Brien, T. P. (2000). Loss of late primitive streak mesoderm and interruption of left-right morphogenesis in the Ednrb(s-1Acrg) mutant mouse. *Developmental biology*, *225*(1), 151-68. doi:10.1006/dbio.2000.9814

Kathiriya, I. S., & Srivastava, D. (2000). Left-right asymmetry and cardiac looping: implications for cardiac development and congenital heart disease. *American journal of medical genetics*, *97*(4), 271-9. Retrieved from http://www.ncbi.nlm.nih.gov/pubmed/11376438

Kirby, M. L., & Waldo, K. L. (1995). Neural crest and cardiovascular patterning. *Circulation research*, *77*(2), 211-5. Retrieved from http://www.ncbi.nlm.nih.gov/pubmed/7614707

Krebs, L. T., Iwai, N., Nonaka, S., Welsh, I. C., Lan, Y., Jiang, R., Saijoh, Y., et al. (2003). Notch signaling regulates left-right asymmetry determination by inducing Nodal expression. *Genes & development*, *17*(10), 1207-12. doi:10.1101/gad.1084703

Lane, P. W. (1960). New Mutants. *Mouse News Letter*, *22*, 35.

Lowe, L. A., Supp, D. M., Sampath, K., Yokoyama, T., Wright, C. V., Potter, S. S., Overbeek, P., et al. (1996). Conserved left-right asymmetry of nodal expression and alterations in murine situs inversus. *Nature*, *381*(6578), 158-61. doi:10.1038/381158a0

McGrath, J., Somlo, S., Makova, S., Tian, X., & Brueckner, M. (2003). Two populations of node monocilia initiate left-right asymmetry in the mouse. *Cell*, *114*(1), 61-73. Retrieved from http://www.ncbi.nlm.nih.gov/pubmed/12859898

Meno, C, Saijoh, Y., Fujii, H., Ikeda, M., Yokoyama, T., Yokoyama, M., Toyoda, Y., et al. (1996). Left-right asymmetric expression of the TGF beta-family member lefty in mouse embryos. *Nature*, *381*(6578), 151-5. doi:10.1038/381151a0

Meno, C, Shimono, A., Saijoh, Y., Yashiro, K., Mochida, K., Ohishi, S., Noji, S., et al. (1998). lefty-1 is required for left-right determination as a regulator of lefty-2 and nodal. *Cell*, *94*(3), 287-97. Retrieved from http://www.ncbi.nlm.nih.gov/pubmed/9708731

Meno, C, Takeuchi, J., Sakuma, R., Koshiba-Takeuchi, K., Ohishi, S., Saijoh, Y., Miyazaki, J., et al. (2001). Diffusion of nodal signaling activity in the absence of the feedback inhibitor Lefty2. *Developmental cell*, *1*(1), 127-38. Retrieved from http://www.ncbi.nlm.nih.gov/pubmed/11703930

Mercola, M. (2003). Left-right asymmetry: nodal points. *Journal of cell science*, *116*(Pt 16), 3251-7. doi:10.1242/jcs.00668

Miller, K. A., Gunn, T. M., Carrasquillo, M. M., Lamoreux, M. L., Galbraith, D. B., & Barsh, G. S. (1997). Genetic studies of the mouse mutations mahogany and mahoganoid. *Genetics*, *146*(4), 1407-15. Retrieved from http://www.pubmedcentral.nih.gov/articlerender.fcgi?artid=1208084&tool=pmcentrez&rendertype=abstract

Nonaka, S, Tanaka, Y., Okada, Y., Takeda, S., Harada, A., Kanai, Y., Kido, M., et al. (1998). Randomization of left-right asymmetry due to loss of nodal cilia generating leftward flow of extraembryonic fluid in mice lacking KIF3B motor protein. *Cell*, *95*(6), 829-37. Retrieved from http://www.ncbi.nlm.nih.gov/pubmed/9865700

Nonaka, Shigenori, Shiratori, H., Saijoh, Y., & Hamada, H. (2002). Determination of left-right patterning of the mouse embryo by artificial nodal flow. *Nature*, *418*(6893), 96-9. doi:10.1038/nature00849

Okada, Yasushi, Takeda, S., Tanaka, Y., Izpisúa Belmonte, J.-C., & Hirokawa, N. (2005). Mechanism of nodal flow: a conserved symmetry breaking event in left-right axis determination. *Cell*, *121*(4), 633-44. doi:10.1016/j.cell.2005.04.008

Pennekamp, P., Karcher, C., Fischer, A., Schweickert, A., Skryabin, B., Horst, J., Blum, M., et al. (2002). The ion channel polycystin-2 is required for left-right axis determination in mice. *Current biology : CB*, *12*(11), 938-43. Retrieved from http://www.ncbi.nlm.nih.gov/pubmed/12062060

Phan, L. K., Lin, F., LeDuc, C. A., Chung, W. K., & Leibel, R. L. (2002). The mouse mahoganoid coat color mutation disrupts a novel C3HC4 RING domain protein. *The Journal of clinical investigation*, *110*(10), 1449-59. doi:10.1172/JCI16131

Phillips, R. J. (1963). New Mutant: non-agouti curly. *Mouse News Letter*, *29*, 38.

Phillips, R. J. (1971). Non-agouti curly (nc). *Mouse News Letter*, *45*, 25.

Pickart, C. M. (2004). Back to the future with ubiquitin. *Cell*, *116*(2), 181-90. Retrieved from http://www.ncbi.nlm.nih.gov/pubmed/14744430

Ramsdell, A. F. (2005). Left-right asymmetry and congenital cardiac defects: getting to the heart of the matter in vertebrate left-right axis determination. *Developmental biology*, *288*(1), 1-20. doi:10.1016/j.ydbio.2005.07.038

Raya, A., Kawakami, Y., Rodriguez-Esteban, C., Buscher, D., Koth, C. M., Itoh, T., Morita, M., et al. (2003). Notch activity induces Nodal expression and mediates the establishment of left-right asymmetry in vertebrate embryos. *Genes & development*, *17*(10), 1213-8. doi:10.1101/gad.1084403

Raya, A., Kawakami, Y., Rodríguez-Esteban, C., Ibañes, M., Rasskin-Gutman, D., Rodríguez-León, J., Büscher, D., et al. (2004). Notch activity acts as a sensor for extracellular calcium during vertebrate left-right determination. *Nature*, *427*(6970), 121-8. doi:10.1038/nature02190

Stang, E., Johannessen, L. E., Knardal, S. L., & Madshus, I. H. (2000). Polyubiquitination of the epidermal growth factor receptor occurs at the plasma membrane upon ligand-induced activation. *The Journal of biological chemistry*, *275*(18), 13940-7. Retrieved from http://www.ncbi.nlm.nih.gov/pubmed/10788520

Sun, Z.-W., Allis, C. D., & Sun Z.W. (2002). Ubiquitination of histone H2B regulates H3 methylation and gene silencing in yeast. *Nature*, *418*(6893), 104-8. doi:10.1038/nature00883

Sweet, H., & Davisson, M. (1995). Remutations at The Jackson Laboratory (Update to Mouse Genome 1993; 91:862-5 - J16313). *Mouse Genome*, *93*, 1030-1034.

Tanaka, Yosuke, Okada, Y., & Hirokawa, N. (2005). FGF-induced vesicular release of Sonic hedgehog and retinoic acid in leftward nodal flow is critical for left-right determination. *Nature*, *435*(7039), 172-7. Macmillian Magazines Ltd. doi:10.1038/nature03494

Walmsley, R., Hishitani, T., Sandor, G. G. S., Lim, K., Duncan, W., Tessier, F., Farquharson, D. F., et al. (2004). Diagnosis and outcome of dextrocardia diagnosed in the fetus. *The American journal of cardiology*, *94*(1), 141-3. doi:10.1016/j.amjcard.2004.03.049

Yamamoto, M., Mine, N., Mochida, K., Sakai, Y., Saijoh, Y., Meno, C., & Hamada, H. (2003). Nodal signaling induces the midline barrier by activating Nodal expression in the lateral plate. *Development (Cambridge, England)*, *130*(9), 1795-804. Retrieved from http://www.ncbi.nlm.nih.gov/pubmed/12642485

Yoshioka, H., Meno, C., Koshiba, K., Sugihara, M., Itoh, H., Ishimaru, Y., Inoue, T., et al. (1998). Pitx2, a bicoid-type homeobox gene, is involved in a lefty-signaling pathway in determination of left-right asymmetry. *Cell*, *94*(3), 299-305. Retrieved from http://www.ncbi.nlm.nih.gov/pubmed/9708732

CHAPTER 4

Conclusions and future directions.[1]

[1]Reference Cota et al., 2006 of this chapter is also Chapter 3 of this dissertation.

The study of spontaneous and chemically-derived mutations in the mouse have enabled the identification of numerous genes with previously unknown roles in regulating the various cellular and morphological process required for proper mammalian development (Lyon, MF and Searle, 1989; Holdener-Kenny et al., 1992; Kasarskis et al., 1998; García-García et al., 2005; Kile et al., 2003; Boles et al., 2009; Herron et al., 2002; Wilson et al., 2005; Stottmann et al., 2011; Sandell et al., 2011). The goal of the work presented in this dissertation was to identify genes with novel roles in regulating the development of the mammalian embryo. The study of the ENU-derived mutant *cetus* presented in Chapter 2 identified a novel leucine-to-proline mutation in the DEAD/H-box helicase, *Ddx11*, that results in severe defects in somitic mesoderm. In Chapter 3, I presented data demonstrating that defects in patterning of the LR axis are responsible for the reduced viability of mice with mutations in the E3 ubiquitin ligase, MGRN1 (Cota et al., 2006). In this chapter I present overall conclusions from each of these studies as well as ideas for future lines of investigation.

Mutations in Ddx11 result in mid-gestation embryonic lethality in the mouse

Loss of sister chromatid cohesion and cohesion-associated factors have been associated with defects in chromosome segregation, as well as defects in embryonic development (Robert V Skibbens, 2005; Dorsett, 2011; Wood et al., 2010). The identification and characterization of defects in chromosome segregation and mitotic progression in $Ddx11^{KO}$ mice is supportive of previous data from the analysis of loss-of-function mutations in yeast, mouse and human that DDX11 plays a critical and conserved role in the establishment of sister chromatid cohesion (Parish et al., 2006; A. Inoue et al., 2007; Farina et al., 2008; R. V. Skibbens, 2004; Leman et al., 2010). Furthermore, the generation of $Ddx11^{KO}$ mice uncovered a specific requirement for this gene in embryonic development (A. Inoue et al., 2007). However, precisely how cohesion establishment factors like DDX11 and its interacting partners (e.g. Ctf18-RFC) themselves

contribute to the process of sister chromatid cohesion and thereby promote genome stability remains unclear.

Previous work done to characterize the null allele of *Ddx11* in the mouse revealed defects in sister chromatid cohesion, and concluded that death of these embryos was due to a failure of proper chorio-allantoic fusion (A. Inoue et al., 2007). In Chapter 2 of this dissertation I present data from my analysis of *cetus* mutants. Positional cloning and complementation analysis of *cetus* revealed a point mutation in *Ddx11* which severely disrupts the function of this gene in mice. *cetus* mutant embryos displayed an extreme and specific reduction of somitic mesoderm, a phenotype which had not previously been described in *Ddx11* mutant embryos.

In order to identify the mechanism underlying the somitic mesoderm defects in *cetus* mutants, I analyzed the expression pattern of the *Ddx11* transcript in embryos by *in situ* hybridization. These experiments found that the *Ddx11* gene was widely expressed throughout the embryonic and extra-embryonic tissues at mid-gestation indicating that the expression pattern of the gene could not alone explain the differential requirement for *Ddx11* within the embryo. Analysis of cell death in gastrulating *Ddx11* mutant embryos showed a massive increase in apoptosis in comparison to wildtype embryos. However, this apoptosis was not confined to the mesoderm of mutant embryos. These results, along with data from analysis of the effects of mutations in genes with similar roles in promoting genome stability that also display a loss of somitic mesoderm; suggest that variations in sensitivity to genomic instability may exist between different cell populations within the embryo. Further studies of cell cycle regulation in the mammalian embryo are needed to fully appreciate the extent of these variations.

Determining the molecular defects in *cetus* mutants

In an attempt to identify the molecular defect in DDX11 caused by the *cetus* mutation, I assayed the ATP hydrolysis and DNA binding activity of recombinant HIS/SUMO-DDX11^{WT}

and HIS/SUMO-DDX11^{cetus} protein. My data suggests that these biochemical activities, while required for proper sister chromatid cohesion (A. Inoue et al., 2007), may not themselves be sufficient for the process. A numbers of studies have shown the helicase activity of FANCJ family helicases, including DDX11, to be both ATP and DNA-dependent (Y Wu et al., 2009; Hirota and J M Lahti, 2000; Farina et al., 2008; Gupta et al., 2007). Future work should directly address the effect of the *cetus* mutation on DDX11 helicase activity. Such studies would definitively answer a prevalent question in the field of cohesion; is helicase activity required for sister chromatid cohesion?

Previous studies have identified physical interactions between DDX11 and components of the cohesin complex as well as cohesion establishment factors and components of the replication fork machinery (Parish et al., 2006; Farina et al., 2008; Leman et al., 2010). It is possible that the *cetus* mutation disrupts one or more of these interactions which is crucial for development of the embryo. In order to begin addressing this possibility, I conducted co-immunoprecipitation experiments to assess the ability of the DDX11^{cetus} protein to interact with the cohesin complex (Appendix A). These experiments, while not exhaustive, showed no defect in the ability of DDX11^{cetus} to interact with RAD21 or SCC1, two core components of the cohesion complex. It remains possible that another known DDX11 protein interaction is disrupted by the *cetus* mutation and future experiments to assess these interactions should be conducted. Alternatively, the *cetus* mutation may disrupt the interaction of the DDX11 with other as yet unidentified effector proteins. This could be addressed by conducting yeast-2-hybrid experiments.

The identification and characterization of the *cetus* mutation in *Ddx11* has identified a previously unreported requirement for this gene in mesoderm development. Despite the relevance to human disease, little is known about the roles of FANCJ helicases in development.

Future studies should be directed at identifying the precise molecular function of DDX11 that is perturbed in *cetus* mutants.

Loss of MGRN1 results in defects in LR patterning

Significant progress has been made in understanding the genetic and molecular mechanisms that pattern the left-right axis over the past fifteen years. Following the initial identification of asymmetric *Nodal* expression in the chick (M Levin et al., 1995), studies in mouse, chick and xenopus have identified a network of asymmetrically expressed genes, ions and transport mechanisms (C Meno et al., 1998; Yoshioka et al., 1998; M. Yamamoto et al., 2003; C Meno et al., 1996; Collignon J. and E J Robertson, 1996; Michael Levin et al., 2002; Aw et al., 2010; Morokuma et al., 2008). How these signals are regulated is less well understood.

In Chapter 3, I present data from the phenotypic analysis of embryonic defects in mice with loss-of-function mutations in *Mgrn1*. The discovery of *situs inversus* in a small proportion of adult *Mgrn1*$^{md\text{-}nc}$ mutant mice raised the possibility that defects in LR axis specification might underlie the lethality in these mutants. In order to address this possibility I assayed the expression patterns of genes required for proper LR-patterning of the embryo in *Mgrn1* mutants. These experiments showed that loss of Mgrn1 results mis-expression of NODAL target genes controlling left-right patterning including *Lefty1*, *Lefty2* and *Pitx2*.

Work in mice by Meno et al. (C Meno et al., 1998) established the foundation for what has become the prevailing hypothesis regarding the mechanism of maintaining left-specific expression domains in the embryo. It is believed that the left-specific expression domain of *Nodal* in the LPM is maintained by antagonism at the level of the NODAL co-receptor, CRIPTO, by LEFTY-1 present in the midline. Data presented in this dissertation demonstrating ectopic right-sided induction of *Nodal* signaling in the LPM in the presence of unperturbed *Lefty-1* expression was among the first to challenge this hypothesis (Cota et al., 2006). More recent

data from zebrafish models suggest that *Lefty-1* in the midline alone is not sufficient to prevent the propagation of *Nodal* and associated downstream nodal signaling to the right LPM and shows evidence for the existence of at least two additional barrier signals (Lenhart et al., 2011). Future studies are required to confirm the relevance of these signals in other model organisms. If these barrier mechanisms are functional in the mouse it would be interesting to examine them in the context of the *Mgrn1* mutations to determine what, if any, role this gene might be playing.

Identifying MGRN1 interacting proteins required for LR patterning

The data presented in Chapter 3 of this dissertation identifies MGRN1 as the first and only ubiquitin ligase which has been shown to date to have a direct role in left-right patterning. Ubiquitination has been implicated in diverse set of cellular processes from protein degradation to receptor trafficking and desensitization (Komander, 2009). Ubiquitin ligase proteins provide specificity to the ubiquitination process by interacting directly with target proteins (Hershko et al., 1986), therefore identifying MGRN1 interacting proteins is essential for determining the precise mechanism of MGRN1-mediated LR patterning. In order to address this, I conducted a series of yeast-2-hybrid experiments (Appendix B). These experiments identified a number of putative MGRN1 interacting proteins, including the previously validated MGRN1 interacting protein, TSG101(Jiao, K. Sun, et al., 2009; B Y Kim, J A Olzmann, et al., 2007). However, none of the MGRN1 interacting proteins identified in these screens have previously reported roles in LR patterning. While it is possible, despite a lack of evidence, that one or more of these proteins does have a role in LR axis specification; it likely that further experiments will be required to identify the interaction required for MGRN1-mediated LR patterning. Yeast-2-hybrid screens using a full-length MGRN1 construct would likely identify additional, more complex, interactions that require multiple regions MGRN1. Once a protein of interest is identified, it will be necessary to determine contribution of MGRN1's ligase activity to these processes using *in*

vitro and *in vivo* ubiquitination assays.

The characterization of patterning defects in *Mgrn1* mutants has expanded the current knowledge of MGRN1-mediated functions in the mouse and has identified MGRN1 as a novel regulator of LR axis establishment. Future studies should be aimed at identifying MGRN1 target proteins and improving our understanding of the role of MGRN1's ubiquitin ligase activity in patterning of the embryo.

In summary, the study of mutant mice has uncovered many genes are required for the proper development of the embryo. Characterization of the embryonic defects present in *Ddx11*^{cetus} and *Mgrn1* mutant mice has uncovered novel roles for these genes. Future studies to characterize the molecular mechanisms used by DDX11 and MGRN1 will add to our understanding of the roles of these proteins during development of the mammalian embryo.

REFERENCES

Aw, S., Koster, J. C., Pearson, W., Nichols, C. G., Shi, N.-Q., Carneiro, K., and Levin, Michael (2010). The ATP-sensitive K(+)-channel (K(ATP)) controls early left-right patterning in Xenopus and chick embryos. *Developmental biology*, **346**, 39-53.

Boles, M. K., Wilkinson, B. M., Maxwell, A., Lai, L., Mills, A. A., Nishijima, I., Salinger, A. P., Moskowitz, I., Hirschi, K. K., Liu, B., et al. (2009). A mouse chromosome 4 balancer ENU-mutagenesis screen isolates eleven lethal lines. *BMC genetics*, **10**, 12.

Collignon J., V. I. and Robertson, E. J. (1996). Relationship Between Asymmetric nodal Expression and the Direction of Embryonic Turning. *Nature*, **381**, 155-158.

Cota, C. D., Bagher, P., Pelc, P., Smith, C. O., Bodner, C. R., and Gunn, T. M. (2006). Mice with mutations in Mahogunin ring finger-1 (Mgrn1) exhibit abnormal patterning of the left-right axis. *Developmental dynamics : an official publication of the American Association of Anatomists*, **235**, 3438-47.

Dorsett, D. (2011). Cohesin: genomic insights into controlling gene transcription and development. *Current opinion in genetics & development*, **21**, 199-206.

Farina, A., Shin, J.-H., Kim, D.-H., Bermudez, V. P., Kelman, Z., Seo, Y.-S., and Hurwitz, J. (2008). Studies with the human cohesin establishment factor, ChlR1. Association of ChlR1 with Ctf18-RFC and Fen1. *The Journal of biological chemistry*, **283**, 20925-36.

García-García, M. J., Eggenschwiler, J. T., Caspary, T., Alcorn, H. L., Wyler, M. R., Huangfu, D., Rakeman, A. S., Lee, J. D., Feinberg, E. H., Timmer, J. R., et al. (2005). Analysis of mouse embryonic patterning and morphogenesis by forward genetics. *Proceedings of the National Academy of Sciences of the United States of America*, **102**, 5913-9.

Gupta, R., Sharma, S., Sommers, J. A., Kenny, M. K., Cantor, S. B., and Brosh, Robert M (2007). FANCJ (BACH1) helicase forms DNA damage inducible foci with replication protein A and interacts physically and functionally with the single-stranded DNA-binding protein. *Blood*, **110**, 2390-8.

Herron, B. J., Lu, W., Rao, C., Liu, S., Peters, H., Bronson, R. T., Justice, M. J., McDonald, J. D., and Beier, David R (2002). Efficient generation and mapping of recessive developmental mutations using ENU mutagenesis. *Nature genetics*, **30**, 185-9.

Hershko, A., Heller, H., Eytan, E., and Reiss, Y. (1986). The protein substrate binding site of the ubiquitin-protein ligase system. *The Journal of biological chemistry*, **261**, 11992-9.

Hirota, Y. and Lahti, J M (2000). Characterization of the enzymatic activity of hChlR1, a novel human DNA helicase. *Nucleic acids research*, **28**, 917-24.

Holdener-Kenny, B., Sharan, S. K., and Magnuson, T. (1992). Mouse albino-deletions: from genetics to genes in development. *BioEssays : news and reviews in molecular, cellular and developmental biology*, **14**, 831-9.

Inoue, A., Li, T., Roby, S. K., Valentine, M. B., Inoue, M., Boyd, K., Kidd, V. J., and Lahti, Jill M (2007). Loss of ChlR1 helicase in mouse causes lethality due to the accumulation of aneuploid cells generated by cohesion defects and placental malformation. *Cell cycle Georgetown Tex*, **6**, 1646-1654.

Jiao, J., Sun, K., Walker, W. P., Bagher, P., Cota, C. D., and Gunn, T. M. (2009). Abnormal regulation of TSG101 in mice with spongiform neurodegeneration. *Biochimica et biophysica acta*, **1792**, 1027-35.

Kasarskis, a, Manova, K., and Anderson, K V (1998). A phenotype-based screen for embryonic lethal mutations in the mouse. *Proceedings of the National Academy of Sciences of the United States of America*, **95**, 7485-90.

Kile, B. T., Hentges, K. E., Clark, A. T., Nakamura, H., Salinger, A. P., Liu, B., Box, N., Stockton, D. W., Johnson, Randy L, Behringer, R. R., et al. (2003). Functional genetic analysis of mouse chromosome 11. *Nature*, **425**, 81-6.

Kim, B. Y., Olzmann, J. A., Barsh, G. S., Chin, L. S., and Li, L. (2007). Spongiform neurodegeneration-associated E3 ligase Mahogunin ubiquitylates TSG101 and regulates endosomal trafficking. *Mol Biol Cell*, **18**, 1129-1142.

Komander, D. (2009). The emerging complexity of protein ubiquitination. *Biochemical Society transactions*, **37**, 937-53.

Leman, A. R., Noguchi, C., Lee, C. Y., and Noguchi, E. (2010). Human Timeless and Tipin stabilize replication forks and facilitate sister-chromatid cohesion. *Journal of cell science*, **123**, 660-70.

Lenhart, K. F., Lin, S.-Y., Titus, T. A., Postlethwait, J. H., and Burdine, R. D. (2011). Two additional midline barriers function with midline lefty1 expression to maintain asymmetric Nodal signaling during left-right axis specification in zebrafish. *Development (Cambridge, England)*, **138**, 4405-10.

Levin, M, Johnson, R L, Stern, C. D., Kuehn, M., and Tabin, C. (1995). A molecular pathway determining left-right asymmetry in chick embryogenesis. *Cell*, **82**, 803-14.

Levin, Michael, Thorlin, T., Robinson, K. R., Nogi, T., and Mercola, M. (2002). Asymmetries in H+/K+-ATPase and cell membrane potentials comprise a very early step in left-right patterning. *Cell*, **111**, 77-89.

Lyon, MF and Searle, A. ed. (1989). Genetic Variants and Strains of the Laboratory Mouse. Second Edi. Oxford University Press, Oxford.

Meno, C, Saijoh, Y, Fujii, H., Ikeda, M., Yokoyama, T., Yokoyama, M., Toyoda, Y., and Hamada, H (1996). Left-right asymmetric expression of the TGF beta-family member lefty in mouse embryos. *Nature*, **381**, 151-5.

Meno, C, Shimono, A., Saijoh, Y, Yashiro, K., Mochida, K, Ohishi, S., Noji, S., Kondoh, H., and Hamada, H (1998). lefty-1 is required for left-right determination as a regulator of lefty-2 and nodal. *Cell*, **94**, 287-97.

Morokuma, J., Blackiston, D., and Levin, Michael (2008). KCNQ1 and KCNE1 K+ channel components are involved in early left-right patterning in Xenopus laevis embryos. *Cellular physiology and biochemistry : international journal of experimental cellular physiology, biochemistry, and pharmacology*, **21**, 357-72.

Parish, J. L., Rosa, J., Wang, X., Lahti, Jill M, Doxsey, S. J., and Androphy, E. J. (2006). The DNA helicase ChlR1 is required for sister chromatid cohesion in mammalian cells. *Journal of cell science*, **119**, 4857-65.

Sandell, L. L., Iulianella, A., Melton, K. R., Lynn, M., Walker, M., Inman, K. E., Bhatt, S., Leroux-Berger, M., Crawford, M., Jones, N. C., et al. (2011). A phenotype-driven ENU mutagenesis screen identifies novel alleles with functional roles in early mouse craniofacial development. *Genesis (New York, N.Y. : 2000)*, **49**, 342-59.

Skibbens, R. V. (2004). Chl1p, a DNA Helicase-Like Protein in Budding Yeast, Functions in Sister-Chromatid Cohesion. *Genetics*, **166**, 33-42.

Skibbens, Robert V (2005). Unzipped and loaded: the role of DNA helicases and RFC clamp-loading complexes in sister chromatid cohesion. *The Journal of cell biology*, **169**, 841-6.

Stottmann, R. W., Moran, J. L., Turbe-Doan, A., Driver, E., Kelley, M., and Beier, D R (2011). Focusing forward genetics: a tripartite ENU screen for neurodevelopmental mutations in the mouse. *Genetics*, **188**, 615-24.

Wilson, L., Ching, Y.-H., Farias, M., Hartford, S. A., Howell, G., Shao, H., Bucan, M., and Schimenti, J. C. (2005). Random mutagenesis of proximal mouse chromosome 5 uncovers predominantly embryonic lethal mutations. *Genome research*, **15**, 1095-105.

Wood, A. J., Severson, A. F., and Meyer, B. J. (2010). Condensin and cohesin complexity: the expanding repertoire of functions. *Nature reviews. Genetics*, **11**, 391-404.

Wu, Y., Suhasini, a N., and Brosh, R M (2009). Welcome the family of FANCJ-like helicases to the block of genome stability maintenance proteins. *Cellular and molecular life sciences : CMLS*, **66**, 1209-22.

Yamamoto, M., Mine, N., Mochida, Kyoko, Sakai, Y., Saijoh, Yukio, Meno, Chikara, and Hamada, Hiroshi (2003). Nodal signaling induces the midline barrier by activating Nodal expression in the lateral plate. *Development (Cambridge, England)*, **130**, 1795-804.

Yoshioka, H., Meno, C, Koshiba, K., Sugihara, M., Itoh, H., Ishimaru, Y., Inoue, T., Ohuchi, H., Semina, E. V., Murray, J. C., et al. (1998). Pitx2, a bicoid-type homeobox gene, is involved in a lefty-signaling pathway in determination of left-right asymmetry. *Cell*, **94**, 299-305.

APPENDIX A

ANALYSIS OF DDX11 INTERACTIONS WITH COHESIN COMPLEX PROTEINS

INTRODUCTION

Previous characterization of the cellular defects present in *Ddx11*^{KO} embryos have provided genetic evidence indicating that DDX11 is required for sister chromatid cohesion and G2-M cell cycle progression in the mouse (A. Inoue et al., 2007). Consistent with these observations, physical interactions between DDX11 and components of the cohesion ring complex, a large ring-shaped multimeric protein complex consisting of four proteins:SMC1, SMC3 and SCC1/RAD21 have also been described (Parish et al., 2006; Leman et al., 2010). While cohesion and cell cycle defects were not directly assayed in the *Ddx11*^{cetus} mutants, it is likely that such defects are present based upon the extensive phenotypic similarity we have seen to the *Ddx11*^{KO} (Chapter 2). In order to address the possibility that the *cetus* mutation might disrupt interactions between DDX11 and the cohesion complex, I conducted a series of immunoprecipitation experiments.

MATERIALS & METHODS

Site-directed mutagenesis

A previously published mammalian expression vector encoding a FLAG-tagged human Ddx11 (ChlR1), pcDNA3-ChlR1-FLAG (DDX11^{WT}-FLAG), was obtained from Eishi Noguchi (Leman et al., 2010). The following set of primers was used to introduce the murine *cetus* mutation (Figure 2.3, Chapter 2) via site-directed mutagenesis in to the pcDNA3-ChlR1-FLAG vector: 5'-ACAGGG GCCTTGCTCCCCTCTGTGGTTGGAG-3' and

5’CTCCAACCACAGAGGGGAGCAAGGCCCCTG T-3’.

Immunoprecipitation (IP)

HEK293T cells were transfected with pcDNA3-FLAG, pcDNA3-ChlR1-FLAG (DDX11^{WT}-FLAG) or pcDNA3-ChlR1^{cetus}-FLAG (DDX11^{cetus}-FLAG) using FUGENE 6 (Roche). Cells were washed twice with ice-cold 1X PBS and lysed with IP lysis buffer (250mM NaCl 50mM Tris (pH 7.5), 1mM Ethylenediaminetetraacetic acid (EDTA), 1% Triton X-100, 0.05% SDS and protease inhibitor cocktail (Roche)). Lysates were cleared by centrifugation at 8,000 rpm for 3 min. Antibodies were pre-bound by 1 hour incubation at 4^{o}C with protein-G magnetic Dynabeads (Invitrogen). Cleared lysates were added to the antibody conjugated beads and incubated for an additional 1 hour at 4^{o}C. Beads were collected and washed four times with IP lysis buffer. Immunoprecipitated proteins were eluted by the addition of 1X SDS loading buffer (0.25 M Tris-HCl (pH 6.8), 10% Glycerol, 1% (w/v) SDS and 0.05% (w/v) Bromophenol Blue) and analyzed by western blot. FLAG-M2 antibody (Sigma), RAD21 (Bethyl Labs), SMC1 (Chemicon) or mouse IgG (Santa Cruz) were used for IP’s and subsequent western blots.

Western Blot

Proteins were denatured by boiling and separated by SDS-PAGE (4-6% w/v acrylamide). Proteins were transferred to polyvinylidene difluoride optimized for fluorescence immunodetection (FL-PVDF) membranes, blocked in either 5% BSA in Tris-buffered saline (pH 7.6). Primary antibody binding was accomplished by overnight incubation of blots at 4^{o}C in Tris-buffered saline (pH 7.6) with 0.1% Tween-20 and 5% BSA. Washes and secondary antibody binding were performed at room temperature in Tris-buffered saline (pH 7.6) with 0.1% Tween-20. Antibodies used included: FLAG-M2 antibody (Sigma, 1:1,500), RAD21 (Bethyl Labs, 1:1,500), SMC1 (Chemicon, 1:1,500), IR Dye 800 or 680LT goat-anti-mouse and goat-anti-

rabbit (LI-COR, 1:15,000). All blots were imaged using an Odyssey CLx infrared imaging system and analyzed using Image Studio Version 2.0 imaging software (LI-COR).

RESULTS & DISCUSSION

In order to assess the effects of the *cetus* mutation on reported interactions between DDX11 and components of the cohesin ring complex (Parish et al., 2006), I introduced the *cetus* mutation in to a previously characterized mammalian expression vector encodinging a FLAG-tagged human DDX11 protein (Leman et al., 2010). The resulting expression constructs were transfected into Hek293T cells (ATCC). Expression of both the DDX11^{WT}-FLAG and the mutant DDX11^{cetus}-FLAG was readily detected in lysates from transfected cells (Figure A1.1 and Figure A1.2) indicating that the introduction of the *cetus* mutation had little effect on the stability of the DDX11-FLAG protein.

As previously reported for the endogenous human DDX11 protein (Parish et al., 2006), components of the cohesion ring complex, SMC1 and RAD21 were readily detected upon immunoprecipitation of the tagged DDX11^{WT}-FLAG with a commercial FLAG antibody (Figure A1.2). The *cetus* mutation did not result in any obvious decrease in either of these interactions in the experiments conducted. These results suggest that the embryonic defects and apparent loss of DDX11 activity observed in *cetus* mutant mice are not due to an inability of the DDX11^{cetus} mutant protein to interact with these components of the cohesin ring complex. My results

CONCLUSIONS

Studies in yeast and human models have identified a role for DDX11 in the establishment of cohesion (Leman et al., 2010; Farina et al., 2008; R. V. Skibbens, 2004). The prevailing hypothesis put forth by Parish et al. (Parish et al., 2006) predicts that DDX11 is required for the loading of the cohesion ring complex on to sister chromatids during DNA replication.

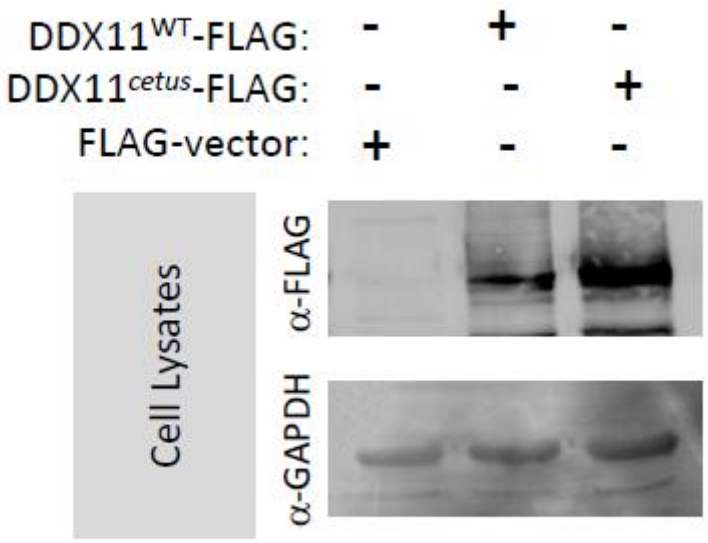

Figure A1.1. Expression of DDX11-FLAG proteins in Hek293T cells. Hek293T cells were transiently transfected with 60ng of FLAG-vector (Lane 1), DDX11^{WT}-FLAG (Lane 2) or DDX11^{cetus}-FLAG (Lane 3). Both the DDX11^{WT}-FLAG and the DDX11^{cetus}-FLAG proteins were readily detected in transfected cell lysates using a FLAG antibody (Sigma). Expression of GAPDH was used as a loading control.

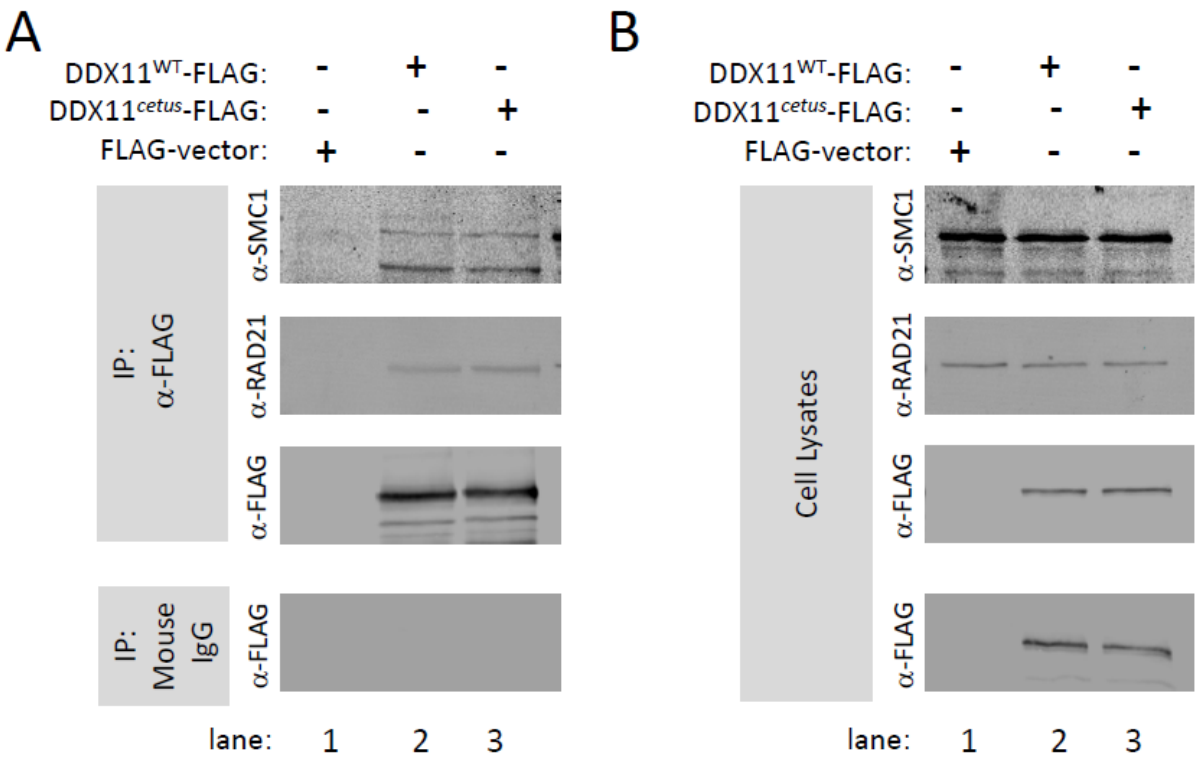

Figure A1.2. DDX11 proteins interact with components of the cohesion ring complex. Hek293T cells were transiently transfected with FLAG-vector (Lane 1), DDX11^{WT}-FLAG (Lane 2) or DDX11^{cetus}-FLAG (Lane 3) were immunoprecipitated with a FLAG antibody (Sigma) and Western blots were performed for components of the cohesion ring complex, SMC1 and RAD21 (A). Immunoprecipitation with mouse IgG was conducted as a negative control for non-specific antibody binding. Endogenous expression of SMC1 and RAD21 as well as the expression of the transfected DDX11 constructs in cell lysates used immunoprecipitation are shown (B).

I have been unable to detect any defects in the interaction between the DDX11^{cetus} protein and components of the cohesin ring complex or in DNA binding (Figure 2.9, Chapter 2). These results may suggest that if DDX11 is required for cohesion loading then neither interaction with cohesion ring complex nor the ability to bind DNA alone is sufficient for the process. Of broader relevance, details on how the cohesin ring complex assembles around sister chromatids remain unclear. It is unknown to what extent cohesion establishment factors like DDX11 influence or are influenced by this assembly (Robert V Skibbens, 2005). Further studies looking at the loading of the cohesion ring complex onto DNA in *Ddx11*^{cetus} mutants would aid in resolving these questions.

ACKNOWLEDGEMENTS

We thank Eishi Noguchi for the generous gift of the pcDNA3-ChlR1-FLAG expression construct. Mark Roberson, Mariana Wolfner, John Schimenti and members of the Garcia-Garcia lab for helpful discussions and comments.

REFERENCES

Farina, A., Shin, J.-H., Kim, D.-H., Bermudez, V. P., Kelman, Z., Seo, Y.-S., and Hurwitz, J. (2008). Studies with the human cohesin establishment factor, ChlR1. Association of ChlR1 with Ctf18-RFC and Fen1. *The Journal of biological chemistry*, **283**, 20925-36.

Inoue, A., Li, T., Roby, S. K., Valentine, M. B., Inoue, M., Boyd, K., Kidd, V. J., and Lahti, J. M. (2007). Loss of ChlR1 helicase in mouse causes lethality due to the accumulation of aneuploid cells generated by cohesion defects and placental malformation. *Cell cycle Georgetown Tex*, **6**, 1646-1654.

Leman, A. R., Noguchi, C., Lee, C. Y., and Noguchi, E. (2010). Human Timeless and Tipin stabilize replication forks and facilitate sister-chromatid cohesion. *Journal of cell science*, **123**, 660-70.

Parish, J. L., Rosa, J., Wang, X., Lahti, J. M., Doxsey, S. J., and Androphy, E. J. (2006). The DNA helicase ChlR1 is required for sister chromatid cohesion in mammalian cells. *Journal of cell science*, **119**, 4857-65.

Skibbens, R. V. (2004). Chl1p, a DNA Helicase-Like Protein in Budding Yeast, Functions in Sister-Chromatid Cohesion. *Genetics*, **166**, 33-42.

Skibbens, Robert V (2005). Unzipped and loaded: the role of DNA helicases and RFC clamp-loading complexes in sister chromatid cohesion. *The Journal of cell biology*, **169**, 841-6.

APPENDIX B

IDENTIFICATION OF MGRN1 INTERACTING PROTEINS

INTRODUCTION

MGRN1 is a C3HC4-RING domain-containing protein that has been shown to function as an E3 ubiquitin ligase both *in vitro* (Lin He et al., 2003) and *in vivo* (Jiao, K. Sun, et al., 2009; Bong Yoon Kim, James A Olzmann, et al., 2007). Protein ubiquitination has been shown to be a key step of signaling in developmental, regulating both components of the canonical WNT and NOTCH pathways (Aberle et al., 1997; Mukai et al., 2010; Hay-Koren et al., 2011; Callow et al., 2011; Berndt et al., 2011; E. C. Lai et al., 2005; Jehn et al., 2002; Qiu et al., 2000). The identification of a direct role for MGRN1 in LR patterning (Chapter 3; Cota et al., 2006) implicated a role for protein ubiquitination in this process which had not previously been identified.

Ubiquitination is a multi-step, hierarchical process whereby the 76-amino acid protein UBIQUITIN is covalently attached to target proteins at lysine or unstable amino-terminal residues. Canonical ubiquitination begins with the binding of UBIQUITIN by an E1 ubiquitin-activating enzyme which, in an ATP-dependent manner, catalyzes in the formation of a thioester bond between the carboxy-termini of the UBIQUITIN molecule and an active site cysteine residue of the E1. The activated UBIQUITIN is then transferred to the active site cysteine residue of an E2 ubiquitin-conjugating enzyme (Schulman and Harper, 2009). Finally an E3 ubiquitin ligase facilitates the transfer of UBIQUITIN from the E2 to the target protein. To date, as many as eight mammalian E1, thirty nine E2 as well as several hundred RING-type E3 proteins have been identified in mammals (Markson et al., 2009; Wenzel et al., 2010; Groettrup et al., 2008) Ubiquitination of proteins has been shown to result in degradation via the ubiquitin-

proteasome system or, in the case of some membrane receptors, changes in receptor trafficking and/or down-regulation of receptor signaling.

As the most downstream component of the ubiquitination process, E3 ubiquitin ligase proteins are the major determinant of specificity in this system. Therefore, the identification of E3 target proteins is essential for determining mechanism for ubiquitin regulation. In order to identify MGRN1 interacting proteins that might play a role in MGRN1-mediated LR pattering events, I performed a series of yeast-2-hybrid experiments.

MATERIALS & METHODS

Yeast-2-Hybrid Screening

Yeast-2-hybrid assays were performed using the ProQuest Two-Hybrid System with Gateway Technology (Invitrogen). *Mgrn1* cDNA fragments encoding regions N- (amino acids 1-278) and C-terminal (amino acids 342-519/532/541) to the RING domain of *Mgrn1* isoforms I, II and III (Figure A2.1) were cloned into the pDEST32 bait vector and screened against a mouse e8.5 embryo cDNA library (ProQuest, Invitrogen). Plasmid DNA was isolated from colonies screened as positive for MGRN1 interactions using a commercial yeast plasmid isolation kit (Clontech). Plasmid DNA was sequenced at the Cornell University Life Sciences Core Laboratory Center (CLC). Gene ontology analysis was performed using the Database for Annotation, Visualization, and Integrated Discovery (DAVID) bioinformatics resource v6.7 (D. W. Huang, Sherman, and Lempicki, 2009a, 2009b).

RESULTS & DISCUSSION

In order to identify MGRN1 interacting proteins that might provide a mechanistic explanation for the left-right patterning defects identified and described in Chapter 3 of this dissertation, yeast-2-hybrid screens were performed using the regions of MGRN1 N- and

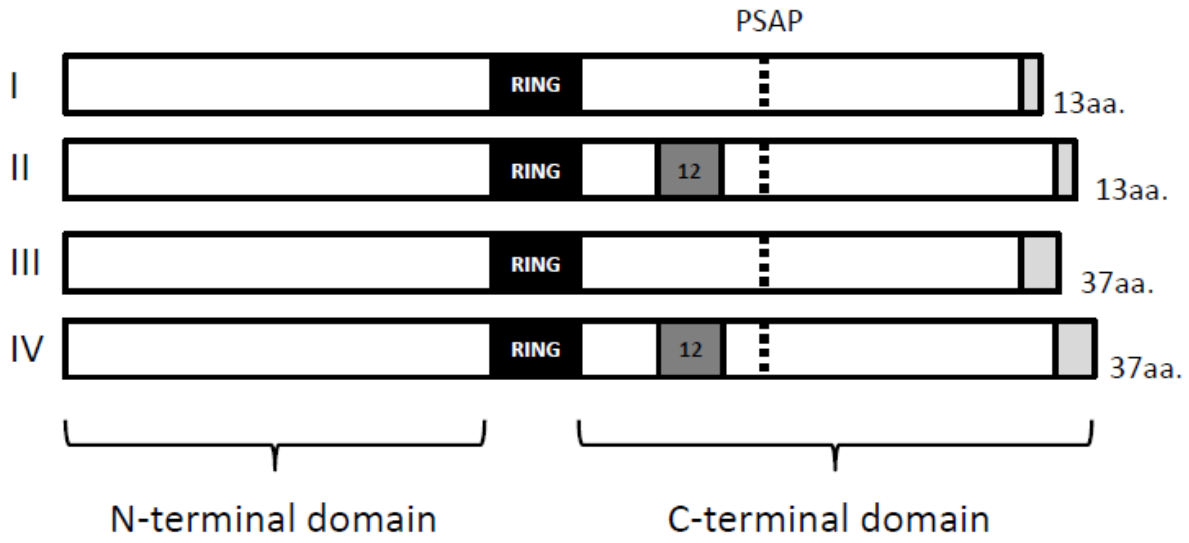

Figure A2.1. ***Mgrn1*** **Isoforms.** *Mgrn1* encodes a C3HC4-RING domain (black box, labeled RING) containing E3 ubiquitin ligase. Alternative splicing of exons 12 (dark grey box, labeled 12) and 17 (light grey boxes, labeled 13aa or 37aa) generate four isoforms (indicated as I, II, III and IV). For yeast-2-hybrid assays, regions were used corresponding to the N-terminal domain or C-terminal domain of isoforms I, II and III. The dotted line indicates the position of the PSAP motif required to mediate interactions with the ESCRT complex protein, TSG101. Figure was adapted from (Jiao, K. Sun, et al., 2009).

Table A2.1. MGRN1 interacting proteins

Gene Symbol	Gene Name	Mgrn1 Fragment
CEP120	centrosomal protein 120	CIII
Epdr1	ependymin related protein 1 (zebrafish)	N
lbp	lipopolysaccharide binding protein	CIII
LdhA	lactate dehydrogenase A	CI
DDX49	DEAD (Asp-Glu-Ala-Asp) box polypeptide 49	CII
Ctsl	cathepsin L	CIII
Snora65	small nucleolar RNA, H/ACA box 65	CIII
HOXA11	homeo box A11	CIII
EEF1G	eukaryotic translation elongation factor 1 gamma	CIII
RBMS1	RNA binding motif, single stranded interacting protein 1	CIII
COL4A4	collagen, type IV, alpha 4	CIII
Rps13	ribosomal protein S13	CIII
gltP	glycolipid transfer protein	CIII
SPHK2	sphingosine kinase 2	CIII
Mt1	metallothionein 1	CIII
RBMS2	RNA binding motif, single stranded interacting protein 2	CIII
NPPB	natriuretic peptide precursor type B	CII
Mrpl23	mitochondrial ribosomal protein L39	CIII
PRKCI	protein kinase C, iota	CIII
GANAB	alpha glucosidase 2 alpha neutral subunit	CI
Rps4	ribosomal protein S4, Y-linked 2	N
RBM10	RNA binding motif protein 10	CIII
CSNK1G2	casein kinase 1, gamma 2	CIII
TSG101	tumor susceptibility gene 101	CI
Rps9	ribosomal protein S9	CIII
Rpl23	ribosomal protein L23	CIII
CD9	CD9 antigen	CII
psmc1	protease (prosome, macropain) 26S subunit, ATPase 1	CI
Gpx5	glutathione peroxidase 5	CIII
CPE	carboxypeptidase E	CI
Prl8a2	prolactin family 8, subfamily a, member 2	CI, CIII
NPPA	natriuretic peptide precursor type A	CIII
ATF1	activating transcription factor 1	N
GNGT1	guanine nucleotide binding protein (G protein)	CIII
Papln	papilin	CI
Ctla2a	cytotoxic T lymphocyte-associated protein 2 alpha	CIII

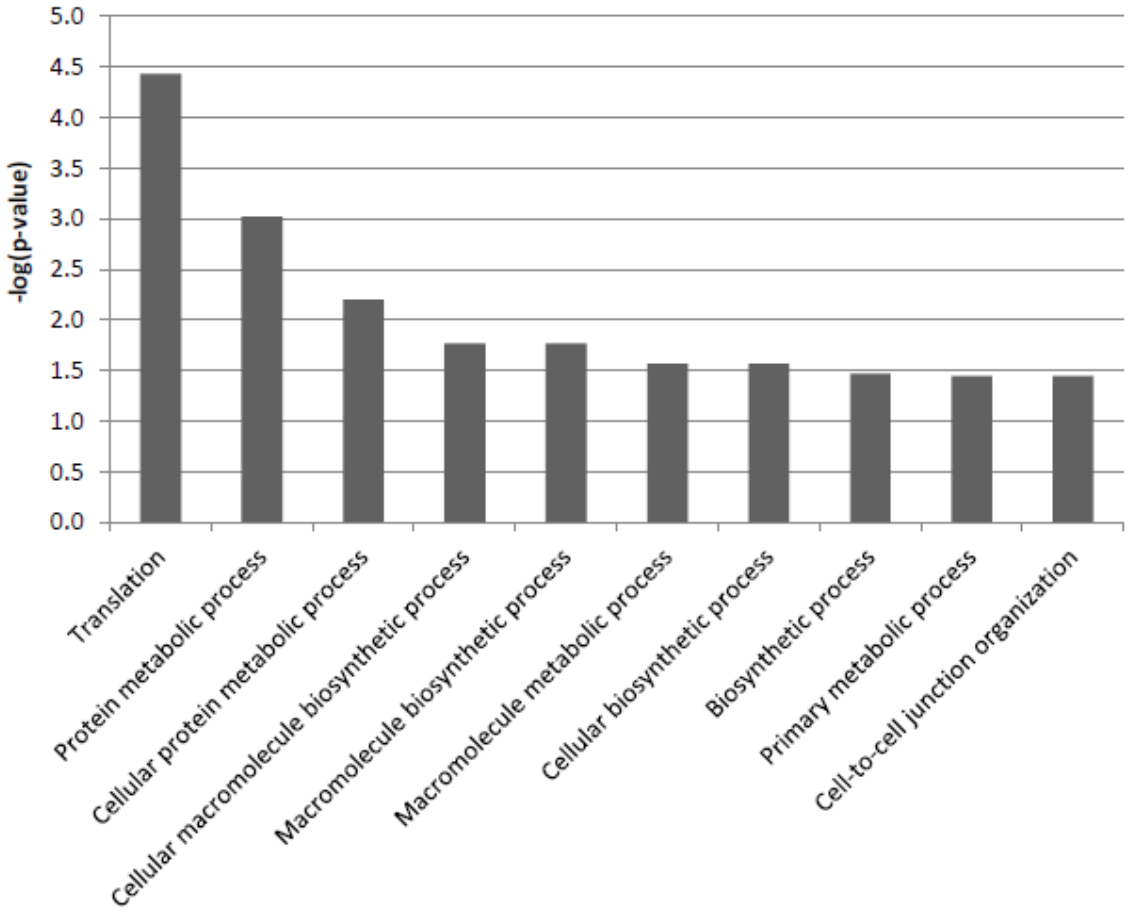

Figure A2.2. Gene Ontology analysis of MGRN1 interactions. Gene ontology analysis of MGRN1 interactions identified by yeast-2-hybrid analysis was performed using the DAVID bioinformatic resource. Represented are the top 10 functional categories of genes most often associated with MGRN1 interacting proteins. The y-axis represents the –log(p-value). All categories exceed a threshold p-value of 0.05 (-log(p-value)=1.3).

C-terminal to the RING domain fused to the DNA binding domain of the yeast transcription factor Gal4 as "bait". A commercial mouse e8.5 cDNA library (ProQuest, Invitrogen) consisting of sequences fused to the Gal4 activation domain was used as "prey". This region of the *Mgrn1* transcript has been shown to undergo alternative splicing which generates four distinct isoforms (Figure A2.1). Previous analysis of transgenic mice expressing each of the four *Mgrn1* isoforms has suggested both overlapping and independent functions for the *Mgrn1* isoforms I, II and III during development. Isoform IV was unable to rescue the developmental defects associated with embryonic lethality in these assays (Jiao, K. Sun, et al., 2009). Thus, *Mgrn1* fragments corresponding to each of these isoforms were assayed.

Yeast-2-hybrid analysis identified 36 potential MGRN1 interacting proteins (Table A2.1), including the previously reported MGRN1 interacting protein, TSG101 (B Y Kim, J A Olzmann, et al., 2007; Jiao, K. Sun, et al., 2009). Gene ontology analysis showed a significant enrichment for genes involved in metabolic processes within the data set of MGRN1 interacting proteins (Figure A2.2) Of particular interest was CARBOXYPEPTIDASE E (CPE), the protein encoded by the gene mutated in Cpe^{fat} mutant mice (Naggert et al., 1995). This enzyme acts as an exopeptidase in the processing of proinsulin insulin (Naggert et al., 1995; Fricker et al., 1996). Previous work has demonstrated that loss of *Mgrn1* in the mouse is able to suppress agouti-mediated insulin signaling and that this suppression results in a global reduction in circulating insulin (Phan et al., 2006). While genetic analysis suggests that the effect of *Mgrn1* on insulin signaling is at the level the MC4R receptor (Phan et al., 2006), evidence supporting a direct interaction between these two proteins is controversial (Overton and Leibel, 2011). Thus the mechanism by which MGRN1 participates in regulation of insulin signaling remains unclear. Future studies confirming a direct interaction between MGRN1 and CPE and investigating the

contribution of this interaction to MGRN1-mediated effects on insulin signaling are needed to address these questions.

CONCLUSIONS

These assays have identified a list of potentially interesting MGRN1 interacting proteins; however they were unsuccessful in identifying interactions with obvious implications in LR patterning. Removal of the catalytic RING domain, intended to prevent ubiquitin-mediated degradation of candidate interacting proteins may have unintentionally prevented the identification of complex protein-protein interactions dependent upon multiple regions of the MGRN1 protein. Such a problem could be circumvented by conducting future yeast-2-hybrid screens using a catalytically inactive version of the MGRN1 protein (Lin He et al., 2003). Regardless, further studies are necessary to identify MGRN1 interactions relevant to its role in LR patterning of the embryo.

ACKNOWLEDGEMENTS

Maria García-García , Mark Roberson, Mariana Wolfner, John Schimenti and members of the Gunn lab for helpful discussions and comments; Jeremy Chow, Sean Hackett and Janice Chan for technical help with the yeast-2-hybrid screens.

REFERENCES

Aberle, H., Bauer, A., Stappert, J., Kispert, A., and Kemler, R. (1997). beta-catenin is a target for the ubiquitin-proteasome pathway. *The EMBO journal*, **16**, 3797-804.

Berndt, J. D., Aoyagi, A., Yang, P., Anastas, J. N., Tang, L., and Moon, R. T. (2011). Mindbomb 1, an E3 ubiquitin ligase, forms a complex with RYK to activate Wnt/{beta}-catenin signaling. *The Journal of cell biology*, **194**, 737-50.

Callow, M. G., Tran, H., Phu, L., Lau, T., Lee, J., Sandoval, W. N., Liu, P. S., Bheddah, S., Tao, J., Lill, J. R., et al. (2011). Ubiquitin Ligase RNF146 Regulates Tankyrase and Axin to Promote Wnt Signaling. *PloS one*, **6**, e22595.

Cota, C. D., Bagher, P., Pelc, P., Smith, C. O., Bodner, C. R., and Gunn, T. M. (2006). Mice with mutations in Mahogunin ring finger-1 (Mgrn1) exhibit abnormal patterning of the left-right axis. *Developmental dynamics : an official publication of the American Association of Anatomists*, **235**, 3438-47.

Fricker, L. D., Berman, Y. L., Leiter, E. H., and Devi, L. A. (1996). Carboxypeptidase E activity is deficient in mice with the fat mutation. Effect on peptide processing. *The Journal of biological chemistry*, **271**, 30619-24.

Groettrup, M., Pelzer, C., Schmidtke, G., and Hofmann, K. (2008). Activating the ubiquitin family: UBA6 challenges the field. *Trends in biochemical sciences*, **33**, 230-7.

Hay-Koren, A., Caspi, M., Zilberberg, A., and Rosin-Arbesfeld, R. (2011). The EDD E3 ubiquitin ligase ubiquitinates and up-regulates beta-catenin. *Molecular biology of the cell*, **22**, 399-411.

He, L., Lu, X.-Y. Y., Jolly, A. F., Eldridge, A. G., Watson, S. J., Jackson, P. K., Barsh, Gregory S, Gunn, T. M., and He L Lu XY, J. A. F. E. A. G. W. S. J. J. P. K. B. G. S. G. T. M. (2003). Spongiform degeneration in mahoganoid mutant mice. *Science (New York, N.Y.)*, **299**, 710-2.

Huang, D. W., Sherman, B. T., and Lempicki, R. A. (2009a). Bioinformatics enrichment tools: paths toward the comprehensive functional analysis of large gene lists. *Nucleic acids research*, **37**, 1-13.

Huang, D. W., Sherman, B. T., and Lempicki, R. A. (2009b). Systematic and integrative analysis of large gene lists using DAVID bioinformatics resources. *Nature protocols*, **4**, 44-57.

Jehn, B. M., Dittert, I., Beyer, S., von der Mark, K., and Bielke, W. (2002). c-Cbl binding and ubiquitin-dependent lysosomal degradation of membrane-associated Notch1. *The Journal of biological chemistry*, **277**, 8033-40.

Jiao, J., Sun, K., Walker, W. P., Bagher, P., Cota, C. D., and Gunn, T. M. (2009). Abnormal regulation of TSG101 in mice with spongiform neurodegeneration. *Biochimica et biophysica acta*, **1792**, 1027-35.

Kim, B Y, Olzmann, J A, Barsh, G S, Chin, L. S., and Li, L (2007). Spongiform neurodegeneration-associated E3 ligase Mahogunin ubiquitylates TSG101 and regulates endosomal trafficking. *Mol Biol Cell*, **18**, 1129-1142.

Kim, Bong Yoon, Olzmann, James A, Barsh, Gregory S, Chin, L.-S., and Li, Lian (2007). Spongiform neurodegeneration-associated E3 ligase Mahogunin ubiquitylates TSG101 and regulates endosomal trafficking. *Molecular biology of the cell*, **18**, 1129-42.

Lai, E. C., Roegiers, F., Qin, X., Jan, Y. N., and Rubin, G. M. (2005). The ubiquitin ligase Drosophila Mind bomb promotes Notch signaling by regulating the localization and activity of Serrate and Delta. *Development (Cambridge, England)*, **132**, 2319-32.

Markson, G., Kiel, C., Hyde, R., Brown, S., Charalabous, P., Bremm, A., Semple, J., Woodsmith, J., Duley, S., Salehi-Ashtiani, K., et al. (2009). Analysis of the human E2 ubiquitin conjugating enzyme protein interaction network. *Genome research*, **19**, 1905-11.

Mukai, A., Yamamoto-Hino, M., Awano, W., Watanabe, W., Komada, M., and Goto, S. (2010). Balanced ubiquitylation and deubiquitylation of Frizzled regulate cellular responsiveness to Wg/Wnt. *The EMBO journal*, **29**, 2114-25.

Naggert, J. K., Fricker, L. D., Varlamov, O., Nishina, P. M., Rouille, Y., Steiner, D. F., Carroll, R. J., Paigen, B. J., and Leiter, E. H. (1995). Hyperproinsulinaemia in obese fat/fat mice associated with a carboxypeptidase E mutation which reduces enzyme activity. *Nature genetics*, **10**, 135-42.

Overton, J. D. and Leibel, R. L. (2011). Mahoganoid and mahogany mutations rectify the obesity of the yellow mouse by effects on endosomal traffic of MC4R protein. *The Journal of biological chemistry*, **286**, 18914-29.

Phan, L. K., Chung, W. K., and Leibel, R. L. (2006). The mahoganoid mutation (Mgrn1md) improves insulin sensitivity in mice with mutations in the melanocortin signaling pathway independently of effects on adiposity. *American journal of physiology. Endocrinology and metabolism*, **291**, E611-20.

Qiu, L., Joazeiro, C., Fang, N., Wang, H. Y., Elly, C., Altman, Y., Fang, D., Hunter, T., and Liu, Y. C. (2000). Recognition and ubiquitination of Notch by Itch, a hect-type E3 ubiquitin ligase. *The Journal of biological chemistry*, **275**, 35734-7.

Schulman, B. A. and Harper, J. W. (2009). Ubiquitin-like protein activation by E1 enzymes: the apex for downstream signalling pathways. *Nature reviews. Molecular cell biology*, **10**, 319-31.

Wenzel, D. M., Stoll, K. E., and Klevit, R. E. (2010). E2s: structurally economical and functionally replete. *The Biochemical journal*, **433**, 31-42.